

HIERARCHICAL HYBRID MATERIALS FROM FLEXIBLE FABRIC  
SUBSTRATES

A dissertation submitted in partial fulfillment of the  
requirements for the degree of  
Doctor of Philosophy

By

WENHU WANG

M.S.EG., Wright State University, 2011

B.E., Sichuan University, 2009

2020

Wright State University

WRIGHT STATE UNIVERSITY  
GRADUATE SCHOOL

Dec 9, 2019

I HEREBY RECOMMEND THAT THE DISSERTATION PREPARED UNDER MY SUPERVISION BY **Wenhu Wang** ENTITLED **Hierarchical Hybrid Materials from Flexible Fabric Substrates** BE ACCEPTED IN PARTIAL FULFILLMENT OF THE REQUIREMENTS FOR THE DEGREE OF **Doctor of Philosophy**.

---

Sharmila M. Mukhopadhyay,  
Ph.D.  
Dissertation Director

---

Philippe Sucusky, Ph.D.  
Director, Ph.D. in Engineering  
Program

---

Barry Milligan, Ph.D.  
Interim Dean of the Graduate  
School

Committee on Final Examination:

---

Willie F. Harper, Jr., Ph.D.

---

Mallikarjuna N. Nadagouda, Ph.D.

---

Hong Huang, Ph.D.

---

H. Daniel Young, Ph.D.

## ABSTRACT

Wang, Wenhui., Ph.D., Engineering Ph.D. Program, Wright State University, 2020.  
Hierarchical Hybrid Materials from Flexible Fabric Substrates.

The goal of this project is to investigate fabrication approaches and structure-property relationships of porous and flexible hierarchical hybrid solids suitable for advanced surface-active devices. Multi-scale hierarchical carbon materials are being fabricated by strong covalent attachment of multiwall carbon nanotube(MWCNTs) arrays on flexible carbon fabric substrates in order to enhance the surface area per unit volume. This was done using chemical vapor deposition (CVD) after functionalizing the surface with a plasma-derived nano-oxide coating. Structural and chemical characterization is performed using scanning electron microscope(SEM), energy dispersive spectroscopy(EDS) and x-ray photoelectron spectroscopy(XPS). Surface area estimates have been made by building structural models from Electron Microscopy data and subsequently validated with direct measurement with BET isotherm analyses. It is seen that calculated specific surface area (SSA) of the material via mass increase during the CVD process is in good agreement with BET gas adsorption measurement of the SSA.

It has been shown that further modification of these surfaces is very effective for tailoring their wettability for selective infiltration of different fluids. These structures have been infiltrated with responsive polymers such as Poly(N-isopropylacrylamide(PNIPAM)s to fabricate smart stimuli-responsive composites.

In addition, palladium nanoparticles(PdNPs) have been attached onto the nanotube carpets. Particle distribution, size variation, and structures have been investigated using Scanning Electron Microscopy (SEM) & Energy Dispersive Spectroscopy (EDS). X-ray photo spectroscopy (XPS) was employed for bonding state analysis.

In-depth understanding of catalytic behavior of these hybrid nanocatalysts (Fabric-CNT-Pd system) has been performed by investigating the catalytic reduction of a model water contaminant triclosan(TCS). The reaction rates, efficiency, and durability have been studied using High Performance Liquid Chromatography (HPLC) and Mass Spectroscopy (MS). Results clearly show unprecedented chemical reduction rates of TCS, implying that PdNPs on these hierarchical porous materials have application potential in next generation nano catalysts suitable for water purification devices.

Additionally, few preliminary studies have been performed in collaboration with other groups to understand the broader applicability of these materials. These include growth of biological cells for enhanced cell differentiation on these materials and gas-responsive electrical properties with potential application in sensing applications.

## Table of Contents

Chapter 1: Introduction and Background .....	1
1.1 Introduction.....	1
1.2 Research Aim and Scope .....	4
1.3 Porous Carbon Supports .....	5
1.3.1 Reticulated Vitreous Carbon foams .....	5
1.3.2 Carbon Fiber Cloth.....	8
1.4 Carbon Nanotube .....	11
1.4.2 CNT Synthesis Techniques .....	18
1.4.3 Applications of Carbon Nanotubes .....	20
1.5 Characterization techniques.....	25
1.5.1 Scanning Electron Microscopy (SEM) .....	25
1.5.2 X-ray Diffraction (XRD).....	25
1.5.3 Energy Dispersive X-ray Spectroscopy (EDS) .....	26
1.5.4 X-ray Photoelectron Spectroscopy (XPS).....	27
1.5.5 Brunauer-Emmett-Teller Surface Area Analysis (BET) .....	27
1.5.6 High Performance Liquid Chromatography (HPLC).....	30
1.5.7 Transmission electron microscopy (TEM).....	31
Chapter 2 Hierarchical hybrid solids: nanotube carpets on porous substrates .....	32
2.1 Introduction .....	32
2.2 Materials and Methods .....	35
2.2.1 Materials.....	35
2.2.2 Synthesis of aligned CNT on carbon fiber cloth .....	35
2.2.3 Electrical Property measurement .....	39
2.2.4 Materials Characterization .....	41
2.3 Results and Discussion .....	42
2.3.1 CNT carpets on ideal carbon surface .....	42
2.3.3 Surface morphology of CNT carpet on carbon fiber cloth.....	48
2.3.4 Analysis and comparison of CNT carpet morphology on different substrates. .....	50
2.3.5 Surface chemistry of CNT carpet .....	56

2.3.5.1 Surface chemistry study of CNT carpet on Fiber cloth.....	56
2.3.5.2 X-ray Diffraction for crystal structure .....	59
2.3.6 Surface area estimates of CNT-carpet enhanced solids: .....	61
2.3.7 Comparison of surface area measurement with gas adsorption .....	71
2.4 Electrical Property measurement.....	77
2.5 Conclusions .....	82
Chapter 3: Surface Wettability Conversion of Hierarchical Carbon Supports.....	84
3.1 Introduction .....	84
3.2 Experimental.....	86
3.2.1 Surface silica coating .....	86
3.2.2 Preliminary contact angle studies on various geometries .....	87
3.3 Results and Discussion .....	91
3.3.1 SOL-GEL silica coating on CNTCFC .....	91
3.3.2 Initial trial of contact angle test of different surface under different condition .	95
3.3.2.1 Detailed contact angle measurement on fabric and foam .....	95
3.4 Conclusion .....	107
Chapter 4 Attachment of nano catalytic particle: Palladium .....	108
4.1 Introduction .....	108
4.2 Experimental.....	110
4.2.1 Materials.....	110
4.2.2 Synthesis of Pd nano catalytic particle.....	110
4.3 Results and Discussions.....	113
4.3.1 Elemental quantification .....	113
4.3.2 Microstructure Characterizaion.....	115
4.3.3 Crystal Structure Characterization .....	121
4.3.4 Chemical Structure of Pd nanoparticles .....	123
4.4 Conclusion .....	125
Chapter 5 Reusable Flexible Hierarchical Hybrid Nanocatalysts for Degradation of Triclosan in water .....	127
5.1 Introduction .....	127

5.2. Experimental.....	132
5.2.1 Materials.....	132
5.2.2 Palladium nanoparticle (PdNP) deposition .....	132
5.2.4 Morphology and Chemistry analysis.....	134
5.3. Results and Discussion .....	136
5.3.1 Attachment of nano catalytic particle: Palladium .....	136
5.3.2 Catalytic reduction of triclosan via hierarchical hybrid material .....	140
5.3.3 Palladium catalyst chemistry analysis.....	149
5.3.4 Degradation pathway study.....	152
5.4. Conclusion .....	160
Chapter 6: Use porous carbon support for stimuli responsive composite .....	161
6.1 Introduction .....	161
6.2 Experimental.....	164
6.2.1 PNIPAM synthesis .....	164
6.2.2 Background mathematical model and water filtration test.....	167
6.2.3 Mechanical strength measurement .....	171
6.3 Results and discussion .....	172
6.3.1 Polymerization .....	172
6.3.2 Fluid flow test.....	177
6.3.4 Mechanical testing.....	183
6.4 Conclusion .....	185
Summary.....	186
Future work.....	189
Reference .....	190
Appendix A: HPLC analysis of Triclosan (Irgasan) .....	229

## List of Figures

Figure 1. 1 RVC foam as received a) physical appearance b) microstructure under SEM 50x .....	6
Figure 1. 2 Carbon fiber cloth as received a) physical appearance b) microstructure under SEM 50x c) microstructure under SEM 1000x .....	9
Figure 1. 3 Molecular construction of different carbon nanotubes using Avogadro	
1.4.1 Physical Properties of CNTs.....	14
Figure 1. 4 . Standard BET adsorption/desorption isotherm of a) carbon fiber cloth (CFC), b) CNT grafted CFC hybrid material .....	29
Figure 2. 1 a) Illustration of plasma buffer layer coating on fiber cloth substrate .	37
Figure 2. 2 Schematic illustration of electrical property measurement .....	40
Figure 2. 3 CNT carpet on ideal carbon(HOPG) surface [149].....	43
Figure 2. 4 a-e SEM image of multiwall carbon nanotubes grown on graphite sample with different surface roughness. (a) pristine graphite sample with a zoomed-out view of aligned CNTs on smooth surface, (b-e) CNTs on graphite sample surface with 1, 5.5, 14.5, 34 micron finish, respectively, (f) histogram plot of carbon nanotube carpet height as the surface roughness varies .....	45
Figure 2. 5 CAD representation and optic image of carbon fiber cloth .....	47
Figure 2. 6 SEM images of the carbon fiber cloth. (a) As received carbon fiber cloth, (b) CNT grafted CFC at low magnification, (c,d) entangled CNTs on two carbon fiber while mechanically separation applied. (d) CNT details from transmission mode image showing the carbon nanotubes are multiwalled CNT with heavy entanglement. ....	49
Figure 2. 7 a) Transmission mode SEM images of CNT on fiber cloth and b) TEM image of multiwalled CNT (c)CNT diameter distribution for inner and outer wall .....	51
Figure 2. 8 CNT diameter variation as a function of time, showing no significant difference can be observed up to 2 hours production time. ....	55
Figure 2. 9 XPS spectra regarding a) carbon fiber cloth survey scan, b) CFC carbon peak fine scan, c) CNTCFC survey scan, d) CNTCFC carbon peak fine scan .....	58

Figure 2. 10 XRD pattern of carbon fiber cloth and CNT-CFC hybrid material ...	60
Figure 2. 11 Carbon fiber cloth weight change according to heat treatment time w/o xylene.....	62
Figure 2. 12 Carbon fiber cloth weight change as a function of thermal CVD runtime.....	64
Figure 2. 13 specific surface area of CNT-CFC hybrid material calculated from the weight gain method.....	70
Figure 2. 14 BET surface area measurement of CNT-CFC hybrid material respect to different CNT growth time .....	72
Figure 2. 15 SSA of CNTCFC hybrid material comparisons from different measurement/calculation methods.....	72
Figure 2. 16 Illustration of N <sub>2</sub> gas molecules interact with both inner and outer walls of CNT.....	76
Figure 2. 17 Electrical Resistance versus length divided by width of CNT/CFC samples for different CNT growth times. ....	79
Figure 2. 18 Conductivity of CNT/CFC samples versus CNTs growing time.....	81
Figure 3. 1 Measurement of the contact angle of a three-phase system .....	88
Figure 3. 2 Schematic representation of goniometer assembly .....	90
Figure 3. 3 Microstructure of SOL-GEL silica coated CNT forest .....	92
Figure 3. 4 Contact angle preliminary test based on carbon fiber cloth. a) as received. b) CNT grafted carbon fabric. c) Silica coated on CNT grafted carbon fiber cloth.....	96
Figure 3. 5 Contact angle preliminary test on RVC foam. a) as received. b) CNT grafted RVC foam. c) SOL-GEL Silica coated CNTRVC.....	99
Figure 3. 6 Selected silicone tube contact angle measurements according to different surface treatment, a) as received b) surface grinded with 120 grit sand paper c) surface etched by peroxide d) surface etched by ammonium hydroxide	103
Figure 3. 7 Contact angle comparison according to different surface treatment..	106
Figure 4. 1 schematic route of Palladium nano particle (PdNP) synthesis.....	112
Figure 4. 2 EDS analysis of fabric samples with different surface modification .	114

Figure 4. 3 Microstructural characterization of Pd attached CNTCFC hybrid material .....	116
Figure 4. 4 Palladium nanoparticle size distribution .....	117
Figure 4. 5 SEM characterization of PdNP attachment on CNTCFC surface with SOL-GEL silica coating .....	120
Figure 4. 6 X-ray diffraction pattern for pristine fabric, CNTCFC hybrid and Pd attached CNTCFC hybrid. ....	122
Figure 4. 7 XPS spectra of a) survey scan of Pd attached CNTCFC hybrid b) high-resolution Pd 3d core level. ....	124
Figure 5. 1 The reactor of triclosan catalytic degradation .....	135
Figure 5. 2 SEM/TEM Micrographs of PdNPs synthesized on CNT-CFC hierarchical substrate .....	138
Figure 5. 3 Normalized PdNP diameter distribution histogram .....	139
Figure 5. 4 Adsorption comparisons of TCS from different materials in water. ...	141
Figure 5. 5 Adsorption comparisons of TCS from different materials in methanol. ....	142
Figure 5. 6 TCS catalytic degradation in a) aqueous environment, b) methanol environment .....	145
Figure 5. 7 Stability and durability test of PdNP loaded CNTCFC hybrid material in a) aqueous environment, b) MeOH environment .....	148
Figure 5. 8 XPS surface analysis of Pd attached CNTCFC hybrid material before dechlorination .....	150
Figure 5. 9 XPS surface analysis of Pd attached CNTCFC hybrid material post dechlorination .....	151
Figure 5. 10 sample liquid chromatogram of TCS at different reaction time .....	154
Figure 5. 11 Typical a,b) LC mass spectrum c) GC-MS acquired .....	157
Figure 5. 12 Triclosan dechlorination and daughter products formation curve ...	159
Figure 5. 13 Proposed pathway of degradation .....	159
Figure 6. 1 Schematic water flow set.....	170
Figure 6. 2 Setup for the compression test .....	171

Figure 6. 3 Optical microscopy image of RVC foam with polymer infiltrated....	175
Figure 6. 4 Composite response to temperature a)below LCST b) above LCST.	176
Figure 6. 5 Thermosensitive valve response on the temperature of constant rate water flow .....	180
Figure 6. 6 Pressure drop as a function of volumetric flow rate at room temperature .....	181
Figure 6. 7 Pressure drop as a function of volumetric flow rate at elevated temperature (50 °C).....	182
Figure 6. 8 Stress-strain curve from a uniaxial compression test on foam samples. ....	184

## List of Tables

Table 1. 1 Material properties of reticulated vitreous carbon (RVC) foam.....	7
Table 1. 2 Material properties of carbon fiber cloth (CFC).....	10
Table 2. 1 CNT inner and outer diameter comparisons based on different substrate. .....	52
Table 2. 2 Estimated values of CNT morphology obtained using SEM analysis..	67
Table 2. 3 Surface area of CNT-CFC hybrid material from BET analysis .....	73
Table 3. 1 Elemental analysis of fiber cloth samples .....	93
Table 3. 2 Contact angle of selected carbon fabric surface with surface modification.....	97
Table 3. 3 Contact angle of selected RVC foam with surface modification .....	100
Table 3. 4 Curved surface contact angle (CA) with different surface treatment ..	104
Table 5.1 The elemental composition obtained from EDS analysis of Pd-NPs fabricated on fiber cloth material.....	139
Table 5. 2 Catalytic rate constant comparisons .....	146
Table 5. 3 Chemical information of Triclosan and Triclosan related daughter product .....	155
Table 6. 1 Parameters of polymerization.....	166
Table 6. 2 Mass measurement comparisons of composite of different support ...	174
Table 6. 3 Permeability of different materials .....	182

## ACKNOWLEDGEMENT

I do not know meaningful enough words to express my genuine appreciation and deep sense of gratitude to those who helped me throughout my dissertation.

Foremost, I would like to express my sincere appreciation to my advisor Dr. Sharmila Mukhopadhyay, words could hardly express my thanks for her never-ending support, encouragement, guidance from the start to the finish. Her wisdom, patience and dedication inspired me, it is my honor to receive her mentorship.

I would also like to express my gratitude to Dr. Mallikarjuna Nadagouda, for the patient guidance and his generous support, I was allowed to conduct experiments in top-notch laboratories, and provided with a precious internship opportunity are all owing to his effort. I must also thank all my dissertation committees for their supportive feedback on my dissertation and genius ideas for my research inspiration. Furthermore, I would like to show my particular thanks to one of my friends/colleagues Dr. Tao Li for his timely help and instruction, without his help some of the experiments would not be possible. For other people who had mentored and helped me I would always be grateful, a special thanks to my senior Hema Vijwani and colleague Soham Parikh, it's my honor to work with such talented people.

Last but not least, I am sincerely thankful, grateful to my parents Xianping Huang and Dongfeng Wang, for their endless sacrifice, caring and unconditional love, all those years, nothing would have been possible without them.

## Chapter 1: Introduction and Background

### 1.1 Introduction

As the exploration of science and technology expands, these days, scientists and engineers are looking for a wide variety of methods to deliberately create materials at the nanoscale with advantageous and enhanced properties. Carbon, as one of the most abundant element in the universe, is playing a key role in nanomaterial, it has a wide range of molecular structures and orbit characteristics ( $sp$ ,  $sp^2$ ,  $sp^3$  hybridization), its allotropes have quite different properties. Novel carbon nanomaterials are being discovered and synthesized, such as carbon nanotube, fullerene, graphene, nanodiamond etc, are with great research interest. No other element is like carbon, as a sole element, is able to form numerous materials with distinct structures and properties. In another word, carbon material itself has almost included all properties of other material owns, it can vary from soft graphite to hard diamond; it can be an electrical insulator or a conductor, even a semiconductor; it can be a thermal conducting or insulating, last but not least, it can be light-absorbing or transparent. Therefore, carbon is showing a promising capability in nanotechnology field.

Surface plays an important role in nanomaterial applications, surface is where material itself interacts with the surroundings. High specific surface area(SSA) will be able to increase the effectiveness and efficiency of a materials due to the available active spots of the material. Therefore, SSA enhancement will be crucial for the performance of the material. There are various ways to achieve higher SSA, cutting down of the solids, or introducing porosity [1, 2]. Either method has its pros and cons. Cutting down solids is able to make solids in form of small particles, powders etc, but agglomeration or handling issues may become a limitation. Extra porosity of the material will definitely increase its SSA while maintaining its original shape, however, mechanical property loss will pull back the further usage of the material. A solution of this is to introduce hierarchy in materials using advanced nano-scale synthetic technology. Inspired from naturally existed hierarchical structure, this kind of structure can be found from biological system to environmental system, such as human dendrite, tree roots etc. [3, 4]

Multi-scale hierarchical materials based on porous supports have been proved to be very useful in a large number of applications due to their unique surface/volume ratio combined with carefully controlled chemistry [5]. The goal of this dissertation is to investigate fabrication and properties of this type of architecture on carbon fiber cloth, which opens up the possibility of adapting this

architecture in a larger variety of flexible and durable devices. In this case, multiwalled-carbon nanotubes(MWCNTs) are grafted onto the carbon fiber cloth, which will not only increase the SSA of the material, but also avoid the potential risk of loose nanomaterials, which are difficult to handle and may pose environmental hazard. After the hierarchical material was formed, based on the surface condition, precisely designed modification is done in order to enhance the potential application for green chemistry [6], electrical properties [7] and nano-scale metallic catalysis or bio scaffolding [8,9].

## 1.2 Research Aim and Scope

This dissertation is intended to identify flexible porous carbon support for CNT grafting, in order to create hierarchical structures, this synthesized hybrid material will be used for further catalytic degradation of aqueous organic pollutant. Main objectives are listed below:

- Synthesis and characterization of CNT grafted CFC hybrid material, investigate the details of surface area change by employing different methods, which includes mathematical model and experimental approach.
- Surface wettability tuning of different material surface
- Surface functionalization and optimization of hybrid material with metallic nanoparticles.
- Investigation of surface functionalization on environmental remediation and catalytic degradation of emerging contaminant in water.
- Preliminary study hierarchical carbon material for broader application, which includes stimuli – responsive polymer incorporation and its influence on dynamic aqueous fluid.

## **1.3 Porous Carbon Supports**

### **1.3.1 Reticulated Vitreous Carbon foams**

Reticulated carbon foams are typically fabricated from the pyrolysis of thermosetting polymer foam, resulting in skeleton or vitreous carbon struts. Reticulated vitreous carbon foams (RVC foams) selected in this study were provided by Ultramet Inc. As shown in Fig. 1.1. Reticulated foam is made up of predominantly amorphous carbon, light weight, fragile, and 3D networking with high solid SSA. Table 1.1 provides the data from the manufacturer.

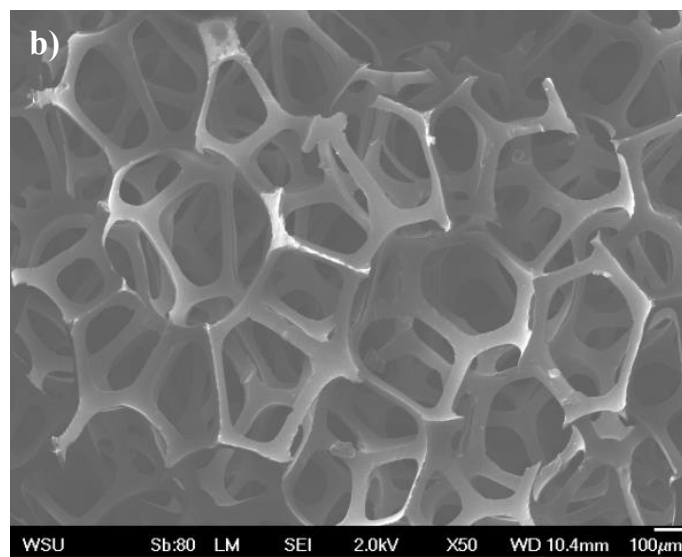
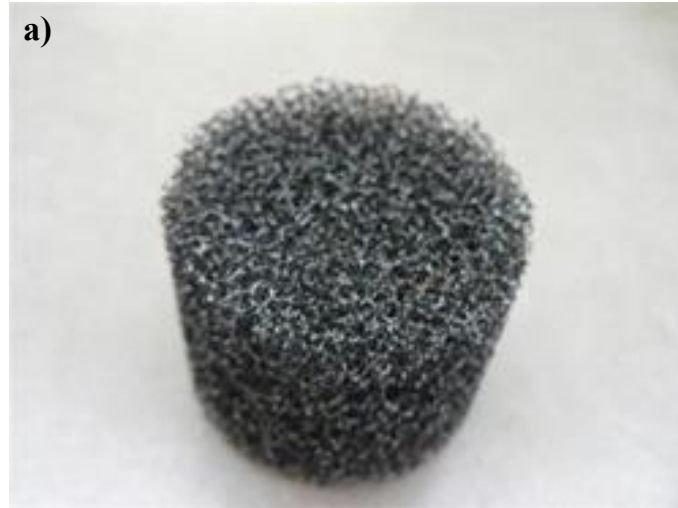


**Figure 1. 1 RVC foam as received a) physical appearance b) microstructure under SEM 50x**

**Table 1. 1 Material properties of reticulated vitreous carbon (RVC) foam**

<b>Physical Properties</b>	<b>RVC foam</b>
Porosity (%)	97
density (g/cc)	0.045
compressive strength at 20 °C (kpa)	762 (ultimate)
Electrical resistivity ( $\Omega$ cm)	0.75
thermal conductivity at 200 °C (W/mK)	0.085
specific heat (cal/g/ °C)	0.3

### **1.3.2 Carbon Fiber Cloth**

Carbon fiber cloth (CFC or CFC), is a fibrous material mostly (usually over 90% or 95%) composed of carbon atoms with high strength and high modulus. In general, CFCs have an average diameter of 5-10 micrometer, in application, they are usually bundled together to form a tow or woven into fabric. CFC has very advantageous properties such as high thermostability, anti-corrosion, good thermal and electrical conductivity and easiness of processing, etc., makes it a modern functional fiber material in the 21<sup>st</sup> century, its unique fibrous nature has decided its applications in aerospace, construction, medical and electronics etc. The CFC selected in this study were obtained from HEXCEL®, HexForce® ACGP206-P. The woven fabric information is provided in Table 1.2.

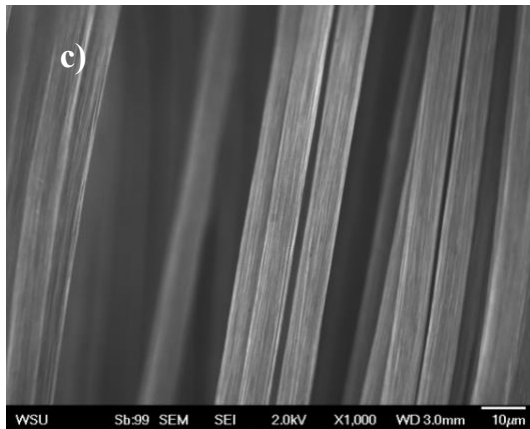
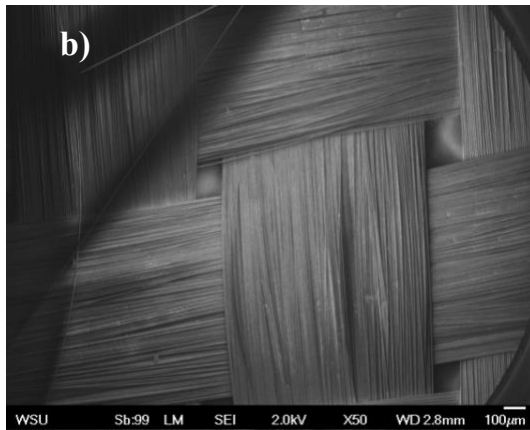
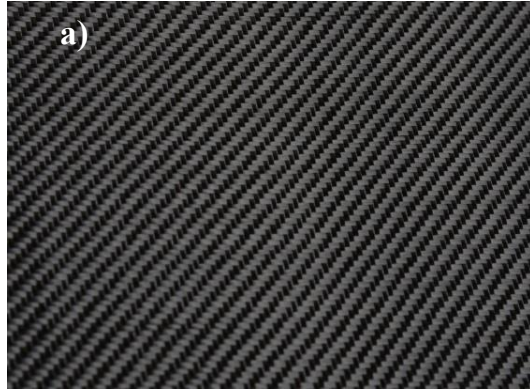


**Figure 1. 2 Carbon fiber cloth as received a) physical appearance b) microstructure under SEM 50x c) microstructure under SEM 1000x**

**Table 1. 2 Material properties of carbon fiber cloth (CFC)**

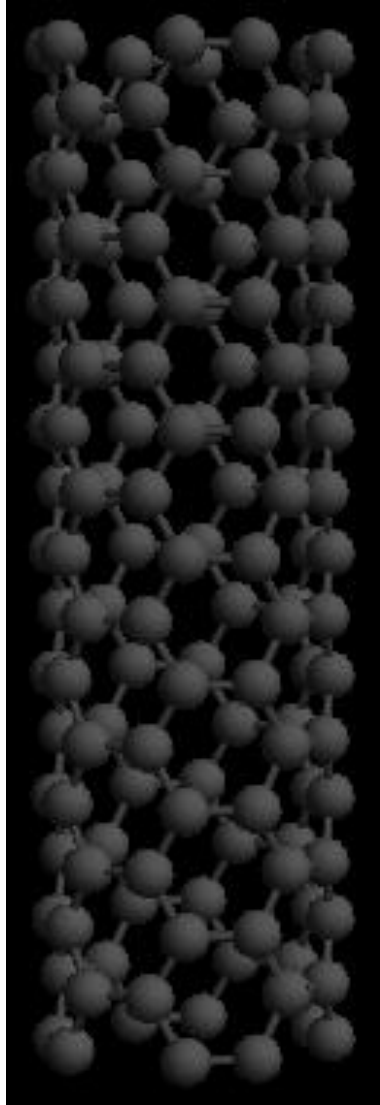
<b>Properties</b>	<b>Carbon Fabric</b>
Weave	Plain
fill yarn/ warp yarn	AS4CGP 3K / AS4CGP 3K
weight (g/m <sup>2</sup> )	205
tensile strength (ksi)	647
tensile modulus (msi)	33.5
Elongation (%)	1.8

## 1.4 Carbon Nanotube

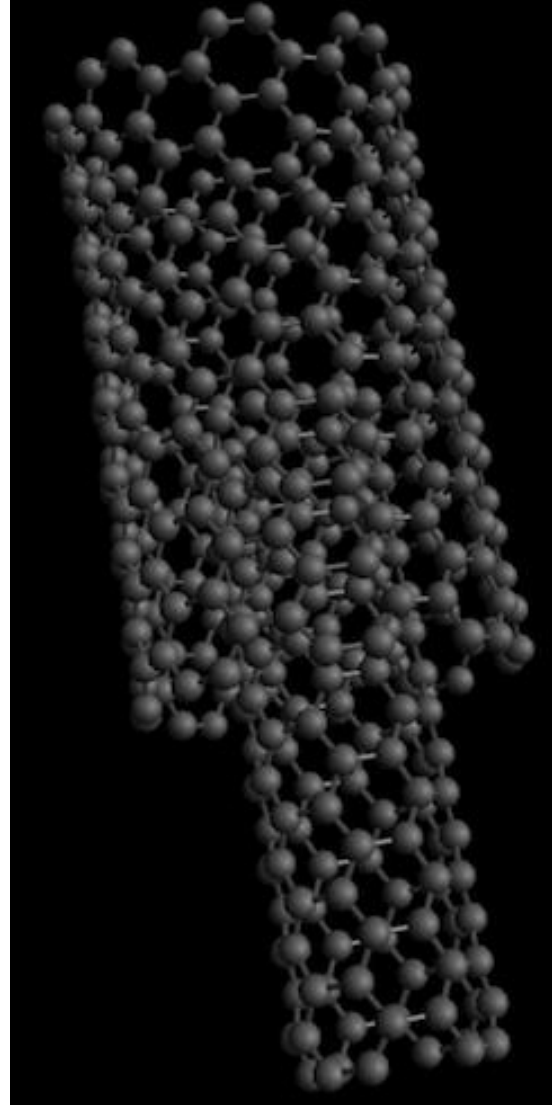
CNT is an allotrope of carbon, it has a standard layered structure, similar to graphite, besides, it is also a special one dimensional hollow structured nanomaterial, with a nano-scaled dimension at radial direction, but at axial direction, length of CNT is usually in mm or even in meters, depends on the synthesis condition [36]. Same as graphite, CNT carbon atoms are bonding with adjacent three carbon atoms via  $sp^2$  hybridization, forming an in-plane hexagonal networking pattern. Since carbon has 4 valent electrons, the 4<sup>th</sup> valence electron is forming a perpendicular out of plane bond through weak Van der Waals force, resulting a 0.34nm distance at the interlayer(radial) direction [10], [11]. This molecular structure makes CNT highly anisotropic. Since its discovery in 1991 [12], there are two major types of CNTs, single wall CNT (SWCNT) and multi-wall CNT (MWCNT), shown in Fig.1.3. Endo et al. showed the first set of SWNT and MWNT in HRTEM images [13]. As the attention increases, soon, CNTs are synthesized using a variety of techniques such as arc-discharge, laser ablation, pyrolysis, electrolysis and chemical vapor deposition (CVD) [14-20] etc. This research focused on CVD method (more detail in Chapter 2) to grow MWCNTs. Several articles have reported theoretical calculations of CNT properties, and it was predicted that SWCNTs had metallic or semi-metallic properties based on

tube chirality but MWCNT were only metallic [7], [21]. CNTs were mechanically tested and the results demonstrated that both SWCNTs and MWCNTs are able to achieve as high as 1TPa young's modulus, which is almost 100 times than steel [37]. From these preliminary studies, CNTs soon started to attract research attention and became a popular research field. Theoretically, the CNT network pattern should maintain hexagonal and cylindrical in axial direction, however, some research conducted on CNT morphology studies showed there is existence of T, L, Y or coil-shaped CNTs [22-25]. Mauricio et al, showed the bending in CNTs, or the appearance of non-cylindrical CNTs are attributed to the surface defects such as pentagon and heptagon shaped rings replacing the hexagonal ring, while pentagon location would create concave, heptagon would form convex [26, 38]. CNTs are unique due to their high aspect ratio, hollow-structure, high tensile strength, and their electrically and thermally conductivity [27-29]. Utilizing one or more factors of CNT will make itself feasible in various applications such as gas storage [30], field emission sources [31], supercapacitors [32], chemical and biosensors [33,34], composites [35], and more. It is important to understand CNT growth mechanism and pattern, as well as the correspondent tailoring for property control. The following chapter is aiming to find out the connections between

growth parameters and resulting CNT morphology, which will be suitable for future property estimation and tuning.



**single wall CNT**



**double wall CNT**

**Figure 1. 3 Molecular construction of different carbon nanotubes using Avogadro**

## **1.4.1 Physical Properties of CNTs**

### ***1.4.2.1 Mechanical Properties of CNT***

CNTs have superior mechanical properties. CNTs have a tensile strength up to 200 GPa, which is over 100 times of steel, but the density of CNTs, is only one sixth of steel. Elastic modulus is a basic measurement of mechanical property of a material. Treacy et al accomplished the earlier studies, by recording the vibration amplitude of CNTs after heated them up with electron beam [39]. Wong et al found out the MWCNT were twice as stiff as SiC nanorod via Atomic force microscopy (AFM) [40]. A lot of research have shown that the young's modulus of CNTs could be over 1 TPa, which is comparable with diamond [37, 41, 42]. This nature of CNT makes itself an excellent candidate for lightweight structural material.

### ***1.4.2.2 Electrical Properties of CNT***

Electron movement inside in CNTs is isotropic, it moves along the axial direction only. This in-plane free to move phenomenon is a characteristic property of conjugated electrons (delocalized  $\pi$  bond) at quantum level. Further studies showed the existence of Fermi point in CNTs, but it only exists in specific types of CNTs [43,44]. As known, there are major three types of CNTs according to its chirality: zigzag, armchair and chiral, it was proven that all armchair CNTs are

metallic, otherwise semiconducting [45-48]. Chen et al had realized the separation of metallic and semiconducting CNT, which are favored by different electronics depending on its application [49, 50].

#### *1.4.2.3 Magnetic Properties of CNT*

Magnetic properties of CNTs are unique. Ajiki et al found out that while CNTs were positioned perpendicular in the magnetic field, the change of magnetic field strength would alter the band gap of CNTs, meanwhile, the periodic change of magnetic field was able to induce band gap of CNT change periodically [51]. By introducing ferromagnetic metal particles onto or into the CNTs, CNTs will be possible used for applications in areas such as magnetic recording and biomedical fields [52, 53, 54].

#### *1.4.2.4 Adsorption Properties of CNT*

Adsorption is a physical phenomenon happens on the surface of a solid, usually, surface properties between the adsorbate gas and correspondent adsorbent solid are strongly related for adsorption process. CNTs have unique hollow tubular shaped structure, as well as high specific surface area (SSA), etc. Those properties have determined CNTs exceedingly good adsorption capabilities [55, 56, 57]. For the nano scale adsorption mechanism, the current well accepted concept is that the adsorption of CNTs are mainly because of the hydroxyl group on the CNT surface.

Recently, research have shown the adsorption can be achieved not only on SWCNTs, as well as MWCNTs. With tunable hydrophilicity and hydrophobicity, low density, chemical stability, CNTs could be used in a range of adsorption process including inorganic, organic and microorganism fields [58-62].

#### *1.4.1.5 Thermal Properties of CNT*

All CNTs are expected to be good thermal conductors along the axial direction, but limited heat exchange ability perpendicular to the axis [63]. Pop et al reported that the conductivity of SWCNTs is nearly  $3500 \text{ Wm}^{-1}\text{K}^{-1}$  at room temperature, almost ten times as high as copper [64]. It is reported the thermal conductance in CNT is governed by phonons, therefore crystallographic defects will strongly affect the CNT's thermal since such defects will cause **phonon to** scatter [65, 66]. Quiton et al from our group investigated the thermal performance of MWCNTs on solid surface as interface material and established the relationship between CNT morphology and thermal resistance [67].

## 1.4.2 CNT Synthesis Techniques

Various of techniques are employed for CNT synthesis, which includes arc discharge [68], laser ablation [69,70], chemical vapor deposition (CVD) [71] and catalytic decomposition of hydrocarbons etc [72].

### 1.4.2.1 Arc Discharge

Arc discharge was the early most method used to synthesize CNTs. In this method, a low-pressure chamber was filled with inert gas, hydrogen (or other hydrogen gaseous source), DC current was used to produce arc between two electrodes kept at certain distance (usually 1mm), the anode was a graphite electrode with catalyst, the cathode was pure graphite. During the process, arc will vaporize the anode graphite, and CNT are deposited onto the cathode. This method usually produces MWCNTs.

### 1.4.2.2 Laser Ablation

Laser ablation is the method used for SWCNTs synthesis. This method is operated below 1200 °C, with inert gas atmosphere (usually helium), high energy CO<sub>2</sub> or neodymium-doped yttrium aluminum garnet (Nd:YAG) laser was used to vaporize high purity graphite. Yudasaka et al reported the choice of catalyst will eventually affect the yield of CNT [73], meanwhile the alloy (such as Ni-Co alloy)

will improve the yield of SWCNTs by 10 to 100-fold comparing with single catalyst.

#### *1.4.2.3 Chemical Vapor Deposition (CVD)*

CVD method is the technique for CNT decoration on given support material. It is widely used method due to its advantages in high yield, simple instrumentation, cost effectiveness, easy to produce. However, this method may induce defects or impurities during the process, purification may be needed [74]. CVD method utilizes either gas/ liquid hydrocarbons as carbon source, transition metal as catalyst. Researchers had found out the catalyst has huge impact on the CNT structure [75-78]. Barney I.T and Karumuri A. had reported that the growth of CNT on predefined surface requires a silica buffer layer [79, 80], Mukhopadhyay *et.al.* successfully deposited a SiO<sub>2</sub> buffer layer onto flat graphite surface using a plasma enhanced chemical vapor deposition (PECVD) [81], followed with a floating catalyst thermal CVD for CNT fabrication. This dissertation focuses on the CVD method to prepare aligned MWCNTs on a flexible carbon support substrate, detailed information will be discussed in chapter 2.

### 1.4.3 Applications of Carbon Nanotubes

#### 1.4.3.1 Electronics

Electrons inside CNTs are able to move only along the axial direction, which makes the CNT resistivity along the longitudinal direction is way smaller than that along the radial direction [82]. As discussed earlier, CNT has either metallic or semiconducting properties according to its chirality [7, 83], armchair SWCNT has similar conductivity as metals, while zigzag SWCNT behaves like semiconductors. CNT have high curvature at the tip, in combination with the good conductivity, CNT tip is able to create strong local electric field at the tip, which enables itself as a good field emitter when the tip is closed, especially MWCNTs [84]. Moreover, Tans et al reported by introducing defects into SWCNTs, SWCNTs can behave like a molecular diode [85].

#### 1.4.3.2 Sensor

At room temperature, CNT has high response rate, high sensitivity and reversibility makes itself an outstanding micro chemical sensor [89-92]. While adsorption process happens CNT walls, its electrical signal (conductivity) will change vastly, for example, NO<sub>2</sub> gas is able to increase conductivity while NH<sub>3</sub> adsorption decreases its conductivity. which makes a good gas sensor. Besides, CNTs have explored its potential application in biomedicine and biosensing.

Especially, CNTs can function as bio-scaffolds for cell or tissue molecules immobilization onto their surface, followed by an electrical signal conversion connected with the recognition of analytes [93-96]. CNTs' physicochemical properties have huge impact on improving biosensing sensitivity and stability, Weizmann et al reported a hybrid biocatalyzed CNT device able to be used for DNA detection at the femtomolar level, as a potential Ebola virus detector [97].

#### *1.4.3.3 Composite*

CNT is called the new generation “super fiber material” due to excellent mechanical properties, as well as large aspect ratio [98]. Additionally, CNTs also maintain other excellent natures, for example, CNTs can be as flexible as carbon fibers, as conductive as metals both electrically and thermally, as anti-corrosive as ceramic materials, therefore, CNT is a good candidate as an ideal reinforcement material for composite. Currently, there are three major field using CNT as composite additives: CNT – metal matrix composite (MMC), CNT-Polymer matrix composite (PMC) and CNT – Ceramic matrix composite (CMC) [99-101]. By combing the advantages of different materials, CNTs reinforced composite has been applied into many research areas or even industrialized, such as electronics, super conductive material, super capacitors, biomedicine and the list goes on.

#### *1.4.3.3 Hydrogen Storage*

With the increasing urge for environment protection, green energy research has attracted more and more attention. Hydrogen fuel is a zero-emission fuel with extremely high energy density, in its application, hydrogen storage is the biggest hump. CNTs as a novel hydrogen storage material shows in atmosphere environment, stored hydrogen can be released out reversibly from the CNT, which is highly valuable [86, 87], besides, those repeatable storing and releasing actions wont deteriorate its storage capability. Therefore, in the fuel cell system, CNTs could act as a substitute of high pressure hydrogen container, which is very promising for electric automobile industry [88].

#### *1.4.3.5 Catalyst Support*

With high specific surface area (SSA), as well as unique cavity structure and adsorption property [103], in addition, CNTs are strong and thermally stable, therefore, CNTs can be used as catalysts and catalyst supports, and presented a higher catalytic activity [102]. By introducing certain surface modification, a variety of functional group can be introduced, hence its catalytic activity will be further enhanced, this dissertation discussed its capabilities as pallidium nanoparticle support, according to its superior hydrogen storage property, CNTs

can be used as catalyst support for hydrogenation, dehydrogenation reactions etc, detailed information is discussed in the latter chapter.

#### ***1.4.3.6 Biomedical application***

Since CNTs discovery in 1991, medical research from both academia and industrial field were trying to make CNTs feasible in various applications such as genetic therapy, therapeutic drug delivery, bio-sensing, orthotics, diagnostics, immunotherapy etc. [104 -107]. Wong *et al* firstly used AFM with CNT tips to investigate amyloid- $\beta$  fibrils of Alzheimer's disease in 1998 [108]. Due to their small dimension, lightweight and ultra-high surface area, CNTs are able to function as an excellent carrier for drug delivery [109]. As the research of the applications of CNT in biomedical and pharmaceutical expands, bio-compatibility and cytotoxicity of CNT are brought onto the table. Studies have shown that there are couple factors determine the toxicity of CNT including CNT dimension, purity and functionalization, by tuning those parameters, CNT toxicity could be minimized for clinic use [110, 111, 112]. Since CNTs are electrical conductive, Mattson *et al* firstly reported the successful growth of neurons on surface modified MWCNTs, which opened the door for the nanotubes as cell growth substrate [113]. Sequentially, Zanello *et al* successfully used MWCNT as scaffold material for osteoblast proliferation [114]. Additionally, CNT has proven itself a

biocompatible candidate for gene therapy, Anderson *et al* demonstrated SWCNT as an effective RNA carriers for gene therapy of pancreatic cancer [115]. CNT has shown itself a worth exploring material for future bio-nanotechnology field.

## **1.5 Characterization Techniques**

### **1.5.1 Scanning Electron Microscopy (SEM)**

Scanning Electron Microscope (SEM), invented by Manfred von Ardenne, is a type of electron microscope that produces images of sample surface by scanning it with finely focused electron beam. Through the interactions between the electron beam and the sample, secondary electrons are excited and emitted from the surface, those secondary electrons carry various of physical information. By collecting, magnification, image reforming of those information, microstructural morphology characterization of the material is accomplished. For this study, JEOL 7401F Field Emission Scanning Electron Microscope (FE-SEM) was used to capture SEM images using secondary and backscatter modes.

### **1.5.2 X-ray Diffraction (XRD)**

X ray diffraction (XRD) is a nondestructive characterization technique for material crystallography, chemical composition and phase analysis. When a monochromized incident x-ray enters a crystal, it will be diffracted into many specific directions after interacts with the atoms in lattice. The direction and intensity of the diffraction line is strongly related to the crystalline structure,

diffraction pattern of each crystal represents its atomic distribution. In this study, PANalytical XPert PRO diffractometer was used to collect sample XRD pattern using Cu as anode material.

### **1.5.3 Energy Dispersive X-ray Spectroscopy (EDS)**

Energy-dispersive X-ray spectroscopy (EDS, EDXS) is an analytical technique allowing the elemental composition of a specimen to be measured. Main principle of this technique is that an incident electron beam will excite an electron from the inner electron shell, and leaves a hole, the outer shell electron will fulfill the hole and simultaneously releases the energy difference in form of X-ray. The energy of this X-ray is measured, since the energy difference between two shells are related to the nature of the emitting element atomic structure, corresponding element is addressed. As an elemental analysis tool, low resolution and the low accuracy of light element is limiting its usage, where supplementary analysis is needed [116]. In this study, Ametek Inc EDS system was used in conjunction with JEOL FE-SEM.

#### **1.5.4 X-ray Photoelectron Spectroscopy (XPS)**

X-ray photoelectron spectroscopy (XPS), also called Electron spectroscopy for Chemical Analysis (ESCA), is a technique used for quantitative analysis of elemental composition, chemical state and bonding state of elements on the surface of a material. It is a surface sensitive technique, thus the analysis is limited only probe into the near surface depth (depends on the instrument, usually less than 10 nm). This technique uses x-ray to irradiate sample surface, excites and emit the inner shell electron of an atom. Each atom produces a characteristic binding energy value, meanwhile, there is chemical shift of the atom if chemical configuration changes even the same atom existing in different molecules, therefore the XPS is a powerful technique for detailed surface chemistry analysis.

In this study, XPS analysis was conducted via a Kratos (Axis Ultra) system using mono-chromatized Al K $\alpha$  (1486.6 eV) as x-ray source, all analysis was performed in ultra-high vacuum environment (UHV $\sim$ 10<sup>-9</sup> torr). Acquired spectra was processed via Casa XPS software (Casa Software Ltd, V2.3.15)

#### **1.5.5 Brunauer-Emmett-Teller Surface Area Analysis (BET)**

Brunauer-Emmett-Teller (BET) theory is a theory correlates the physisorption of gas molecules on a solid material surface to the specific surface area (SSA) of the

material [117]. In this analysis, Quantachrome NOVA 2200e series was used for the BET surface area analysis, employing nitrogen as adsorbate, liquid nitrogen was used to maintain the temperature of the analysis (77 K). Standard BET adsorption/desorption isotherm was shown in Fig. 1.4, adsorption process is to stick the gas molecules onto the surface of solid, all available sites on the sample was equally, with increasing pressure, the gas adsorption increases correspondingly. When the adsorption finishes, the desorption process will start, by decreasing the gas pressure, desorption process will proceed.

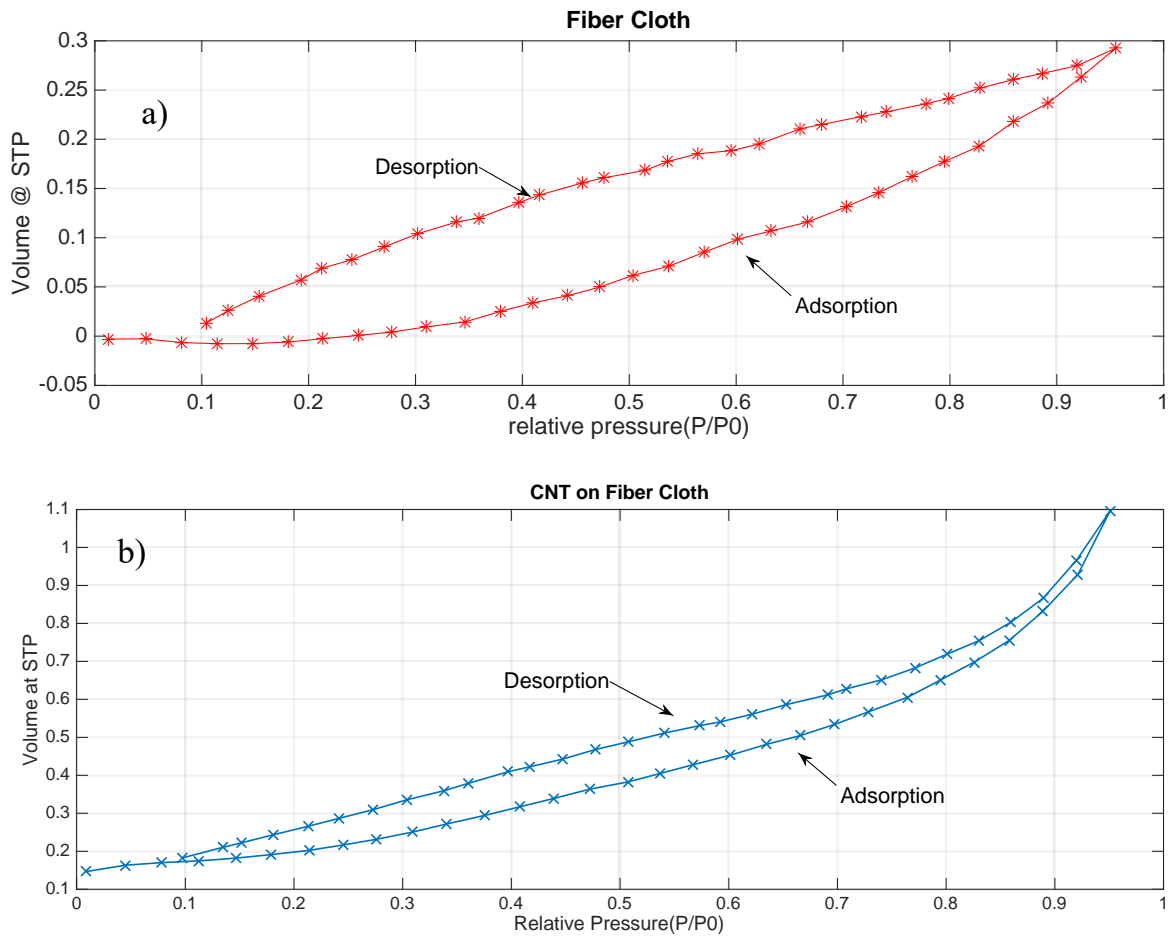


**Figure 1.4 . Standard BET adsorption/desorption isotherm of a) carbon fiber cloth (CFC), b) CNT grafted CFC hybrid material**

### 1.5.6 High Performance Liquid Chromatography (HPLC)

High-performance liquid chromatography (HPLC; also named as high-pressure liquid chromatography) is an analytical technique used for separation, qualification and quantification of a sample mixture in a solvent. In the operation, analyte is injected into the stream of mobile phase, which is usually a miscible combination of water and organic solvent. The mixed mobile phase will move toward a definite direction through a column. Inside the column there is stationary phase immobilized on the support particles, or on the inner wall of the column tube. Based on the affinity of the mobile phase and stationary phase, each component inside the analyte will move at different velocities, therefore each component of the analyte will be pass through (or stay inside) the column at different time period, which is called retention time. The retention time is the time for a particular analyte to pass through the column and reach the detector under certain conditions (elution strength, pressure, etc), it represents the intermolecular interaction(affinity) between the components in mobile phase (analyte) and the stationary phase. In this study, HPLC system used was Waters Micromass Quattro Micro equipped with a mass spectrometer for liquid chromatography (LC-MS) and an auto sampler, column used was Waters Xselect CSH C18 3.5  $\mu\text{m}$ , 4.6x50 mm.

Since HPLC method is tuned based on the particular chemical, detailed HPLC method for this study is shown in Appendix A.

### **1.5.7 Transmission electron microscopy (TEM)**

Transmission electron microscopy (TEM) is another electron microscopy technique. In comparison with SEM, TEM incident electron beam is passing through the sample to form an image. In general, TEM is capable of imaging a significantly higher resolution and magnification, makes it an essential characterization tool for nanomaterial and nanotechnology. In this study, Thermo Scientific™ Talos™ F200X Field Emission Scanning Transmission Electron Microscope was used for analysis.

## Chapter 2 Hierarchical hybrid solids: nanotube carpets on porous substrates

### 2.1 Introduction

Many engineering applications rely on interactions between solid and fluid phases, and the capability of the engineering device is determined by the available surface area that interacts with the fluid phase. Nanoscale materials provide significant advantage of large specific surface area, but lack the structural integrity and pose potential environmental problems due to rapid proliferation and ingestion [118]. Introducing pores or defects on the larger solids therefore increase their surface area availability, but predictably, this method is also limited by the loss of mechanical strength [119] with increasing porosity. In many naturally occurring bio-materials such as capillaries, dendrite roots and microvilli, this issue is addressed by the use of hierarchical surface architectures where the larger solid scaffold is enriched with progressively smaller functional components that interact with their surrounding fluids such as air, water, or bio-fluids [120,121]. In recent years, many researchers as well as our group have been investigating this approach by engineering hierarchically structured solids that comprise a bulk supporting material and strongly bonded arrays of nanotubes and nanoparticles [122-127].

This approach of creating hierarchical solids can be very powerful because substrate materials can be selected based on physical (flexible/rigid, thick/thin,

permeable/impermeable) or chemical needs(inert/active, hydrophilic/hydrophobic), their surface area increased by several orders of magnitude by attaching nanotube arrays as needed. However, it is grossly under-utilized in the design of engineered materials due to interfacial control challenges. The growth of vertically-aligned CNT on flat model substrates like silicon or alumina has been reported [128-130], but the growth of vertically-aligned CNT on porous structure has received minimal attention. Few studies for growing CNT on such porous structures have been limited to metal or oxide foams [131,132]. In one isolated study, “hairy foam structures” were reported, which demonstrates synthesis of carbon nanofibers on nickel-catalyst coated carbon foam structures [133].

Recently, a series of systematic investigations has been reported by our team [134-138], where CNT were grown on porous substrates of different geometries and compositions after a plasma-enhanced nanoscale oxide layer (silica) was used to activate them [134,139]. These materials were seen to be durable and effective in a wide range of applications ranging from composite enhancement [140,141] to adsorption [142], catalysis [102], electrochemistry [143], biodegradation [144] and bio-sensing/bio-scaffolding [145,146].

Whereas significant improvement in useful properties is clearly demonstrated in the above publications, control and scale-up of these materials for large scale

applications will need in-depth understanding of processing-structure-property relationships of the CNT carpet on substrates. It is important to investigate how these nano-features permeate through inner pores, what types of morphology they will have and how much useful surface area they add for different applications. The goal of this chapter is to focus on such issues specific to three-dimensional carbon substrates having open interconnected porosity. A common used carbon substrate – carbon fiber cloth has been investigated. Key parameters that influence the permeation, attachment and growth of aligned CNT through the inner pores have been analyzed. Detailed morphological analysis was carried out using Field Emission Scanning Electron Microscopic (FE-SEM), to estimate CNT diameters, densities, and lengths of CNT arrays. We have developed analytical models to estimate CNT surface areas using the microstructural analysis method and verified using their weight gain data and literature estimates of CNT densities [30]. The surface area estimates are also correlated with adsorption of gas atoms in BET surface area analysis, in order to understand the availability of surface sites for various applications.

## 2.2 Materials and Methods

### 2.2.1 Materials

Analytical grade reagents used in this study were the following: Hexamethyl-dimethylsiloxane (99.5%, HMDSO,  $(\text{CH}_3)_6\text{Si}_2\text{O}$ , Sigma-Aldrich chemicals), Ferrocene (99%,  $\text{C}_{10}\text{H}_{10}\text{Fe}$ , Alfa-Aesar Ltd), and Xylene ( $\text{C}_6\text{H}_4\text{C}_2\text{H}_6$ , PTI Process Chemicals). Other materials are de-ionized water (DI water) and laboratory grade high purity argon and hydrogen gases. Carbon fiber cloth was provided by Hexcel, ACGP206-P weave.

### 2.2.2 Synthesis of aligned CNT on carbon fiber cloth

Carbon Fiber fabric samples were cut into square pieces about 10 cm by 10 cm in size. Aligned carbon nanotubes were fabricated on flexible carbon fiber cloth (CFC) supports using a two-step process: microwave plasma enhanced chemical vapor deposition (PECVD) of silica buffer layer followed by floating catalyst chemical vapor deposition (CVD) of carbon nanotubes. The two-step CNT fabrication technique was invented and optimized from earlier research [134-136]. In this study, process variables were modified and optimized suitable for various porous structures and were carefully monitored, as described in this section.

### ***Silica buffer layer deposition via PECVD***

Silica( $\text{SiO}_x$ ) deposition was carried out in a plasma reactor (V15GK, PlasmaTech Inc.), using gas mixture of HMDSO and oxygen in cyclic steps. Schematic representation of the PECVD process is shown in Figure 2.1a. CFC was coated with uniform silica buffer layer on both front and back side.

### ***Carbon nanotube growth via thermal CVD***

Samples after silica coating subsequently moved to a thermal CVD reactor, consisting of a single crystal quartz tube in a three-zone programmable furnace system (OTF-1200X-III, MTI Corporation Ltd), shown in Fig 2.1b. Samples were placed vertically inside the tube. A mixture of carbon source and catalyst solution was injected into the reactor via an infuse pump (Pump 11 Elite, Harvard apparatus) from a steel syringe under  $\text{H}_2$  reducing environment, while xylene is the carbon source and ferrocene is the catalyst. The entire thermal CVD process contains three stages, pre-heat, growth and cool down, this process is optimized from previous studies [17-20]. It was seen that the key factors will influence the final CNT growth are: CVD run time, furnace temperatures (pre-catalyst and CNT-growth zone), gas composition and flow rates, catalyst and source (Fe/Xy) flow rates, and silica coating thickness[134-138].

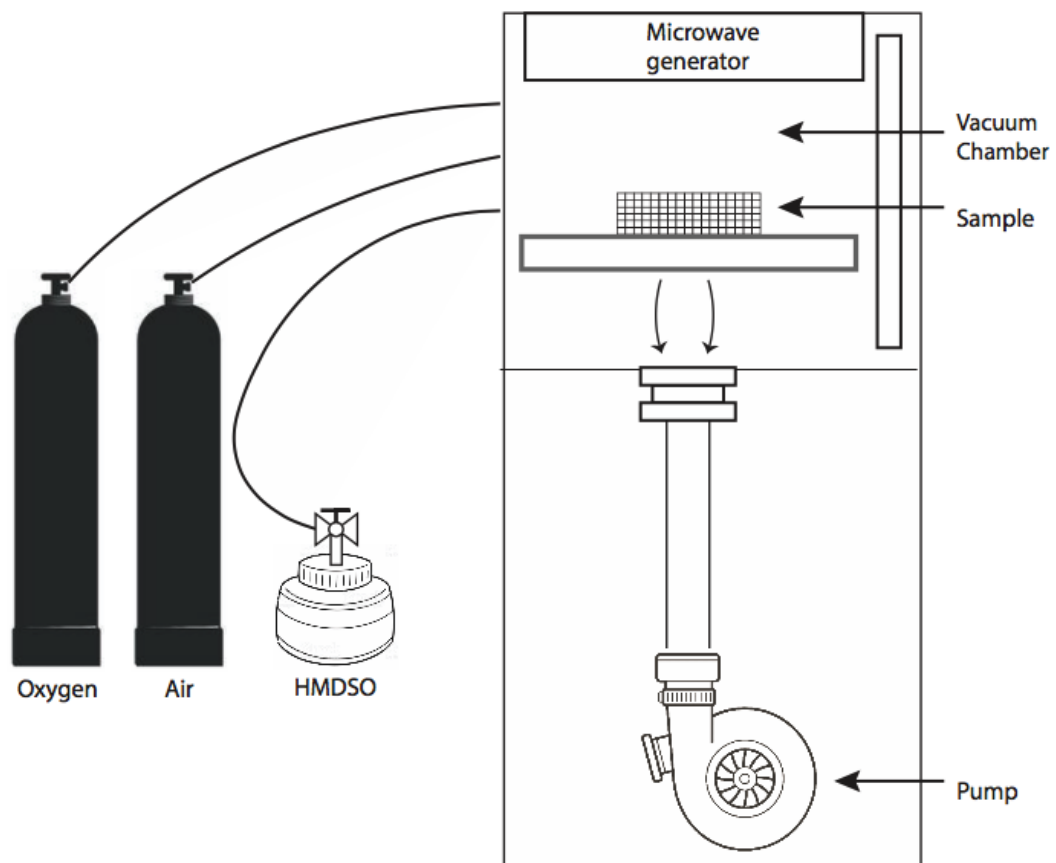


**Figure 2. 1 a) Illustration of plasma buffer layer coating on fiber cloth substrate**

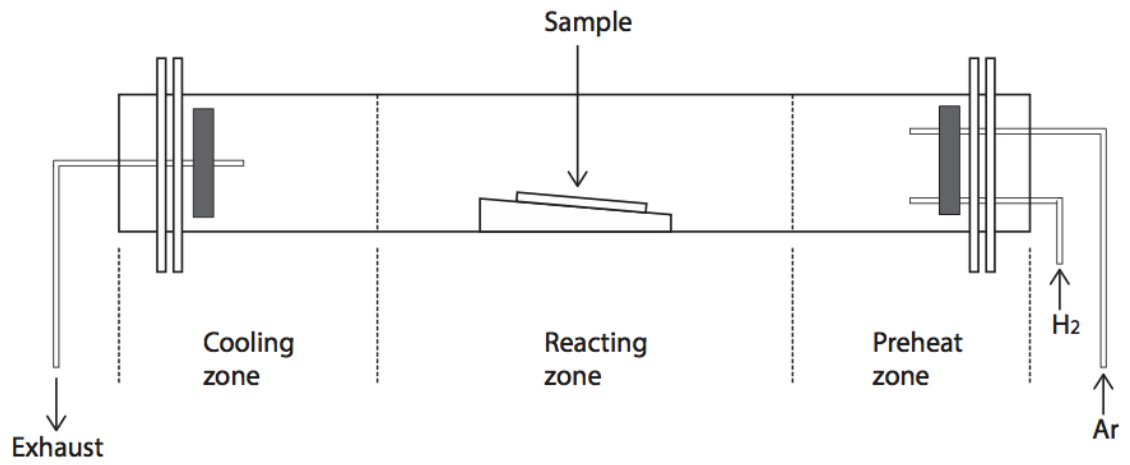


**Fig. 2.1 b) Schematic illustration of thermal CVD process**

### **2.2.3 Electrical Property measurement**

Two-point method was used for R measurement by Keithley 172A multimeter. A mixture of silver paste and paint was applied to both ends of each sample for appropriate leads. During electrical measurement, samples were kept in a box to prevent possible contamination and to minimize airflow. Fig 2.2 exhibits diagram of measurement cell.

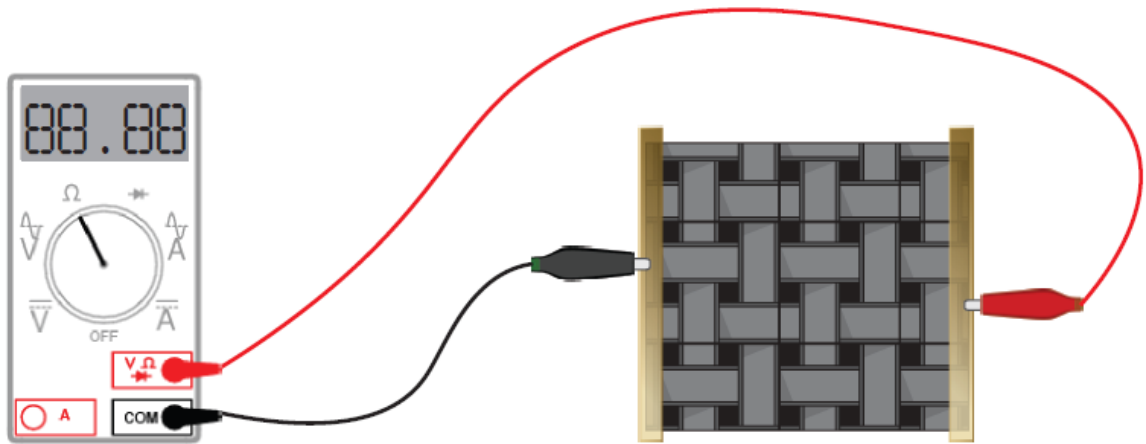


**Figure 2. 2 Schematic illustration of electrical property measurement**

#### 2.2.4 Materials Characterization

Micro-structural images of hierarchical hybrid material were observed using JEOL 7401F field emission scanning electron microscope (FE-SEM). Statistical analysis of SEM micrographs was performed using Image J imaging software. Surface chemical characterization was performed using X-Ray photoelectron spectroscopy (XPS) with a Kratos (Axis Ultra) system and mono-chromatized Al K $\alpha$  (1486.6 eV) source in ultra-high vacuum (UHV~10<sup>-10</sup> Torr) environment. To correct the issue of surface static charging in these scans, a standardized value of 284.4 eV was assigned to C 1s spectrum from graphitic carbon, a known binding energy value for carbon-carbon bonding in *sp*<sup>2</sup> graphite [148]. X-ray diffraction (XRD) patterns were obtained by a PANalytical XPert PRO diffractometer, using a mono-chromotized Cu K $\alpha$  radiation ( $\lambda$ = 1.5418 Å) at 25 kV and 0.4 mA. XRD data was collected in the range of 20° < 2 $\Theta$  < 90° diffraction angle. Surface area measurement is carried out via a Quantachrome instrument NOVA e-Series 2000 model. Brunauer-Emmett-Teller(BET) method was used to measure the specific surface area(SSA), N<sub>2</sub> gas adsorption/desorption isotherm was obtained at 77K.

## 2.3 Results and Discussion

### 2.3.1 CNT carpets on ideal carbon surface

In order to study more details of the CNT growth on the carbon substrate, ideal flat carbon support highly oriented pyrolytic graphite (HOPG) were utilized. Earlier investigators in this team [149] have performed systematic studies on HOPG to understand the influence of the growth parameters, such as buffer layer thickness reactor conditions and growth time. It was reported that, on ideal flat surface having optimal buffer layer thickness and deposition conditions, CNT carpet height increased linearly with the deposition time of CVD, at about a rate of 1.66  $\mu\text{m}/\text{min}$ . Figure 2.3 shows an image of CNT carpet on HOPG substrate after 60 minutes of CVD deposition at 720 Celsius.

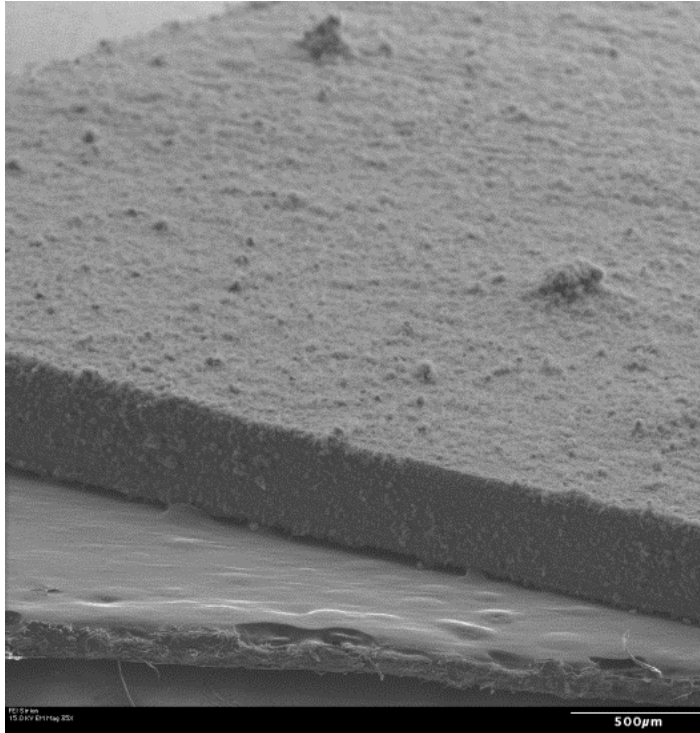


**Figure 2. 3 CNT carpet on ideal carbon(HOPG) surface [149]**

In this study, the influence of surface roughness was investigated by using the same parameters to deposit CNT growth layers on HOPG surfaces that were intentionally roughened using abrasive polish. Standard abrasive sandpapers, with grits conforming to ANSI B74.12-2018 specifications, were used and their corresponding estimated root mean square roughness (RMS) values were used as reference. Before polishing, pristine HOPG substrates were determined to have a RMS roughness values of 4.17 nm as measured by atomic force microscope (AFM). However, the sandpaper polished samples could not be measured by AFM directly, since the finish roughness is beyond the detection limit of AFM. Therefore, the estimated roughness related to each commercial sandpaper grits has been plotted in the data [150].

Figure 2.4 shows the SEM images of CNT carpet on HOPG samples as a function of roughness. All ANSI grit sizes was converted into surface roughness-root mean square (RMS) values according to their published data.

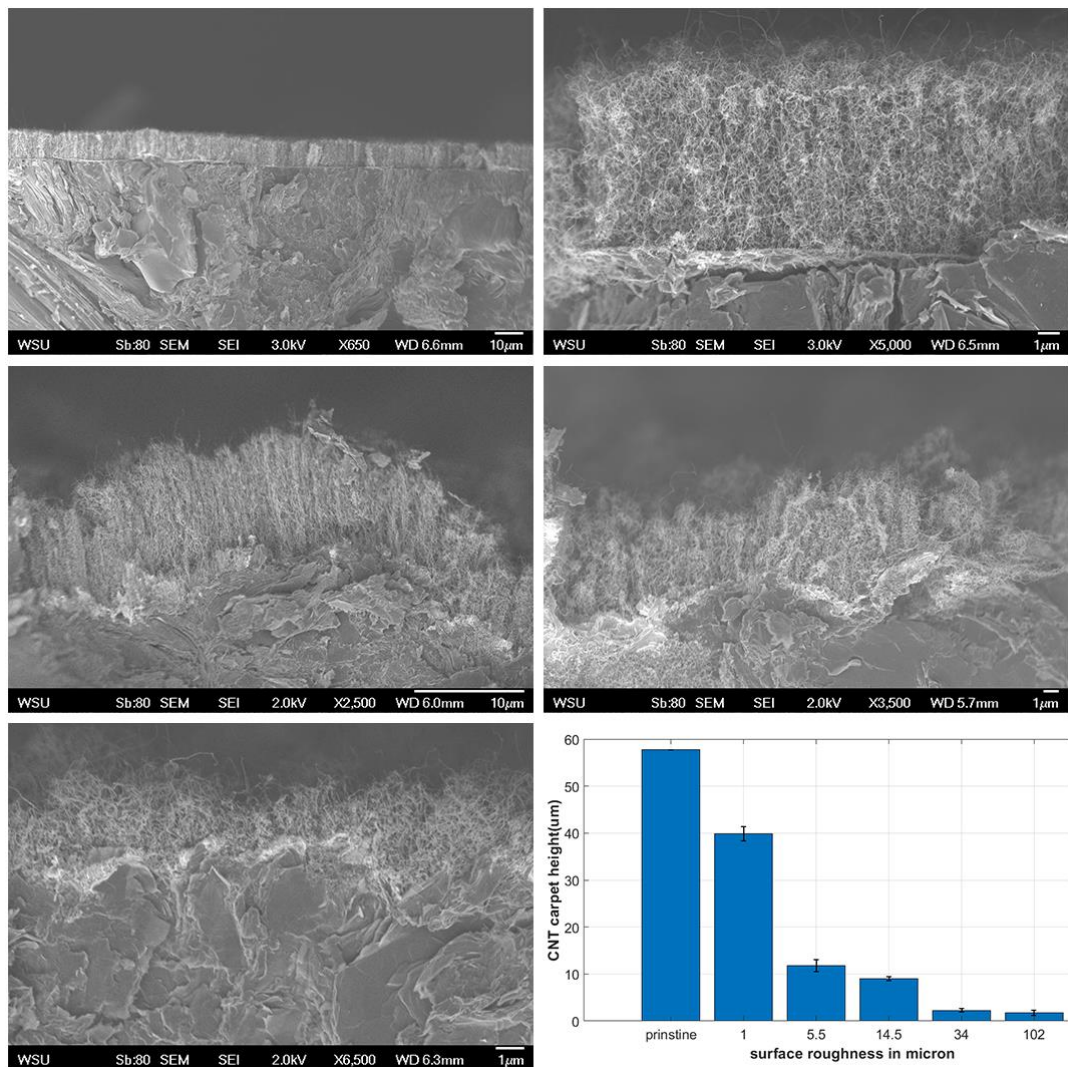


**Figure 2. 4 a-e SEM image of multiwall carbon nanotubes grown on graphite sample with different surface roughness. (a) pristine graphite sample with a zoomed-out view of aligned CNTs on smooth surface, (b-e) CNTs on graphite sample surface with 1, 5.5, 14.5, 34 micron finish, respectively, (f) histogram plot of carbon nanotube carpet height as the surface roughness varies**

It can be clearly seen that the sample surface with higher roughness tends to have shorter CNTs, and the alignment of the CNTs is reduced with roughness. This is not unexpected, since buffer layers follow the substrate contour, and individual nanotubes are expected to grow normal to the surface at each point. Therefore, CNT strands growing on rough surfaces are not exactly parallel, and may be hindering each other's growth during formation.

These results indicate that while rough and uneven surfaces do support healthy and robust CNT carpet growth, their alignment and carpet lengths will depend upon the substrate morphology, and hence there is need for substrate-specific investigation for different applications. The uneven surface for our study is more complex: it consists of porous weaved microfiber cloth, an CAD illustration of the fiber cloth is shown in Figure 2.5. Resulting morphology of CNT carpet on these substrates are shown in next section, and compared with earlier studies on carbon foam.

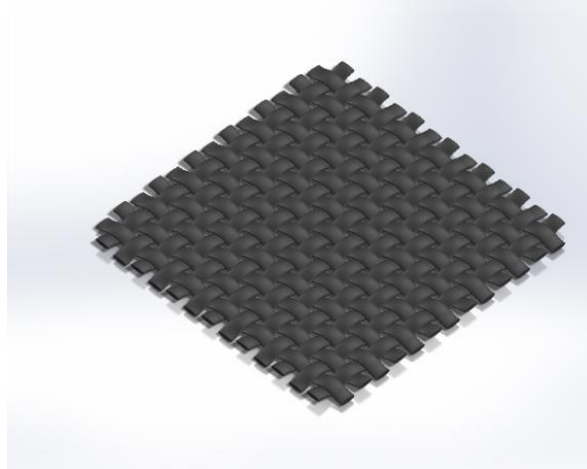


**Figure 2. 5 CAD representation and optic image of carbon fiber cloth**

### **2.3.3 Surface morphology of CNT carpet on carbon fiber cloth**

Fig 2.6 shows electron microscopy images of carbon fiber fabric before and after CNT growth. It is observed each fiber of the carbon cloth, which is smooth to begin with, shown in 2.6a, gets coated with carbon nanotube arrays, which can eventually overlap and entangle with arrays of adjoining fibers (Fig 2.6b). Since the entire cylindrical surface of carbon fibers are coated with a dense fuzzy layer of CNTs, the interface between the individual CNT and fiber substrate cannot be seen in SEM images., Figure 2.6-c, d, shows that aligned CNTs on two individual fibers get entangled and can be stretched as they are mechanically pulled apart. 2.6e shows the grown CNTs have a uniform size and shape, detailed analysis of the CNTs on CFC are in the following section.

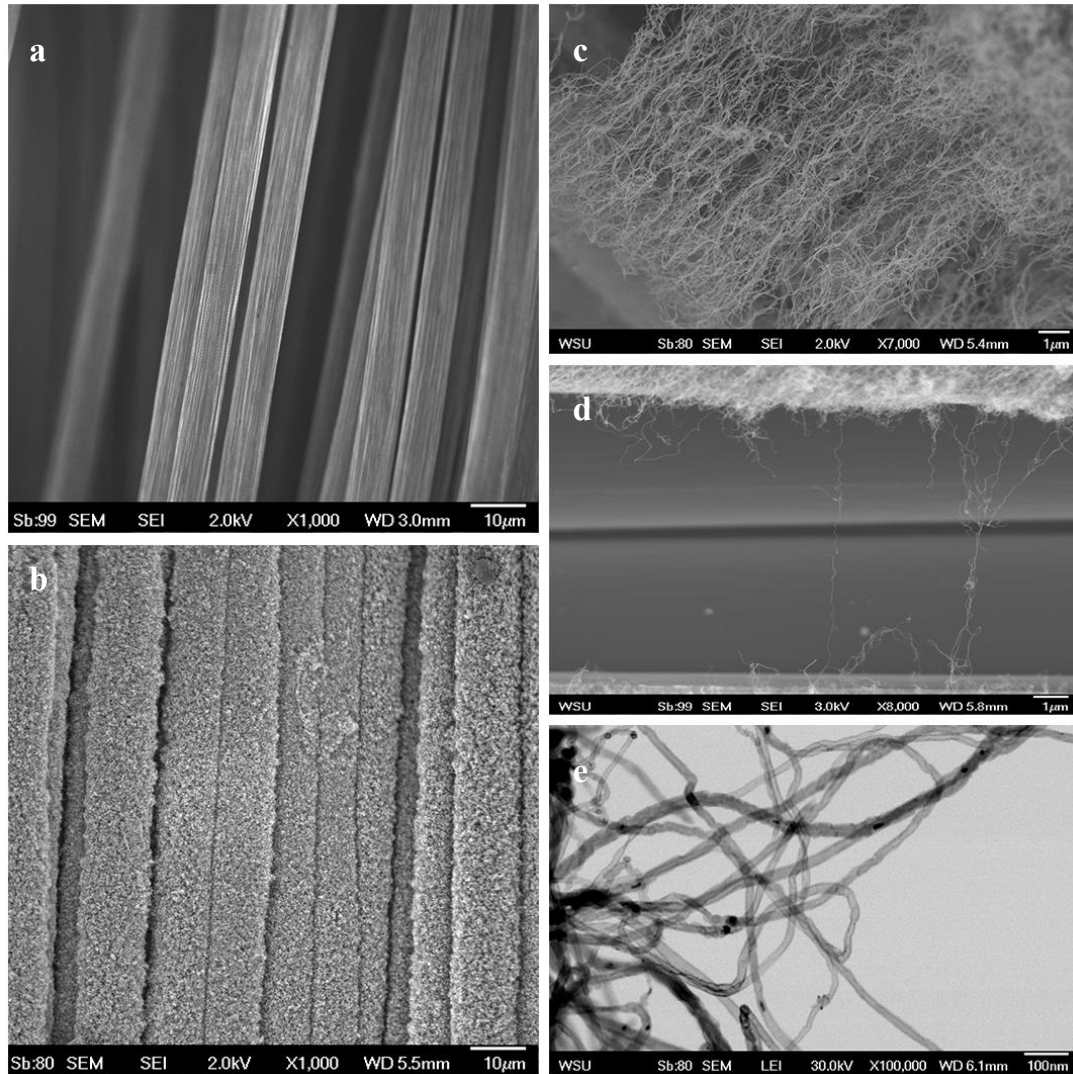


**Figure 2. 6 SEM images of the carbon fiber cloth. (a) As received carbon fiber cloth, (b) CNT grafted CFC at low magnification, (c,d) entangled CNTs on two carbon fiber while mechanical separation applied. (e) CNT details from transmission mode image showing the carbon nanotubes are multiwalled CNT with heavy entanglement.**

### **2.3.4 Analysis and comparison of CNT carpet morphology on different substrates.**

One important property of CNT carpets that will be useful for all future applications is the dimension of the individual CNT in each strand. Whereas the overall length of the CNT carpet can easily be tuned with CVD growth time, it is important to understand their inner and outer diameters, which determines the number of graphene layers in each cylinder, the weight, density, surface area, and related engineering properties. It is also important to understand if and how these features may change from one geometry to another.

The first question to address is how the CNT diameters may depend on substrate geometry. Fig. 2.7 shows a histogram of measured CNT diameters on carbon fiber cloth, indicating both inner and outer diameters. In these samples, the mean inner diameter is  $9.9 (\pm 0.76)$ , mean outer diameter was about  $22.4 (\pm 1.84)$  nm, respectively. This result can be compared with those reported on ideal flat surface, HOPG graphite and Reticulated Vitreous Carbon foams (RVC) investigated by Quinton et al [149] and Vijwani et al [151] in previous studies, included in Table 2.1.

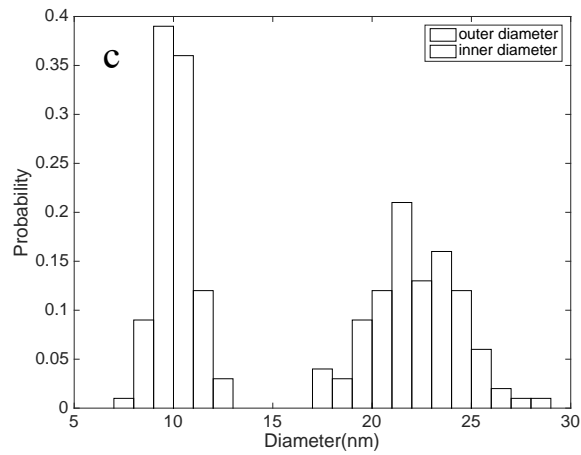
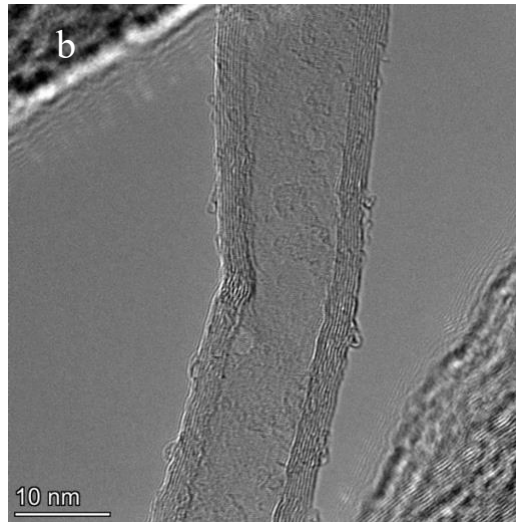
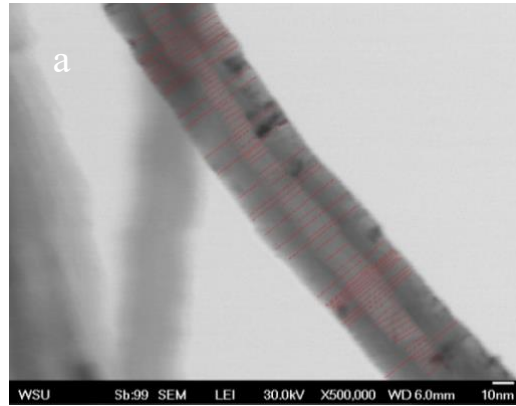


**Figure 2. 7 a) Transmission mode SEM images of CNT on fiber cloth and b) TEM image of multiwalled CNT (c)CNT diameter distribution for inner and outer wall**

**Table 2. 1 CNT inner and outer diameter comparisons based on different substrate.**

<b>sample</b>	<b>inner diameter (nm)</b>	<b>outer diameter (nm)</b>
CNT on graphite [149]	10	19
CNT on RVC [151]	$9 \pm 1.35$	$18 \pm 2.2$
CNT on CFC	$10 \pm 0.76$	$22 \pm 1.84$

From the table 2.1 above, we can see the CNT on different substrates show the similar average inner diameter, but outer diameter may have more substrate to substrate variation. More notably, the carbon fiber cloth shows slightly thicker CNT strands on average. This is most probably controlled by the catalyst size, i.e, the size of metal nanocatalyst that gets stabilized on the substrate. In the floating catalyst thermal CVD process used here, catalyst particles are continuously being deposited on substrates, and are growing by either agglomeration with nearby particles, or by absorbing the incoming catalyst-containing precursor (Ferrocene) [151]. It is possible both phenomenon happen simultaneously. Compared to the ideal flat surface of HOPG, the curved surface of the of the individual carbon fibers , as well as the grooves caused by weaving of the fiber into cloth, can increase the possibility of catalysts that are anchored on the surface, and have more chance to build up and agglomerate into larger nanocatalysts before nucleating nanotubes. On the other hand, the highly porous RVC foam create more open channels for CVD precursors to permeate the inner surfaces, which offers less possibility of excessive iron trapping and nanocatalyst agglomeration. This may lead to the smaller catalyst particle size therefore thinner CNTs.

Next important question to answer is, would the CNT diameters change with deposition time for given growth conditions, i.e, would the average diameter of

CNT carpets change with deposition time, as the CNT strands grow in length and entangle, perhaps offering newer type of nucleation/growth sites. To address these, detailed measurements of average CNT thickness were performed as a function of CVD deposition time, as shown in Fig.2.8, Less than 10% diameter variation was observed from samples with different CNT growth time, it is clearly indicated from these measurements that the average CNT diameter does not vary with CNT growth time. It must be noted that, since this is a statistical average of large forest of nanotubes, atomistic variations at local nucleation sites may be missed. What this study shows is that no visible significant changes that will be relevant for engineering applications could be detected at the microstructure scale.

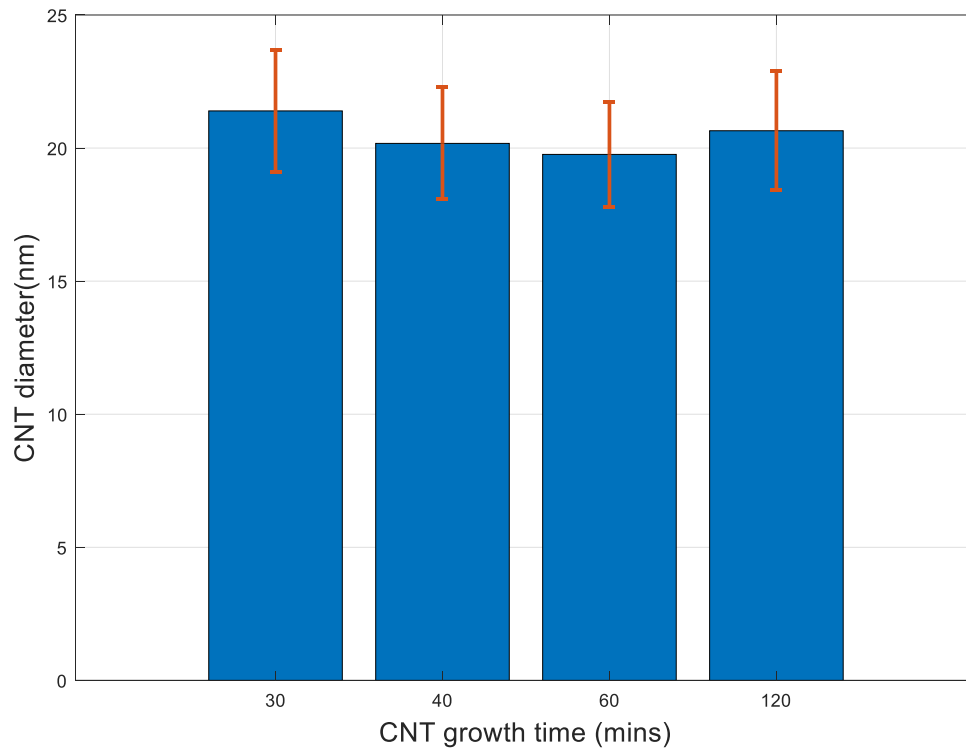


**Figure 2. 8 CNT diameter variation as a function of time, showing no significant difference can be observed up to 2 hours production time.**

## 2.3.5 Surface chemistry of CNT carpet

### 2.3.5.1 Surface chemistry study of CNT carpet on Fiber cloth

The X-ray Photoelectron Spectroscopy (XPS) analysis on the pristine CFC and CNTCFC hybrid material is shown in Figure 2.9. 2.9a, 2.9c represents the survey scans of the material, it can be observed pristine CFC has main surface composition comprised of carbon and oxygen, while CNTCFC sample is purely carbon based. Fine scans give more details of the carbon composition. 2.9b. The deconvolution of C 1s spectrum shows a main component at 284.5 eV, which is attributed to the graphitic hexagonal carbon bonding (C-C  $sp^2$  hybridization), the peak at 286.3 eV is assigned to the C-O bonding, and the  $\pi-\pi^*$  peak is located at 291.3 eV. In contrast, the deconvolution of XPS C 1s spectra of CNTCFC hybrid material is very different, seen from 2.9d. Likewise, main peak of aromatic carbon bonding (C-C  $sp^2$ ) from the hexagonal walls of CNTs. The peak at 285.3 eV is referred to the C-CH  $sp^3$  hybridization, it is because of the defects in the hexagonal structure. Broad satellite peak at 291 eV is attributed to the  $\pi-\pi^*$ . There is significant evidence showing that the high resolution and narrow C 1s peak of CNTCFC hybrid material gives pure graphitic carbon, also, the higher degree of

*sp*<sup>2</sup> contribution will inevitably considered with better conductivity compared with the pristine CFC.

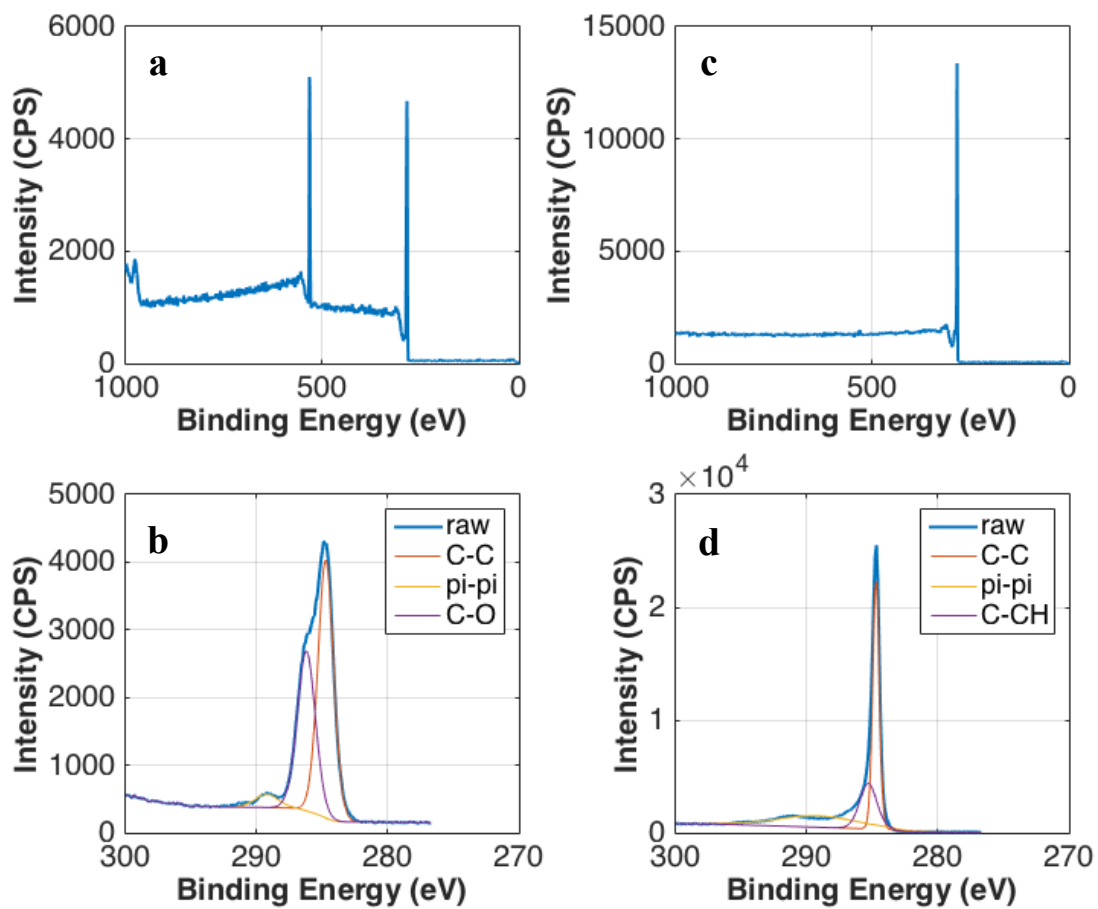


**Figure 2. 9 XPS spectra regarding a) carbon fiber cloth survey scan, b) CFC carbon peak fine scan, c) CNTCFC survey scan, d) CNTCFC carbon peak fine scan**

### 2.3.5.2 X-ray Diffraction for crystal structure

Structural investigation was performed using X-Ray Diffraction (XRD). Figure 2.10, the blue line shows the XRD pattern for as-received carbon fiber cloth, indicating that it has two major peaks at  $2\theta$  values of 7 and 26, where the prominent peak at  $26^\circ$  corresponds to (0 0 2) plane, a characteristic peak of hexagonal structure of graphitic carbon. Both peaks at 5.5 and 26 are producing broad diffracted peaks, which is due to the lower crystalline quality. In Fig. 2.10, red line represents the CNTCFC hybrid material. The intensity of (0 0 2) plane, which represents layered graphitic carbon structure is increased, and sharper. This proves the increase of crystallinity. Same time, the large broad peak at  $2\theta$  values of 5.5 disappears, due to the more ordered structure and disappearance of amorphous carbon, same time, the peaks at  $42^\circ$ ,  $50^\circ$  both corresponds to the graphitic structure of carbon, there is significant evidence showing the crystal structure of the material surface has changed and become graphitic, which is from CNT.

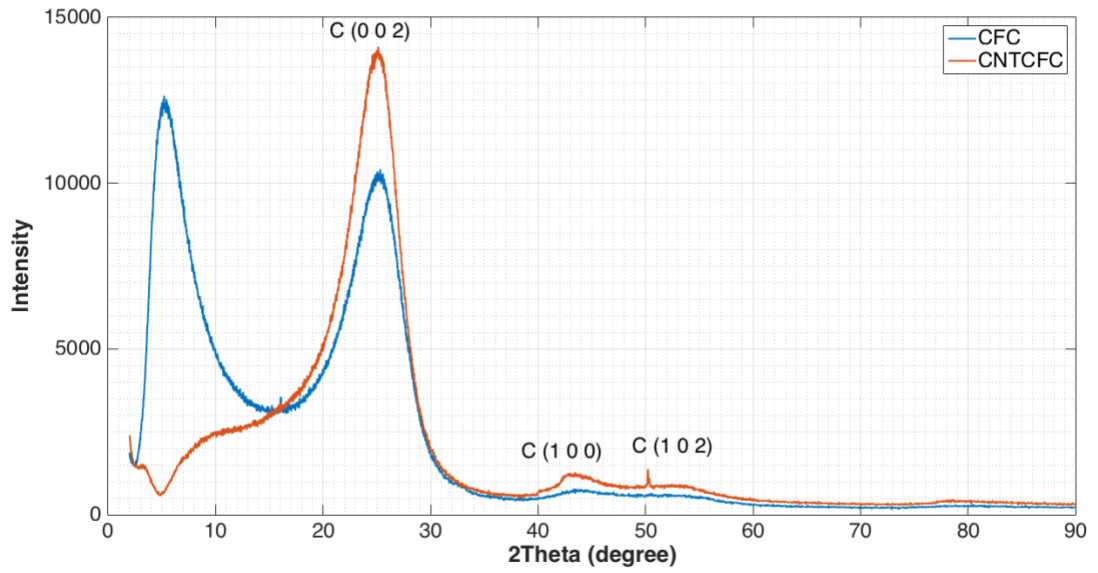


**Figure 2. 10 XRD pattern of carbon fiber cloth and CNT-CFC hybrid material**

### **2.3.6 Surface area estimates of CNT-carpet enhanced solids:**

The specific surface area of the nanotube carpets has been estimated using the microstructural information of CNT morphology. The idea is to understand under what conditions this estimate would correlate with gas adsorption on the surface. This part of the study has been focused on carbon fiber fabric, with the idea of exploring their potential as flexible surface-active devices.

It must be noted that there are several steps involving plasma and thermal treatments during carbon nanotube carpet growth, and each step may inherently include some weight change before CNTs are actually formed. Therefore, in order to accurately measure the weight gain caused by CNT growth, the weight loss of original substrate caused by each step without CNT growth is carefully measured by simulating the entire process under identical conditions, without the chemical precursor for CNT growth. Fig. 2.11 shows the normalized weight change of the carbon fiber fabric substrate due to each step, without the CNT precursors.

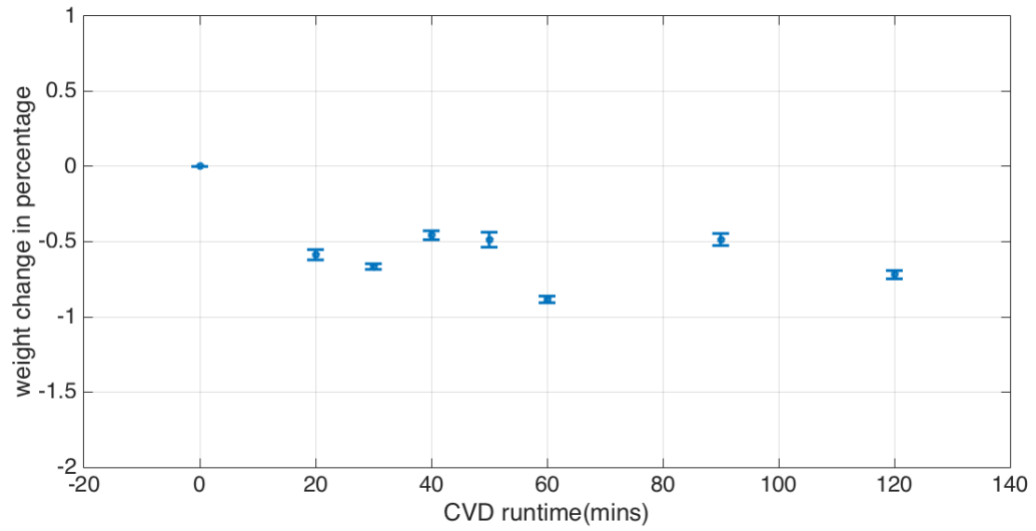


**Figure 2. 11 Carbon fiber cloth weight change according to heat treatment time w/o xylene**

It is obvious that plasma coating and the heat treatment will cause the sample weight loss, before the CNT growth leads to weight increase. It can be seen that, the carbon fiber cloth samples experience a 1% weight loss after both plasma treatment and the heat treatment. This correction is then applied to the original weight of the substrate before estimating the weight gain due to CNT grafting.

Figure 2.12 shows the net weight change of the substrate from each step including during these processes.

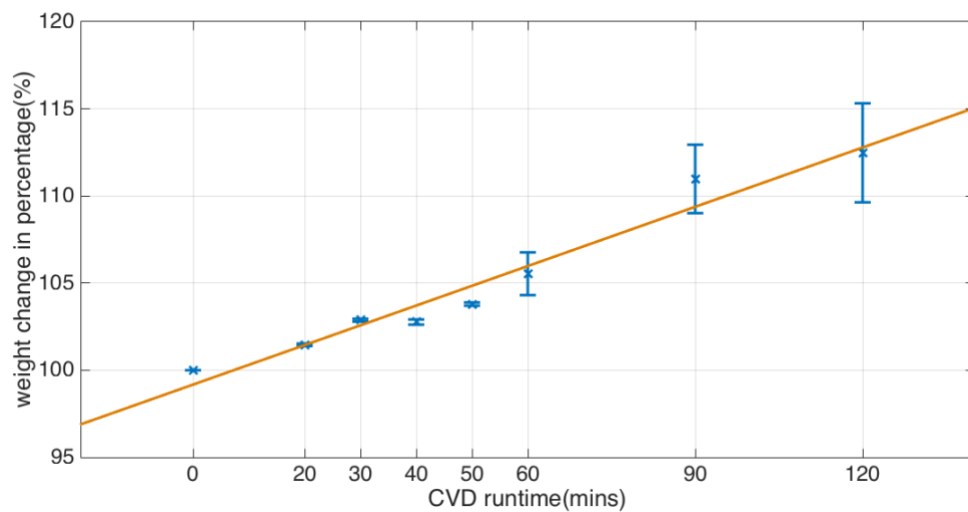


**Figure 2. 12 Carbon fiber cloth weight change as a function of thermal CVD runtime**

The corrected weight change is then calculated using following equation,

$$\text{weight change\%} = \text{basevalue} + \frac{m_{CNT-CFC} - m_{CFC}}{m_{CFC}} \quad (1)$$

where,  $m_{CNT-CFC}$ ,  $m_{CFC}$  represent CNT grafted CFC and untreated CFC mass

The base value is the weight loss correction due to thermal and plasma treatments. The corrected weight change as a function of thermal CVD runtime is plotted and shown in Fig 2.16, and it can be seen that the weight increase follows a linear pattern as the thermal CVD runtime increases.

In order to convert weight gain into total surface area of nanotubes created, mass density of CNT needs to be estimated. This is obtained from the mass density analysis of MWCNT reported in the literature [147] that takes into account the outer and inner diameters of CNT, or the number of graphene walls in each nanotube. The outer and inner diameters for these samples were obtained using SEM/STEM images. In MWCNT in general, the inter-wall distance,  $d_i$  is approximately 0.34 nm, measurement from TEM (Fig2.7b) matches as reported by Ajayan et al [148]. Therefore, the average number of nanotube walls ( $n$ ) in MWCNT can be given by equation 2. The mass density of MWCNT ( $\rho_{CNT}$ ) is obtained by applying the SEM data from our samples to equation 3 below, which is used here to relate nanotube density to its diameter and number of walls.

$$n = \frac{D_o - D_i}{2 * d_i} + 1 \text{ ---- (2)}$$

$$\rho_{MW} = \frac{4000}{1315} \left[ \frac{n}{D_o} - \frac{d_i * n(n-1)}{D_o^2} \right] \text{ ---- (3)}$$

Here,  $D_i$  and  $D_o$  are inner and outer diameters of MWCNT,  $d_i$  is inter-wall spacing,  $n$  is number of walls in MWCNT, and  $\rho_{CNT}$  is the mass density of MWCNT. Some of these values are tabulated in. In the mathematical calculation of the CNT SSA on the substrate, several assumptions are kept: 1) all carbon nanotubes are treated as a single carbon nanotube with the same diameter, which in our SEM observation is 22.4 nm. 2) area density of CNT arrays is homogeneous throughout the whole. Related parameters are tabulated in Table 2.2.

**Table 2. 2 Estimated values of CNT morphology obtained using SEM analysis**

<b>Estimated CNT Morphology Values</b>		
<b>Avg. Outer Diameter, <math>D_o</math></b>	22.4	nm
<b>Avg. Inner Diameter, <math>D_i</math></b>	9.9	nm
<b>Avg. Number of walls, n</b>	19	#
<b>Density of MWCNT, <math>\rho_{CNT}</math></b>	1.79	g/cm <sup>3</sup>

Using the above values, the specific surface area (SSA) (m<sup>2</sup>/g) of individual CNT, *i.e.* the surface area to mass ratio of the CNT can be determined by equation 4.

$$SSA_{CNT} = \frac{SA_{CNT}}{m_{CNT}} = \frac{SA_{CNT}}{V_{CNT} * \rho_{CNT}} = \frac{4}{D_o * \rho_{CNT}} \times 10^3 \quad \text{---- (4)}$$

Where,  $M_{CFC-CNT}$  is total mass of CFC-CNT sample after CNT growth,  $M_{CNT}$  mass of CNT (mass difference after CNT growth) grown on CFC sample, and  $SA_{CNT}$ ,  $V_{CNT}$ , and  $m_{CNT}$  is the surface area, volume, and mass of an individual CNT respectively, need to mention  $10^3$  comes from the unit conversion from the calculation, since the resulting SSA is in m<sup>2</sup>/g. The calculated SSA of CNT is 99.8 m<sup>2</sup>/g, this calculated result is furthermore compared with experimental results from BET analysis. The goal of this chapter was to examine if surface area estimates obtained from the two predictive methods compare well with each other, and how they relate to the experimental observation of surface gas adsorption.

The surface area of the whole CNT-CFC hybrid material is made of two parts,  $SSA_{CNT}$  and  $SSA_{CFC}$ , so the total SSA of CFC-CNT hybrid material ( $SSA_{CFC-CNT}$ ) is then given by equation 5

$$x * SSA_{CNT} + (1 - x)SSA_{CFC} = SSA_{CNT-CFC} \quad \text{---- (5)}$$

where  $x$  is the weight percentage of CNT at corresponding growth time, which can be obtained from the weight change of sample.  $SSA_{CNT}$ ,  $SSA_{CFC}$  and  $SSA_{CNT/CFC}$  are specific surface area of carbon nanotube, carbon fiber cloth and CNT grated fiber cloth, respectively. Fig 2.13 is showing the calculated SSA of CNT-CFC based on eq.5, a linear pattern is observed as CNT growth time increase, a 0.1 m<sup>2</sup>/g/min growth rate is extrapolated from the plot.

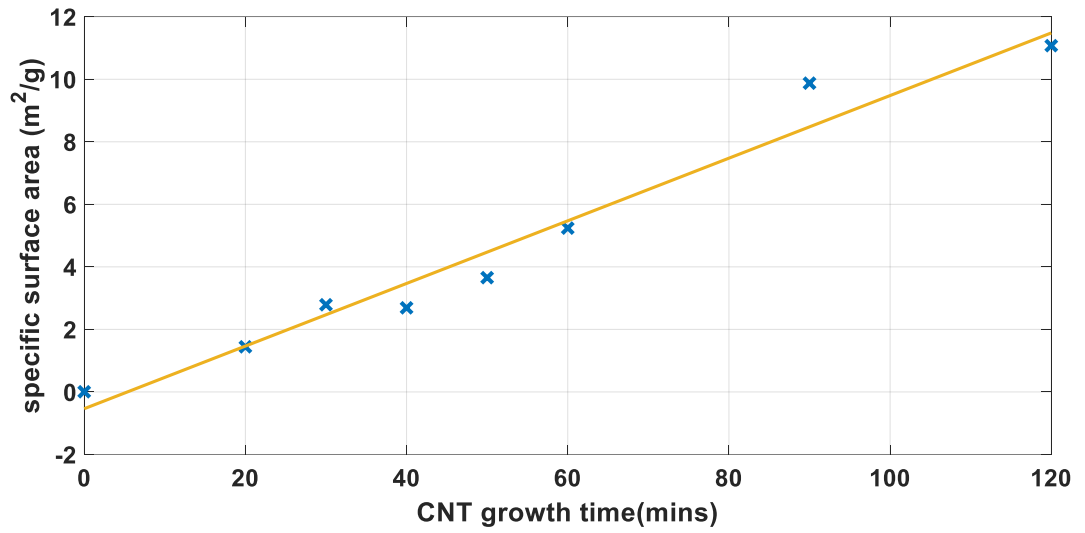
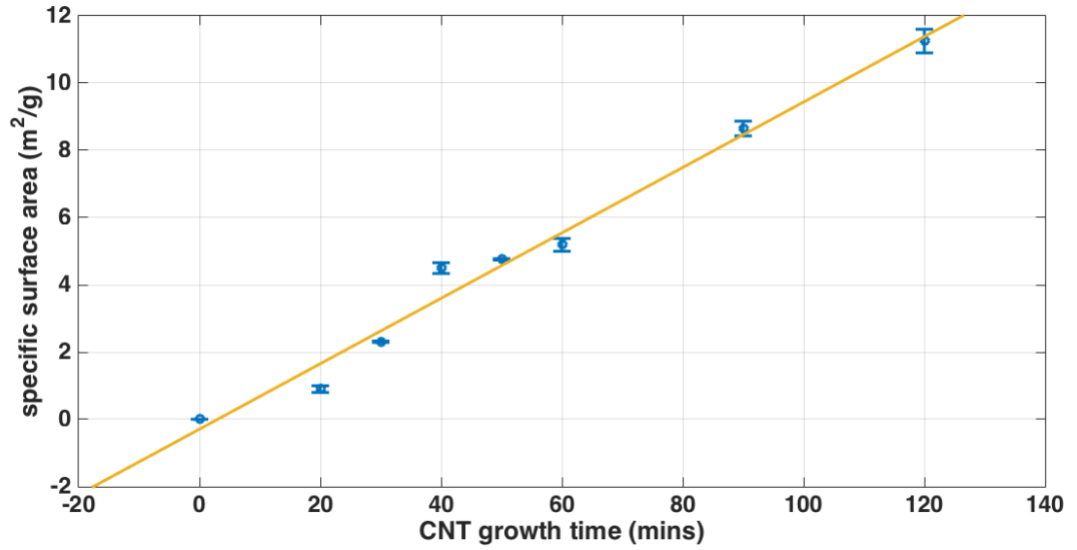


**Figure 2. 13 specific surface area of CNT-CFC hybrid material calculated from the weight gain method**

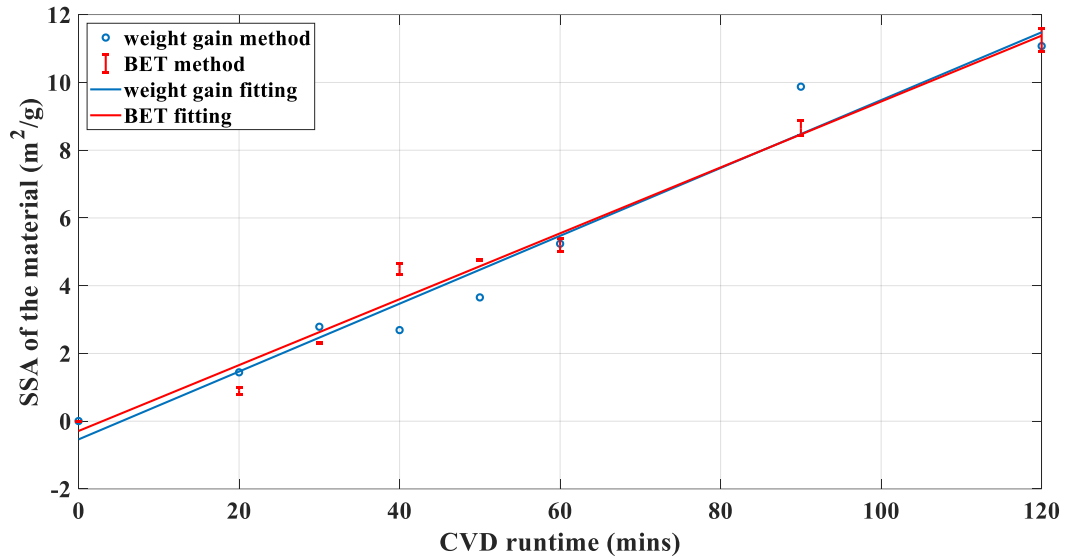
### 2.3.7 Comparison of surface area measurement with gas adsorption

Fig. 2.14 shows the surface measurement via BET method, nitrogen gas adsorption/desorption isotherm used to calculate surface area. The SSA from manufacture is given as 0.006 m<sup>2</sup>/g. It can be seen the surface area increases from 0.006 m<sup>2</sup>/g to 5.19 m<sup>2</sup>/g for the one hour CNT growth time, and up to 11.25 m<sup>2</sup>/g as the CVD runtime increased to 2 hours, which, eventually, is around 2000 times surface area increase. A comparison plots were created in order to shoulder to shoulder compare the material specific surface area change as CNT growth time increases, shown in Fig 2.15. The results showed the despite the SSA of hybrid material from BET analysis is not perfectly matching the with value of SSA from weight gain method. Both approaches have good agreement in SSA increase rate, which is 0.1 m<sup>2</sup>(g\*min)<sup>-1</sup>. During the calculation, couple of major assumptions were made, however the resulting SSA increase rate is close enough to be identical, which can provide significant evidence for future material property estimation.

Since there is a good match of the growth rate observed, conversely, the SSA of CNT(SSA<sub>CNT</sub>) can be calculated by reversing Equation 5, the reason for doing this is to find out the SSA<sub>CNT</sub> from experimental BET test, and find out the trend of the growth. Calculated result is documented in table 2.3



**Figure 2. 14 BET surface area measurement of CNT-CFC hybrid material respect to different CNT growth time**



**Figure 2. 15 SSA of CNTCFC hybrid material comparisons from different measurement/calculation methods**

**Table 2. 3 Surface area of CNT-CFC hybrid material from BET analysis**

<b>CVD runtime(mins)</b>	<b>average SSA(SSA<sub>CNTCFC</sub>)(m<sup>2</sup>/g)</b>	<b>SSA of CNT(SSA<sub>CNT</sub>)(m<sup>2</sup>/g)</b>
0	0.005	0
20	0.9	108.0229
30	2.31	102.3476
<b>40</b>	<b>4.5</b>	<b>130.3869</b>
50	4.76	107.8196
60	5.19	82.58134
90	8.65	71.63675
120	11.25	68.81511

From the table above, the  $SSA_{CNT}$  is kept above 99.8  $m^2/g$ , which reference number calculated from weight gain method, up to 50 mins of growth. Afterwards, the  $SSA_{CNT}$  starts to drop and eventually, plateaus around 70  $m^2/g$ . This can be attributed to the gradual entanglement of the denser and denser CNT forest, and the heavy entanglement will be hindering the gas molecules passing through the hybrid material. Interestingly, one singular point was observed, 40 mins of CVD (in bold in table 2.3), which outputs an above average  $SSA_{CNT}$ , a significant 30% SSA increase was observed. A triplicate test was conducted for data verification, a consistent data was collected. One possible explanation for this phenomenon is, since it is clearly the CNTs studied in this work are hollow structured multiwall carbon nanotubes. Therefore, during the standard BET test, the surface used for  $N_2$  adsorption is not limited on the outer side of CNTs, the inner surface may have gas molecules adsorbed on at the same time. Especially while CNTs are short, CNTs are not closed and its inside surfaces are still useful for maximizing the overall surface area. This assumption can be supported by Quinton et al [19] previous work. The growth mechanism in our process is neither solely tip-growth or bottom-growth, but a mixed growth model. As a result, partially bottom growth CNTs have open ends, which eventually kept the  $SSA_{CNT}$  always above the theoretical calculated value 99.8  $m^2/g$ , and reached a maximum point when CVD

runtime reaches 40 mins. A schematic illustration model was constructed using Avogadro, shown in Fig 2.16.

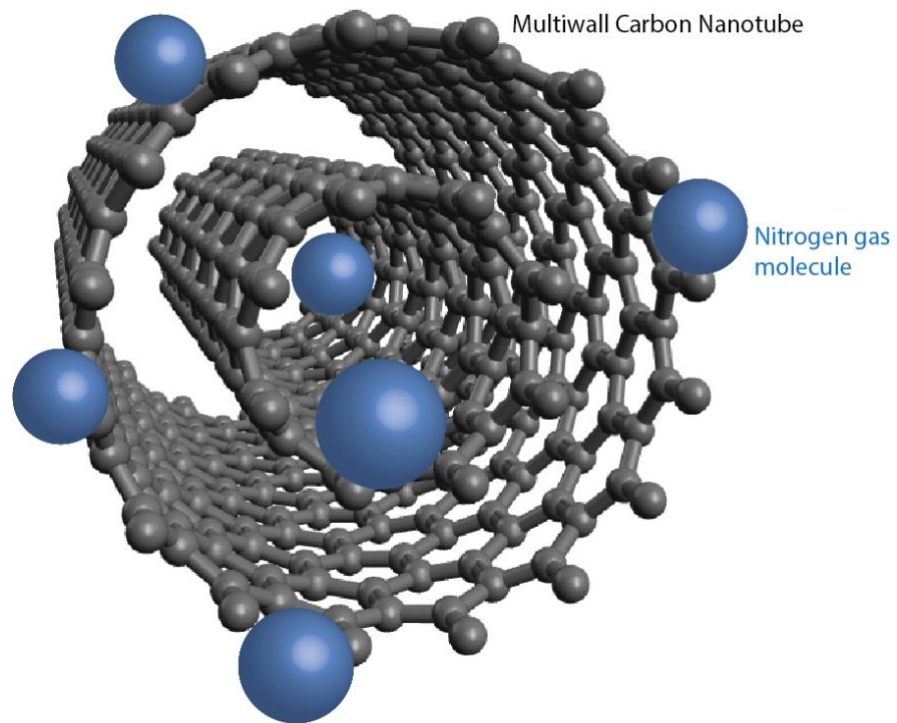


**Figure 2. 16 Illustration of  $N_2$  gas molecules interact with both inner and outer walls of CNT**

## 2.4 Electrical Property measurement

Electrical resistance,  $R$ , depends on geometry of sample as well as material. Assume that  $l$ ,  $A$  and  $\rho$  are the length, cross- section area and resistivity of sample, respectively. Therefore, we can use the equation below:

$$R = \rho l / A \quad (5)$$

As the cross- section, itself, is width ( $w$ ) times thickness ( $t$ ), so:

$$R = \rho l / wt \quad (6)$$

Based on equation 6, electrical resistance versus length to width ratio, would yield resistivity over thickness. In this study, a single sheet of CFC was enhanced with different lengths of CNT carpet, and the resistance of different lengths of sample measured. The thickness of the sample (carbon fiber cloth) can be assumed to be a constant value for all lengths.

Fig 19 below shows the normalized electrical resistance at different CNT growth time, result exhibits electrical resistance for samples having different CNT growing time. For all samples, from raw carbon fibers to 3 hrs CNT growth, electrical resistance linearly changes versus length over width ratio ( $L/W$  ratio). The slopes of curves are directly proportional to resistivity. The electron transport in MWCNTs is believed to be diffusive/ quasi ballistic, in contrast SWCNTs.

Besides, quantum dots may exist in CNTs and because of strong Carbon- Carbon bonds electro-migration can easily occur even in high current densities, thus, the higher density of CNTs, in other words longer growing time, would ease electron transport. Electrical conductivities of CFC specimens of 1, 2 and 3 hours of CNT growth were found to be approximately 580, 850 and 1420 S/Cm, respectively. Based on experiments, electrical conductivity of 3 hours sample was about 15 times greater than the pristine one.

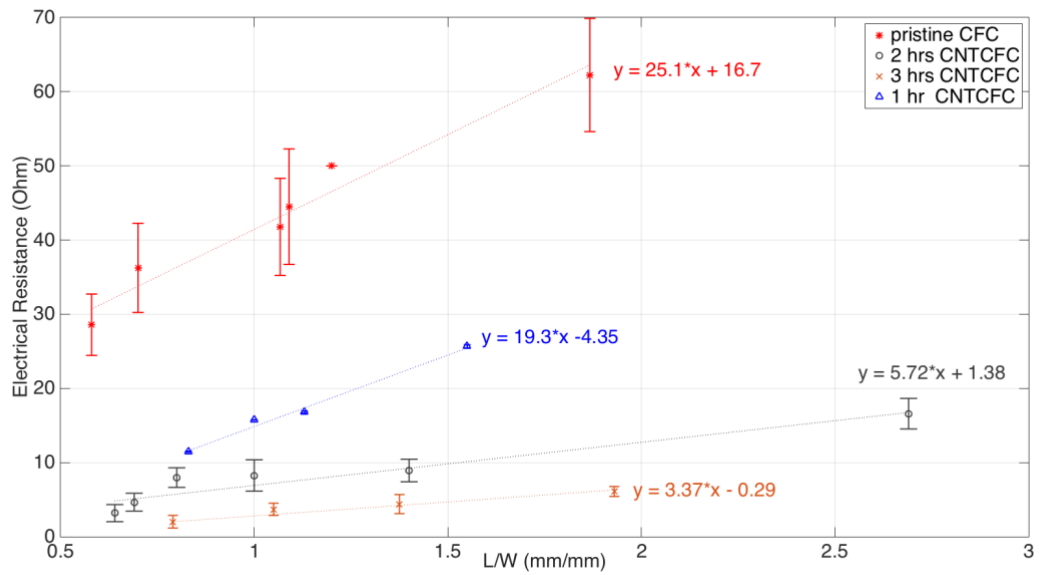


**Figure 2. 17 Electrical Resistance versus length divided by width of CNT/CFC samples for different CNT growth times.**

As predicted, increasing CNT growth time would decrease the electrical resistance. Longer CNT growing time bears longer CNTs and interlinking of CNT strands, meaning more available transport paths for electrons. Fig 20 shows conductivity values as a function of CNT growth time for samples with different CNT growth time. eight groups of samples. The electrical conductivity linearly increases with CNTs growing time. The calculated conductivity shows 15 times increase, from raw CFCs, 95 S/cm, to 1488 of the 3 hours CNTCFC sample. These increases can be justified in two probable ways. Longer growing time, would bear more condensed structure, and thus; intertube spacing will be smaller. Moreover, in a longer growth time it is, the lengths of CNTs would linearly increase, consequently results in a linear increase in conductivity. On the other hand, larger bundles of CNT (or CNT forest) could be developed which could create greater contact area enhancing conductance. In addition, higher growth time, amorphous carbon, which causes degradation in conductivity, would have less chance to stand and might be eliminated and turned into crystalline phases which possess greater electrical conductance.

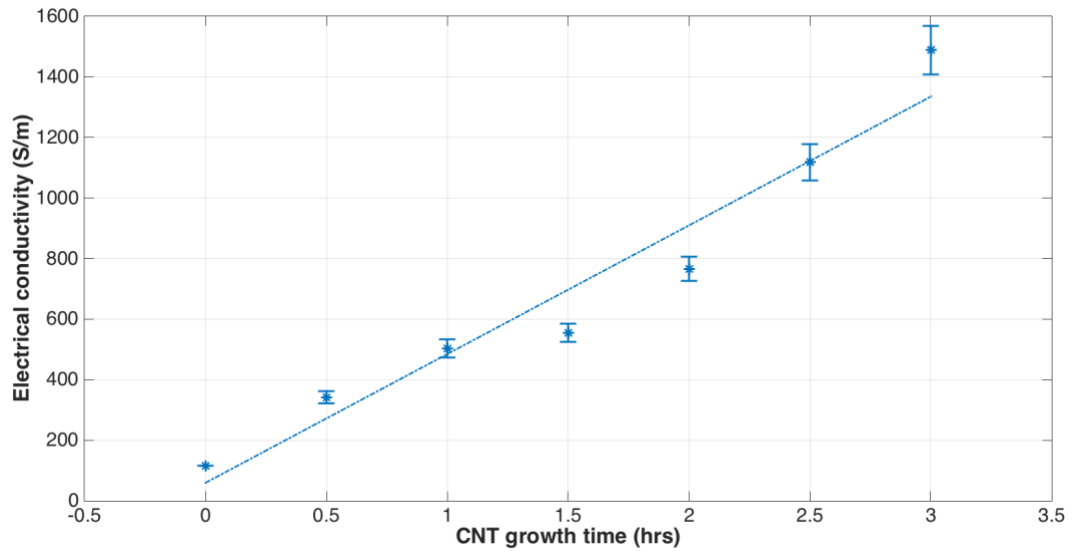


**Figure 2. 18 Conductivity of CNT/CFC samples versus CNTs growing time**

## 2.5 Conclusions

This chapter investigates the multi-scale structural and functional aspects of porous three-dimensional carbon solids, consisting of flexible carbon cloth that are enriched with carpet-like arrays of covalently bonded carbon nanotubes (CNT). Earlier publications have demonstrated that CNT carpet enhancement of solids show promise in enhancing surface activity of porous materials. This study provides in-depth analysis of the multi-scale morphology aspects of such solids, with emphasis on processing-structure-property relationships relevant to surface-applications in different service conditions. Model porous substrate –flexible woven fabric sheet, has been investigated. Its surfaces is enriched with carpet-like arrays of carbon nanotubes using a two-step technique: The first step involves creating a surface buffer layer using microwave plasma deposition. This is followed by floating catalyst chemical vapor deposition. In-depth characterization has been performed using Field Emission- Scanning Electron Microscope (FE-SEM), X-ray diffraction (XRD) and x-ray photoelectron spectroscopy (XPS). It is seen that while the process parameters need to be optimized for surface geometry and porosity of the substrate, two variables that have maximum impact, and can be used for tuning CNT carpet morphology are the thickness of the oxide buffer layer, and CVD deposition times.

For the model sample investigated, increase in surface area caused by attachment of cylindrical nanotubes was estimated from detailed microstructural characteristics (diameter, length, spacing etc.) of CNT carpets and correlated well with weight gain measurements. These values were compared with direct gas adsorption surface area measurements using BET analysis in order to understand the availability of surface sites for different service conditions. It is seen that both methods have a good agreement of SSA of the CNT grafted carbon fiber cloth. Last but not least, electrical property measurement was conducted, linear relationship between CNT surface area and conductivity was established, indicating predictable physical properties governing by the SSA of the material, while using this geometry independent two-step CVD method. These studies indicate that novel hierarchical porous structures with tailorable surface morphologies can be created for unique surface properties related to adsorption, catalysis, electrical, thermal and electrochemical activities.

## Chapter 3: Surface Wettability Conversion of Hierarchical Carbon Supports

### 3.1 Introduction

Many material processing techniques such as joining, solidification, and composite processing [152] involve multi-phase phase interactions. This is also important for surface related properties such as catalysis, sensing, corrosion, surface reaction etc...Wetting depends on intermolecular interaction between solid and liquid species when brought together. Wetting degree (wettability) depends on the interfacial energies between different phases. In the previous chapter, the surface area of porous substrates was increased significantly by attaching CNTs, which could enhance the activities due to more available active sites on the material [153]. Furthermore, it is also suggested, and shown in the next chapter, that CNT-grafted porous material could have more catalytic effect in various applications when functionalized with metal nanoparticles, such as Pd, Pt [154, 155]. In these applications, surface wettability plays an important role when the materials interact with solution phases. In this chapter, different material's surface wetting was studied, different surface modifications were applied to samples with different surface morphology (flat, curved, porous). Surface wettability tuning was conducted in order for different materials be applicable at various environment.

Surface energy and chemistry of the CNT grafted support can be controlled by oxidative functionalization via either gas-phase or liquid-phase oxidation. However, common oxidative methods, such as chemical etching or plasma etching, induce significant structural damage to CNT and compromise CNT carpet integrity. [156] Additionally, surface absorbed/adsorbed species do not gift permanent wettability conversion [157] and will easily undergo desorption process while exposed to heat or reducing atmosphere. In some extreme cases, desorption seems to occur even in the dark and vacuum environment [158] which makes it hard to obtain permanent wettability required for certain applications such as contaminated water purification. An alternative approach investigated here is to coat the CNT carpet with a silica layer(film) via a sol-gel method. This non-destructive way is desired for a sensitive substrate.

## 3.2 Experimental

### 3.2.1 Surface silica coating

A thin silica layer is coated on the porous substrate(RVC foam and carbon fiber cloth) via acid catalyzed SOL-GEL method. Chemical used as silica source is Tetraethyl orthosilicate (TEOS).

Solution ratio = ethanol : water : TEOS = 50:50:1

- PH value adjusted into 3, stirred for 1 hour
- Dipping time 1 hour, stir bar removed
- Air dry for 12 hours,
- hot plate dry in air for 12 hours
- Annealed at 500 degree C (CVD furnace used)

Silica coating is checked using EDS to quantitatively measure the silica content change, as well, the surface morphology is observed by using SEM.

### 3.2.2 Preliminary contact angle studies on various geometries

Contact angle is defined as the angle between the tangent of the liquid-gas interface and the tangent to the solid surface at the contact line where all three phases meet, toward the liquid as shown in Figure 3.1. Contact angle is first modeled and formulated by Thomas Young with the interfacial energy of the three-phase system [159], as given in equation (3.1)

$$\gamma_{SG} = \gamma_{SL} + \gamma_{LG} \cos\theta \dots \dots \quad 3.1$$

where  $\gamma_{SG}$  solid-gas interfacial energy;  $\gamma_{SL}$  is solid-liquid interfacial energy;  $\gamma_{LG}$  is liquid-gas interfacial energy;  $\theta$  is apparent contact angle. Young's equation is derived from the equilibrium of surface free energy or vector balance of surface tension. In the point of surface free energy, a water droplet will remain static state when the global surface free energy reaches minimum. Young's equation can also be balanced by balancing the surface tension horizontal components at the three-phase point.

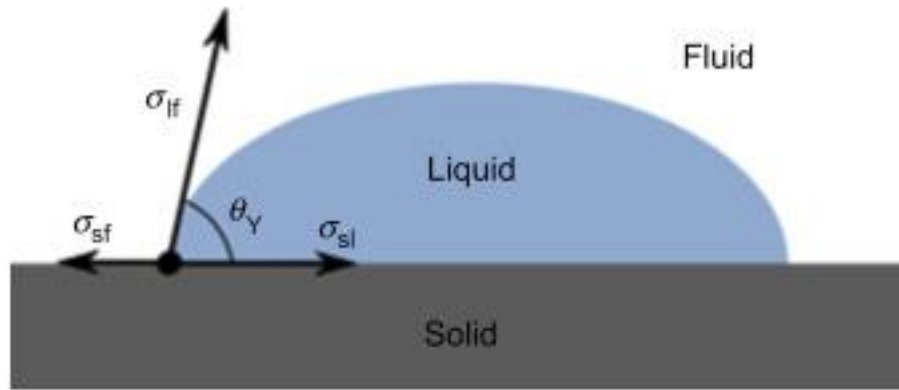


**Figure 3. 1 Measurement of the contact angle of a three-phase system**

We are interested in seeing contact angle vary with different geometry. In this chapter, surfaces studied include curved surface – silicone tube, rigid porous carbon surface – RVC foam and flexible carbon woven fiber cloth. Influence of surface modifications on changes in wettability were also studied. Modification approaches include mechanical abrasive polishing, chemical etching, plasma etching, etc.

A static contact angle was measured by analyzing the liquid droplet on prepared solid surface. Solid Works was used for the data processing. A lab made goniometer was optimized to improve the quality of the pictures. Inspired by the previous work of Lamour *et.al.* [160], similar station was set up, schematic illustration is shown in Fig 3.2. A cardboard with both ends open was covering the sample from the top. One end of the dark box was covered with a translucent paper, which functions as a light diffuser generating a homogeneous background. Pictures with sharper and clearer contour could be taken after adding a diffuser. Each test 5  $\mu$ l of distilled water was pumped and placed gently on the sample surface by a pipette.

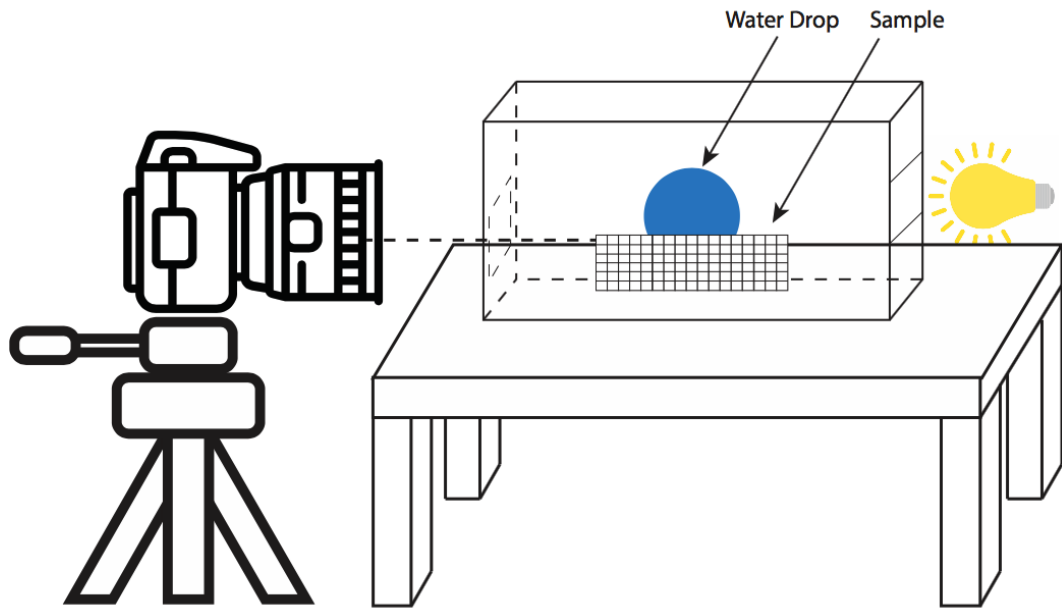


**Figure 3. 2 Schematic representation of goniometer assembly**

### 3.3 Results and Discussion

#### 3.3.1 SOL-GEL silica coating on CNTCFC

Two groups of samples are randomly collected in this analysis, top view SEM images were taken at multiple random locations of two sets of samples. Detailed images are shown in Figure 3.3. From Fig 3.3, it's clearly all CNTs remain undamaged, which was expected since the SOL-GEL is a nondestructive coating method. Silica coated CNTs do look the same as non-coated, however, there is significant evidence showing surface charge build-up (shinning spots), which is attributed to the electric insulating silica layer. Furthermore, there is no significant evidence of overall clumping happens, and the CNT can be seen well distributed in these images, some overlapping is observed. Still, locally, there are some spots showing clump phenomena (circled out in red), some CNT are stick together and the pictures become very cloudy. Therefore, dispersion may become a potential issue for application of the CNT hybrid material, since silica layer is electrically insulating, this may hinder the electrical properties of the material. Additionally, in order to see more details on the silica coating on the fiber cloth sample, elemental analysis was conducted to compare the chemical compositions using EDS, result is shown in Table 3.1.

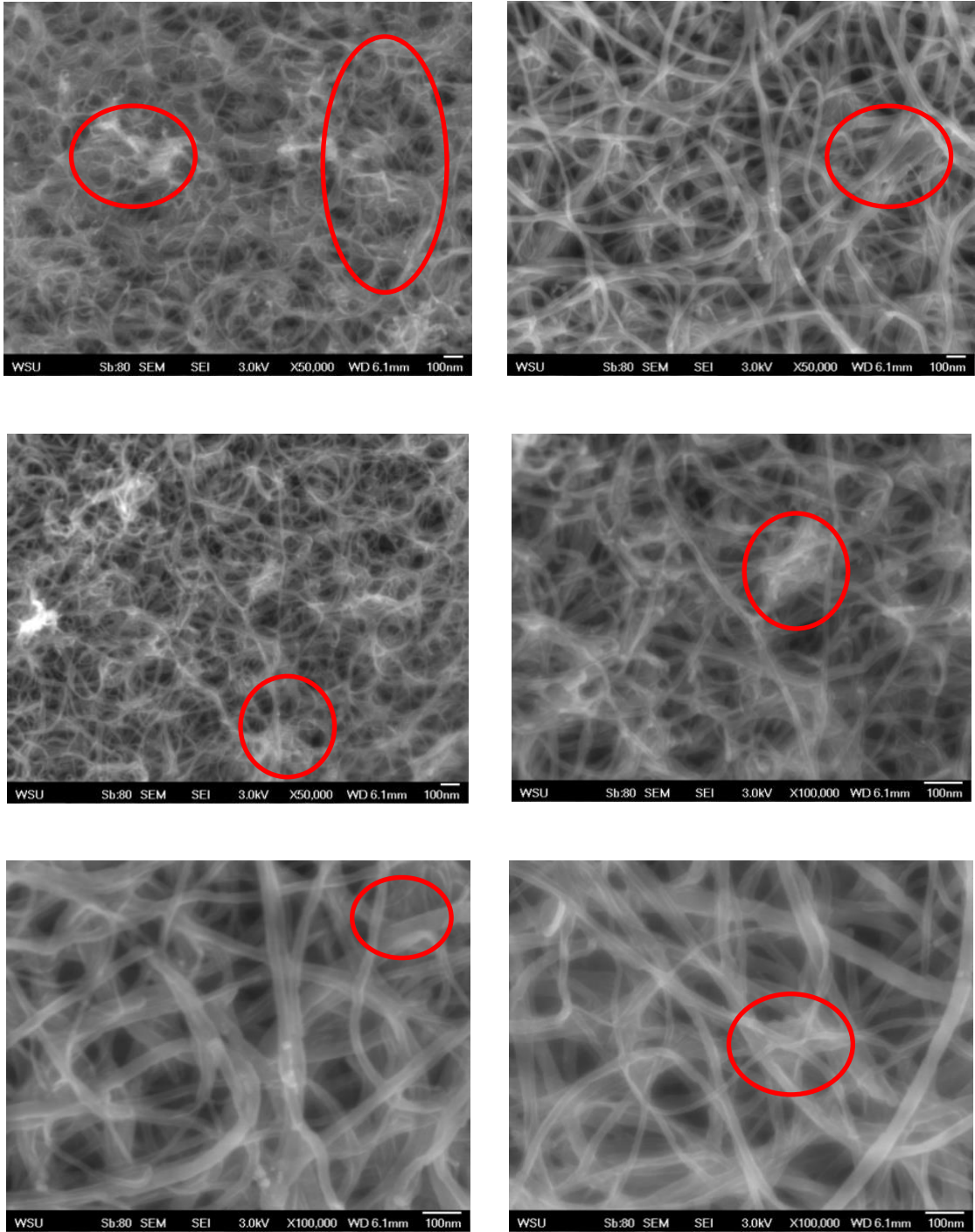


**Figure 3. 3 Microstructure of SOL-GEL silica coated CNT forest**

**Table 3. 1 Elemental analysis of fiber cloth samples**

<b>Sample</b>	<b>Atomic percentage (%)</b>			<b>Weight percentage (%)</b>		
	C K	O K	Si K	C K	O K	Si K
<b>CFC</b>	96.17	3.83	0	94.96	50.4	0
<b>CNT-CFC</b>	97.21	2.28	0.1	94.94	2.97	0.23
<b>TEO-CNT-CFC</b>	91.68	05.05	03.27	86.45	06.35	07.20

Three groups samples were characterized in EDS, in order to compare the elemental change of the sample through each step of surface modification. Table 3.1 tabulated the pristine carbon fiber cloth (CFC), CNT grafted fiber cloth hybrid material (CNT-CFC) and the TEO coated hybrid material (TEO-CNT-CFC). Firstly, for the all group, iron(catalyst) element information was excluded in this analysis since the focus is the influence silica coating. From the table above, there is significant evidence showing trace of silicon with the SOL-GEL silica coating, comparing to the pristine fiber cloth and CNT grafted fabric. Silicon peak from CNTCFC sample is attributed to the plasma coated silica buffer layer ( $\text{SiO}_x$ ), since the buffer layer is at nano scale, very minimum amount was able to be traced from EDS. The SOL-GEL silica coating is proven successful and complete.

### **3.3.2 Initial trial of contact angle test of different surface under different condition**

#### **3.3.2.1 Detailed contact angle measurement on fabric and foam**

A detailed study of contact angle measurement was conducted on two types porous carbon substrate. Carbon fiber cloth (CFC) and Reticulated Vitreous carbon foam (RVC). Both supports have gone through identical surface treatment, including CNT grafting and SOL-GEL silica coating.

From the figure 3.4 and table 3,2 shown below, we can see the carbon fiber holds a hydrophilic surface, after CNT grafting, the surface become hydrophobic, however, if SOL0GEL silica is successfully coated on the CNTCFC surface, the surface wettability will be reverted, which means back to hydrophilic. Quantitative comparison in the table 3.2 shows the surface wettability of the carbon fabric after SOL-GEL coating has almost restored.

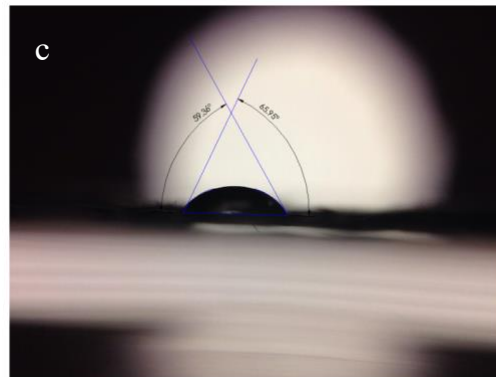
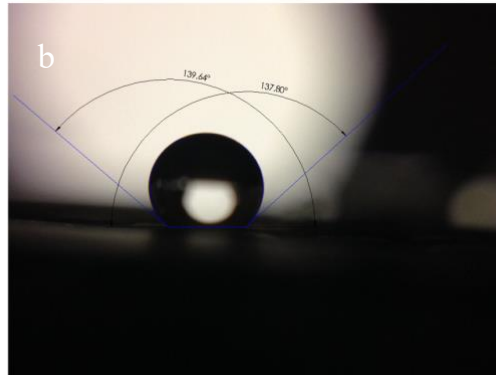
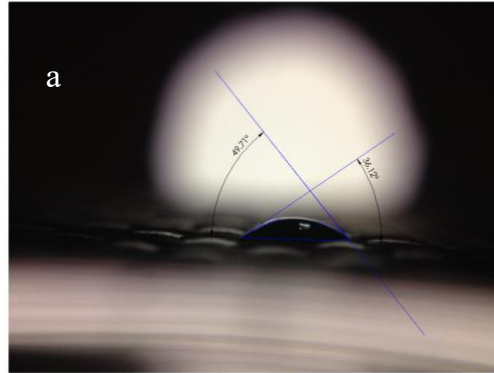


**Figure 3. 4 Contact angle preliminary test based on carbon fiber cloth. a) as received. b) CNT grafted carbon fabric. c) Silica coated on CNT grafted carbon fiber cloth.**

**Table 3. 2 Contact angle of selected carbon fabric surface with surface modification**

<b>Substrate</b>	<b>Average contact angle(°)</b>
Carbon Fiber Cloth (CFC)	39.5
CNT- CFC	141.3
TEO-CNT-CFC	51.7

RVC foam surface contact angle holds a different result, apparently, untreated RVC foam has a hydrophobic surface, after grafted by CNT, the surface become more hydrophobic, which is termed as super hydrophobic, however, if one layer of silica is coated on the CNT grafted fabric surface, the surface wettability will be changed dramatically into hydrophilic. Quantitative results are given as table 3.3, result showing with the CNT grafting, CNTRVC material is able to achieve a super hydrophobic surface. Meanwhile, SOL-GEL silica is able to convert the wettability into completely hydrophilic.

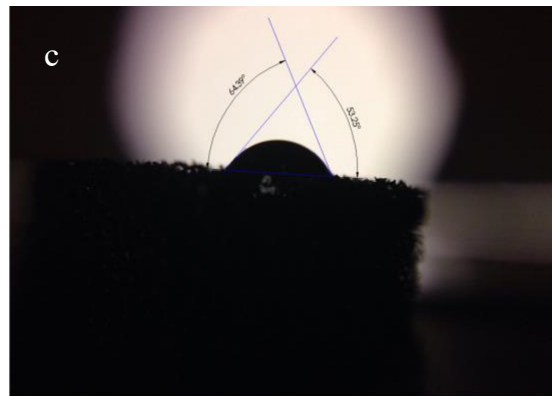
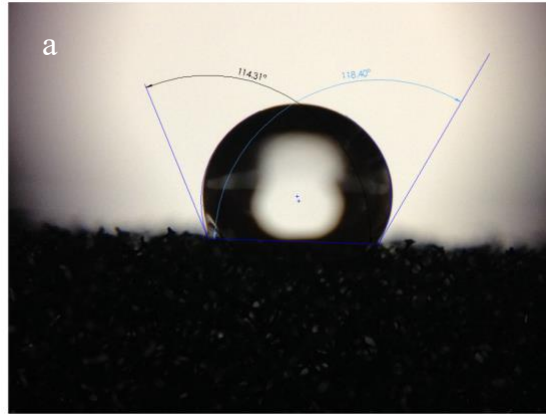


**Figure 3. 5 Contact angle preliminary test on RVC foam. a) as received. b) CNT grafted RVC foam. c) SOL-GEL Silica coated CNTRVC.**

**Table 3. 3 Contact angle of selected RVC foam with surface modification**

<b>Substrate</b>	<b>Average contact angle(°)</b>
Carbon RVC	116.2
CNT+ Carbon RVC	150.4
Silica + CNT+ RVC	58.5

### 3.3.2.2 Preliminary contact angle studies on cylindrical polymer tube

Systematic study of contact angle (CA) tuning was achieved in sections above. Since both porous and flat surface CA were studied in this group, a preliminary surface CA test was conducted. Various surface treatment was conducted on a selected commercial silicone curved surface. All engineering activities were conforming to ASTM E407 for chemical etching and ANSI B74.12-2018 for surface mechanical roughening [161, 162]. Since ASTM E407 is for metal etching, slightly adjustment was made. Sample contact angle measurement is illustrated as in Fig.3.6. Likewise, the true contact angle is an average of left-side and right-side measurement. Various approaches were utilized for different surface finish including both physical and chemical method, which includes peroxide (used as received), hydrochloric acid(10M), ammonia(10M), nitric acid(10M) and silicon carbide sandpapers with different grids from Buehler. All CA measurements were taken in triplicate for data validation. A complete CA summary tabulated in table 3.4 and plotted in Fig 3.7 for comparisons. From the results shown from Fig. 3.7, we can observe the following findings.

First, the untreated silicone tube possesses a hydrophobic surface, which has a contact angle around 95 degrees. By different surface treatment, the surface will become hydrophobic or reverse to hydrophilic, in this case, we can see with 120

grit sand paper grinding, as well as 120 grit sand paper grinding followed by plasma silica oxygen etching, both give the highest contact angle, around 110 degrees. If the surface is treated with chemicals, generally the surface change into hydrophilic, among all, ammonium hydroxide surface etching and ammonium hydroxide followed by silica plasma coating present the lowest contact angle, which is around 60 degrees.

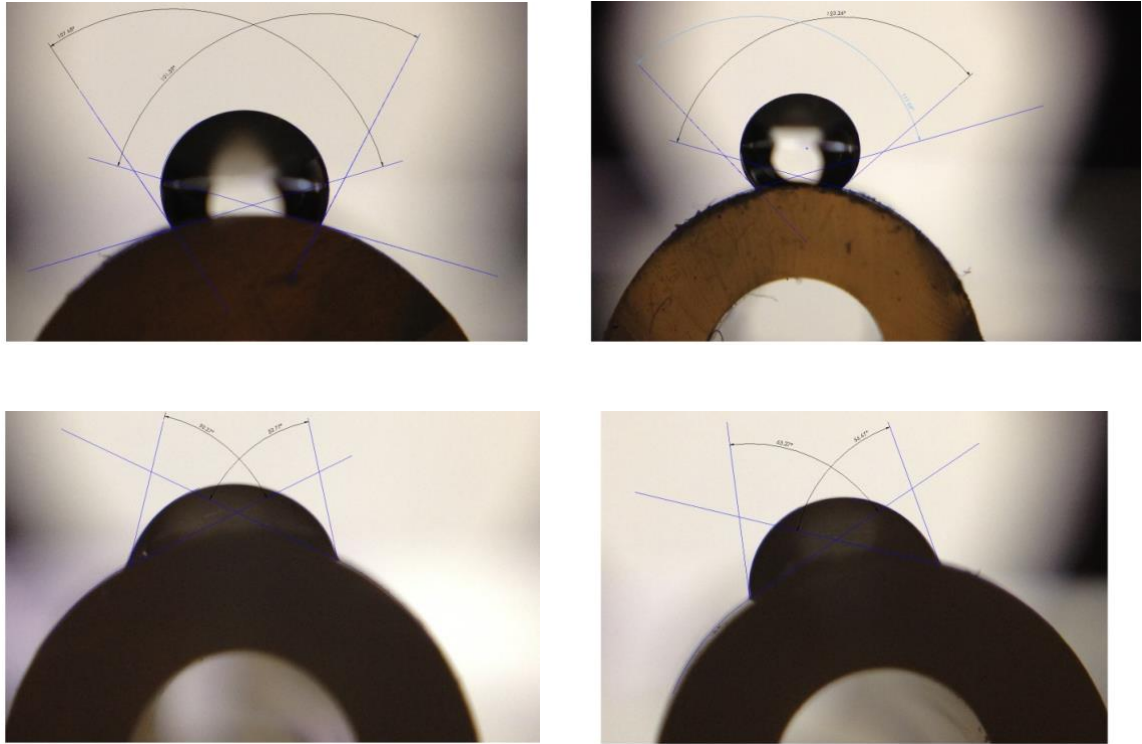


**Figure 3. 6 Selected silicone tube contact angle measurements according to different surface treatment, a) as received b) surface grinded with 120 grit sand paper c) surface etched by peroxide d) surface etched by ammonium hydroxide**

**Table 3. 4 Curved surface contact angle (CA) with different surface treatment**

<b>Samples</b>	<b>Average CA(°)</b>	<b>Standard error(°)</b>
pristine	97.57	7.15
pristine + plasma SiOx	100.30	3.64
pristine + plasma SiOx + plasma O2	81.24	4.35
sandpaper grit 120	108.83	10.02
sandpaper grit 120 + plasma SiOx	102.03	6.53
sandpaper grit 320	108.90	14.91
sandpaper grit 320 + plasma SiOx	97.15	4.69
sandpaper grit 600	97.82	2.16
sandpaper grit 600 + plasma SiOx	88.27	5.72
Peroxide	65.35	5.89
Peroxide + plasma SiOx	58.90	7.79

HCL	85.24	5.78
HCL + plasma SiOx	48.23	7.28
HNO3	95.33	1.29
HNO3 + plasma SiOx	83.86	3.63
Ammonia	93.11	3.48
Ammonia + plasma SiOx	65.06	5.24

### Overall View of Contact Angle

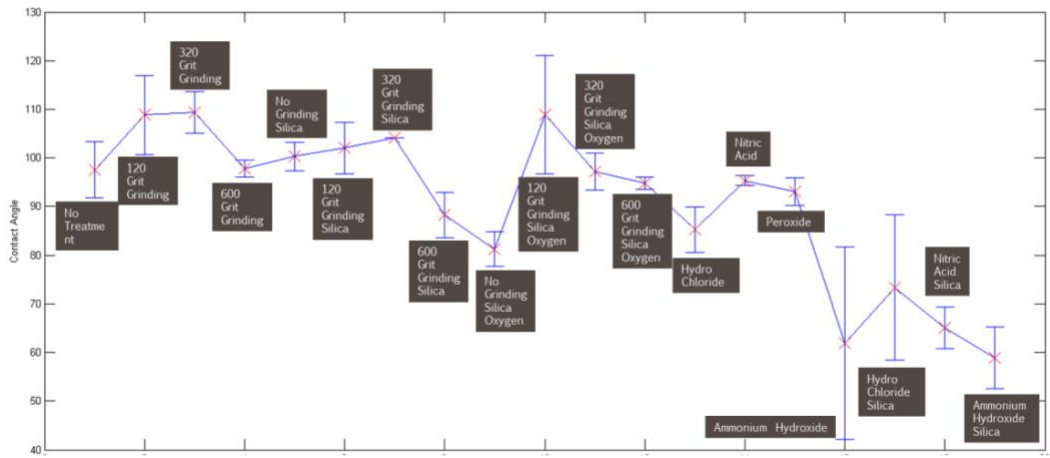


**Figure 3. 7 Contact angle comparison according to different surface treatment**

### 3.4 Conclusion

This chapter focuses on surface wettability of different materials and techniques of modifying that. preliminary studies were performed on a hydrophobic engineering material, where chemical etching with oxidizing liquids converted them to hydrophilic. Detailed studies of contact angle on the hierarchical carbon surfaces were performed. CNT coated surface is presenting a superhydrophobic property, however, with a SOL-GEL silica coating of the surface, the hydrophobic surface could be made into hydrophilic. Previously, our group has also proven another approach to change the wettability of the CNT carpet, by using microwave ionized oxygen plasma. In the former technique, the wettability was reversible, and excessive care was needed to control plasma power and reaction time, to prevent CNT damage. In contrast, SOL-GEL is a non-destructive method for the wettability modification, all CNTs will remain intact under SEM.

## Chapter 4 Attachment of nano catalytic particle: Palladium

### 4.1 Introduction

Metal nanoparticles (NPs) have found potential applications in many research fields including bio-medical, electronic, environmental, catalytic, and sensing that can constructively be used to advance current large number of cutting-edge applications [163-167]. Transition metal NPs have been attracting increasing attention due to their considerably high chemical activity and specificity of the interaction. NPs exhibiting distinct physical and chemical properties in comparison to their bulky state counterpart because of their large SSA. Among all transition metals, Pd had shown its remarkably catalytic activity and its unique ability to absorb hydrogen gas, as well as for molecular hydrogen splitting, forming a new intermetallic phase - palladium hydrate [168]. However, loose NPs can cause handling issues, recovery difficulties, health and environmental hazards. this concern can be directly targeted by attaching NPs onto larger substrate [169-172]. The limiting factor now therefore is the SSA that the supporting material can provide. Previous chapter, CNTs arrays were grafted on carbon fiber cloth forming exceptionally high SSA hybrid material. Supported Pd NPs are widely used for automotive exhaust catalysis, hydrogenation, dehalogenation, etc. For many surface sensitive applications, attaching nanoparticles of precious metals on high

SSA supports becomes economically and ecologically desirable for effectiveness of the system [173, 174]. The hierarchical hybrid material (CNTCFC) used in this study is the ideal support for anchoring Pd NPs due to its enhanced surface area and robust structure [175].

In the past, this group had demonstrated that Pd NP can be attached on rigid porous foams [176]. This study explores the possibility of obtaining a flexible hybrid carbon material such as carbon fiber cloth, that supports Pd NPs. Influence of surface tuning on NP size and deposition density was studied. Microstructural spectroscopic characterizations and chemical state analysis were carried out by comparing the nanoparticles on different hierarchical substrate by SEM, EDS and XPS.

In this study, three types of substrate were compared for the Pd NPs attachment, which are pristine fabric (CFC), CNT grafted fabric (CNTCFC) and SOL-GEL silica coated CNTCFC (TEO-CNTCFC), elemental, microscopic and crystallographic analysis were conducted respectively.

## 4.2 Experimental

### 4.2.1 Materials

All the reagents used in this study were of analytical grade as received; those include Tetra-amine Palladium (II) Nitrate solution (TAPN, 99.9%, 5% Pd, Alfa-Aesar Ltd.). Other materials are de-ionized water and methanol (Certified ACS grade, Fisher Scientific). Ultra-high purity hydrogen gas ( $H_2$ , 99.99%), and laboratory grade argon gas (Ar, 99.9%) were used.

### 4.2.2 Synthesis of Pd nano catalytic particle

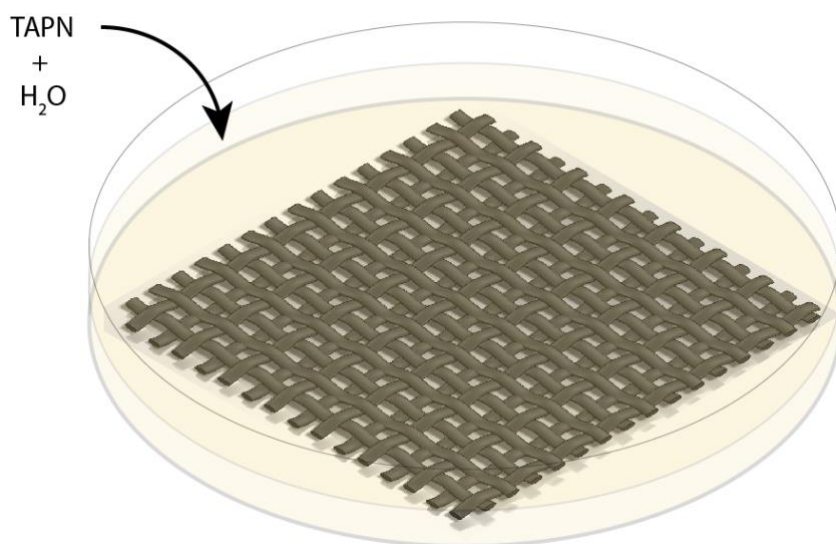
PdNPs were synthesized by the liquid-phase synthesis method combined with thermal calcination process, the CNTCFC hybrid material was immersed in precursor solution (stage I), and then dried in a tube furnace followed by heat treatment at elevated temperatures (stage II). Palladium is attached as a metallic form. Argon gas and hydrogen gas are the inert protective gas and reductive gas, respectively. The deposition is achieved on all three fabric support mentioned above. The process used in this study was developed earlier in this group [176]. Schematic illustration of each stage is shown in Fig 4.1.

### *Precursor Equilibrium-Adsorption – Stage I*

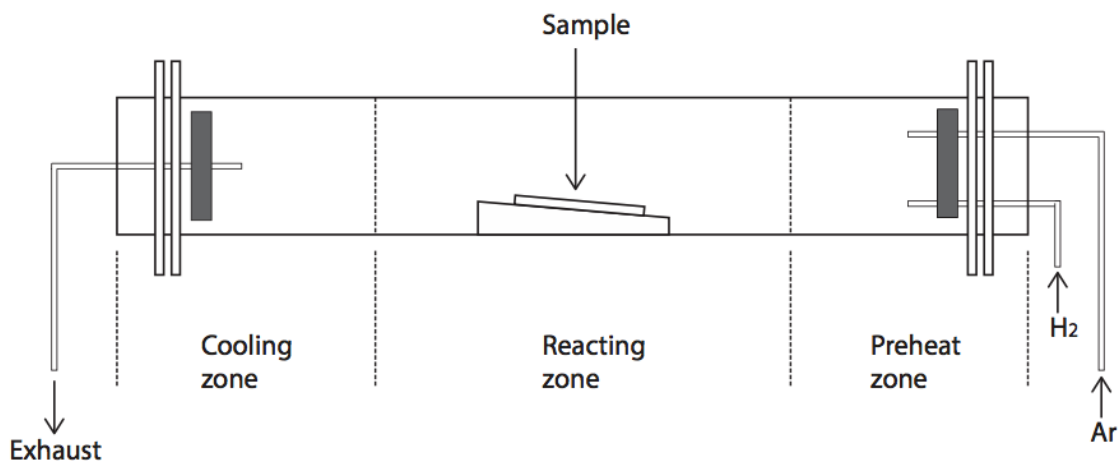
Tetraamine palladium (II) nitrate (TAPN) of known concentration (62.5 mM TAPN) is used as the metal precursor solution. The rinsed carbon fiber cloth is immediately immersed in aqueous precursor solution of TAPN for 1 hour. Excessive remaining solution on the sample is washed away by rinsing in methanol and DI water.

### *Thermal Treatment and Reduction – Stage II*

The thermal reduction is carried out in a quartz tube (length 1400 mm, inner diameter 70 mm). This thermal treatment includes three steps as drying, calcination, and reduction. In the drying step, samples were dried at 100 °C for 12 hrs. In the calcination step, samples were heated up to 400 °C in 30 mins and kept for 2 hrs. Heating rate is controlled by computer in order to prevent nanoparticle coalescence. Calcination was carried out in argon atmosphere, amines and nitrates groups of TAPN will be decomposed in the calcination step. In the reduction step, samples were subsequently heated up to 450 °C (10 °C/min) for 2 hrs using hydrogen as the reducing gas and Ar as the carrier gas. Furnace was thereafter cooled down to room temperature with the presence of H<sub>2</sub> and Ar.



**Precursor Equilibrium-Adsorption – Stage I**



**Thermal Treatment and Reduction – Stage II**

**Figure 4. 1 schematic route of Palladium nano particle (PdNP) synthesis**

## 4.3 Results and Discussions

### 4.3.1 Elemental quantification

Elemental quantification studies on PdNP grown on various surface modified structures are shown in Fig 4.2. EDS data was collected at 20 kV accelerating voltage and probe current of 12 mA. From the data, it can be seen that higher palladium content was obtained on the TEO-CNTCFC surface compared to CNT-CFC and CFC surfaces. EDS quantification revealed that higher Pd content was obtained with improved surface wettability. Pd loading increases over three times while the CNT surface becomes hydrophilic. It is worth to point out that bare fiber cloth was not be able to be a support for the nano particles, in another word, without CNT attachment, Palladium nanoparticle could not be successfully deposited onto the fabric surface.

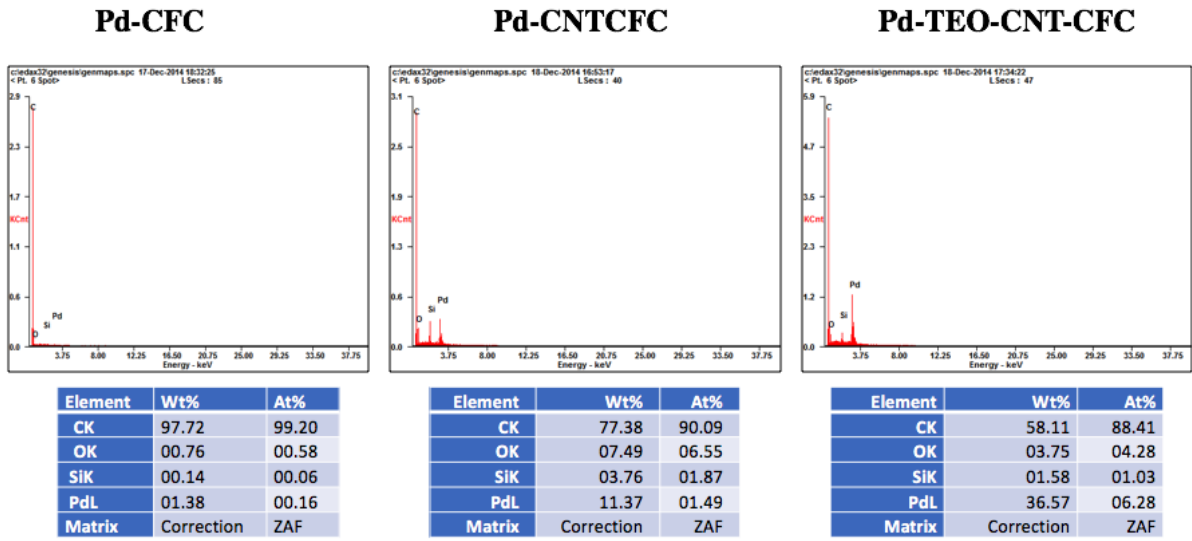


**Figure 4. 2 EDS analysis of fabric samples with different surface modification**

### 4.3.2 Microstructure Characterizaion

From the EDS analysis, we know only CNT grafted fabric is the right candidate for PdNP deposition, therefore, SEM analysis were conducted and compared for both CNTCFC and TEO-CNTCFC samples.

#### 4.3.2.1 Pd-CNTCFC

Fig 4.3 shows the microstructural analysis of Pd-CNTCFC sample, SEM and TEM images were taken. It can be seen that large amount of Pd particles are deposited onto the CNT carpet. Meanwhile, NP particle size seems evenly distributed. The particles sizes distribution investigations were achieved using Image J. Shown in the histogram in Fig 4.5. Multiple microstructure images were analyzed for particle size distribution. For the diameter measurement, a total of 10 images were collected for data processing. It can be clearly seen from the histogram that the majority of particles fall between 8-13 nm and observed to have variation particle distribution. The mean particle diameter for the Pd-CNTCFC samples is 10.9 nm with a standard error of 1.83 nm.

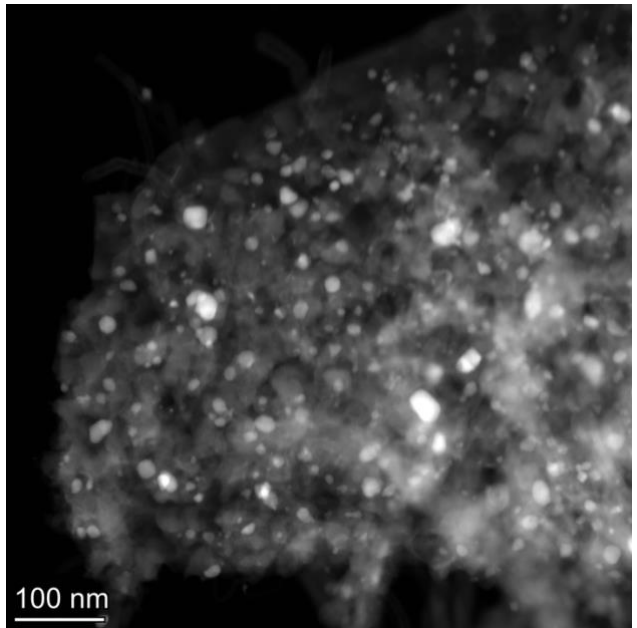
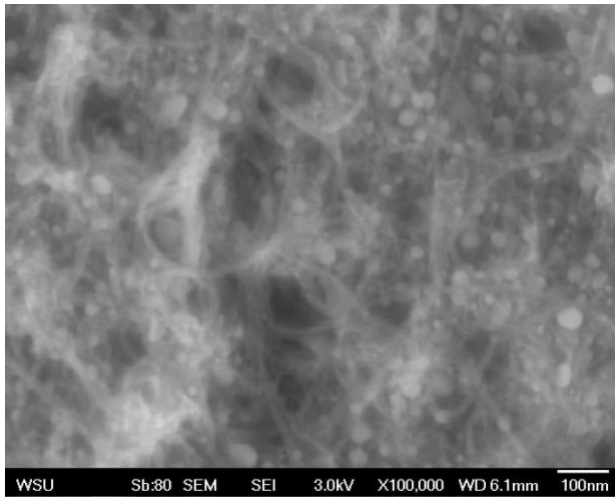
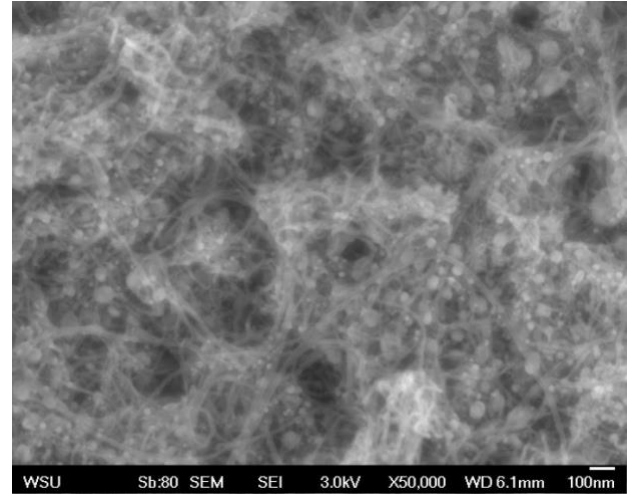
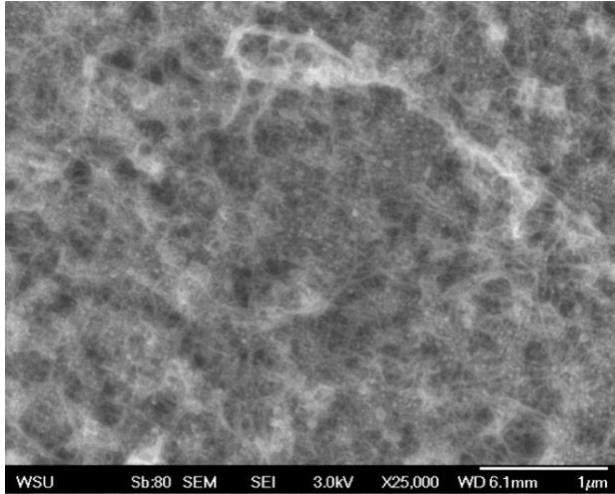


**Figure 4. 3 Microstructural characterization of Pd attached CNTCFC hybrid material**

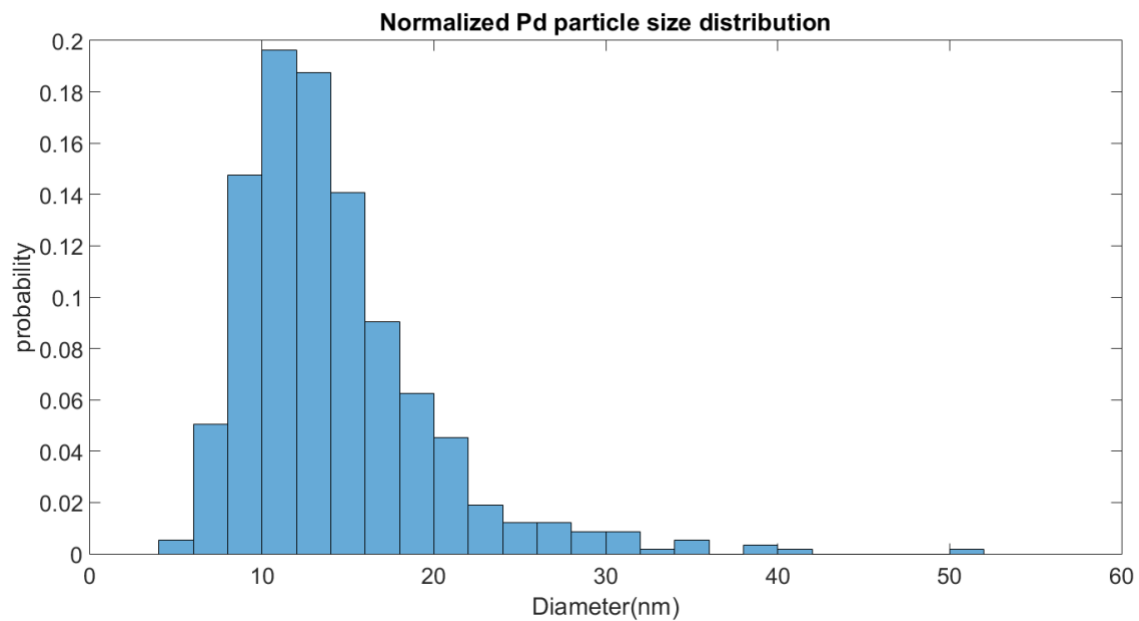


**Figure 4. 4 Palladium nanoparticle size distribution**

#### 4.3.2.2 Pd-TEO-CNTCFC

From previous chapter, it is known that SOL-GEL silica coating was a successful approach for surface wettability tuning. Here, since the TAPN is an aqueous precursor, surface affinity is playing a significant role for the nanoparticle loading, from the EDS analysis, it is clear that with the wettability tuning, Pd loading is increased by 4 times. CNTCFC exhibits a hydrophobic surface, therefore, hydrophilic counterpart of CNTCFC was used to compare the palladium nanoparticle deposition on the hybrid material surface.

Fig 4.5 shows the micrograph of the SOL-GEL silica coated CNTCFC for PdNP attachment. From the SEM images there is, as well, showing the clamping part of the CNT tubes, which was resulting from the silica coating. Additionally, there is significant evidence that large scale particles are appearing, which is attributed to the agglomeration of smaller Pd nanoparticles. Unfortunately, these large and not evenly distributed nanoparticles are not desired for further usage. Therefore, even the TEO-CNTCFC group will have an increased Pd loading, but this surface hydrophilic modification is not a good approach for nanoparticle to disperse evenly throughout the surface, direct deposition of Pd onto the CNT support proves to be a better method. This agglomeration can be resulting from over-

accumulation of TAPN on the nanotube, and eventually forming large size particles.

Since CNTCFC becomes the only suitable candidate for the palladium nanoparticle attachment, further XRD and XPS analysis will be only conducted on the CNTCFC group for Pd loading (Pd-CNTCFC).

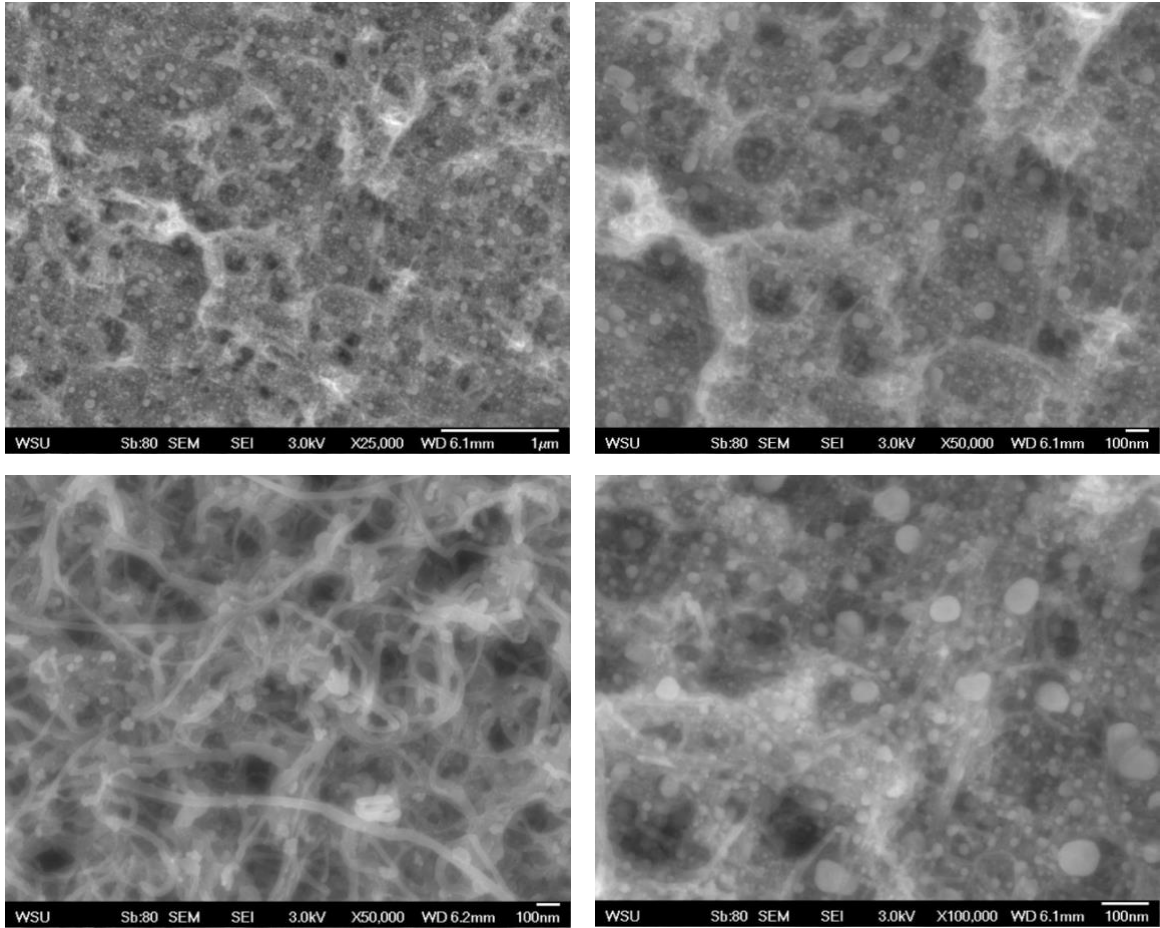


**Figure 4. 5 SEM characterization of PdNP attachment on CNTCFC surface with SOL-GEL silica coating**

### 4.3.3 Crystal Structure Characterization

Figure 4.6 shows the XRD patterns obtained from palladium nanoparticles on CNT fiber cloth (Pd-CNTCFC) in comparison with the pristine fabric and CNTCFC. By comparing the XRD diffractogram of the three, we can see the surface change after each modification was applied. The main peak at  $2\theta = 26^\circ$  corresponds to carbon (0 0 2) plane in all three samples, which is the characteristic peak of hexagonal structure of graphite and CNT, and another peak of C (1 0 2) shows at  $50^\circ$  of CNTCFC group. As for the XRD pattern of Pd-CNTCFC, additional peaks appeared at  $2\theta$  values of  $40^\circ$ ,  $46^\circ$ ,  $69^\circ$ , and  $82^\circ$ , corresponds to the Pd(1 1 1), Pd(2 0 0), Pd(2 2 0), Pd(3 1 1) crystal planes, are in good agreement with those reported in the literature, which are the characteristic diffraction peaks of a face-centered-cubic (fcc) crystal phase of palladium nanoparticles [177, 178, 179].

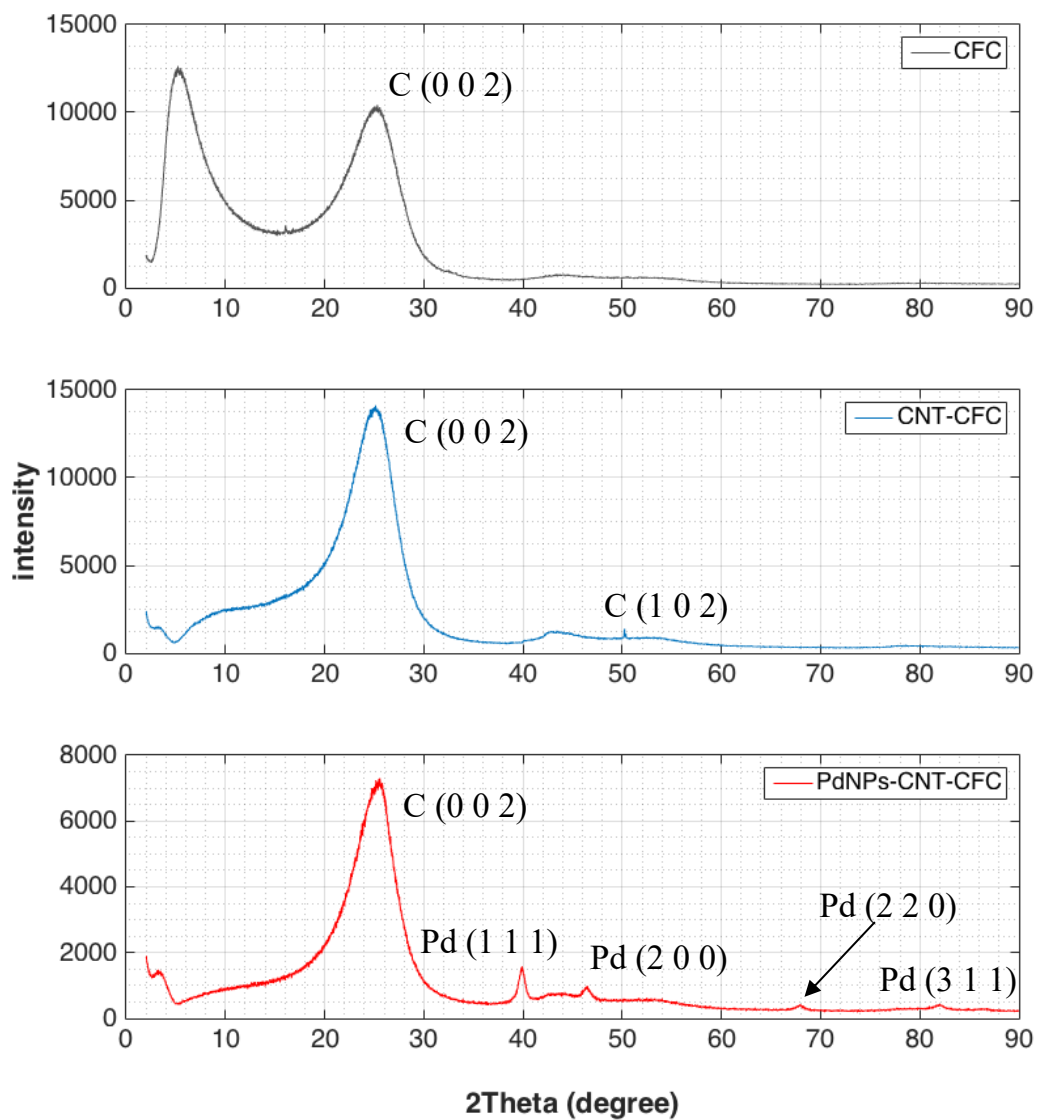


**Figure 4. 6 X-ray diffraction pattern for pristine fabric, CNTCFC hybrid and Pd attached CNTCFC hybrid.**

#### 4.3.4 Chemical Structure of Pd nanoparticles

Fig 4.7 shows the XPS spectra of Pd nanoparticle attached CNTCFC hybrid material. Three distinct peaks were observed in the XPS survey spectra (Fig 4.7a) at 285 eV, 334 eV and 531 eV, corresponding to C *1s*, Pd *3d* and O *1s*, respectively. Two well-resolved strong peaks at 335.3 and 340.6 eV can be attributed to the Pd *3d<sub>5/2</sub>* and Pd *3d<sub>3/2</sub>*, respectively (Fig 4.7b), which match the typical peaks of metallic Pd<sub>0</sub>.

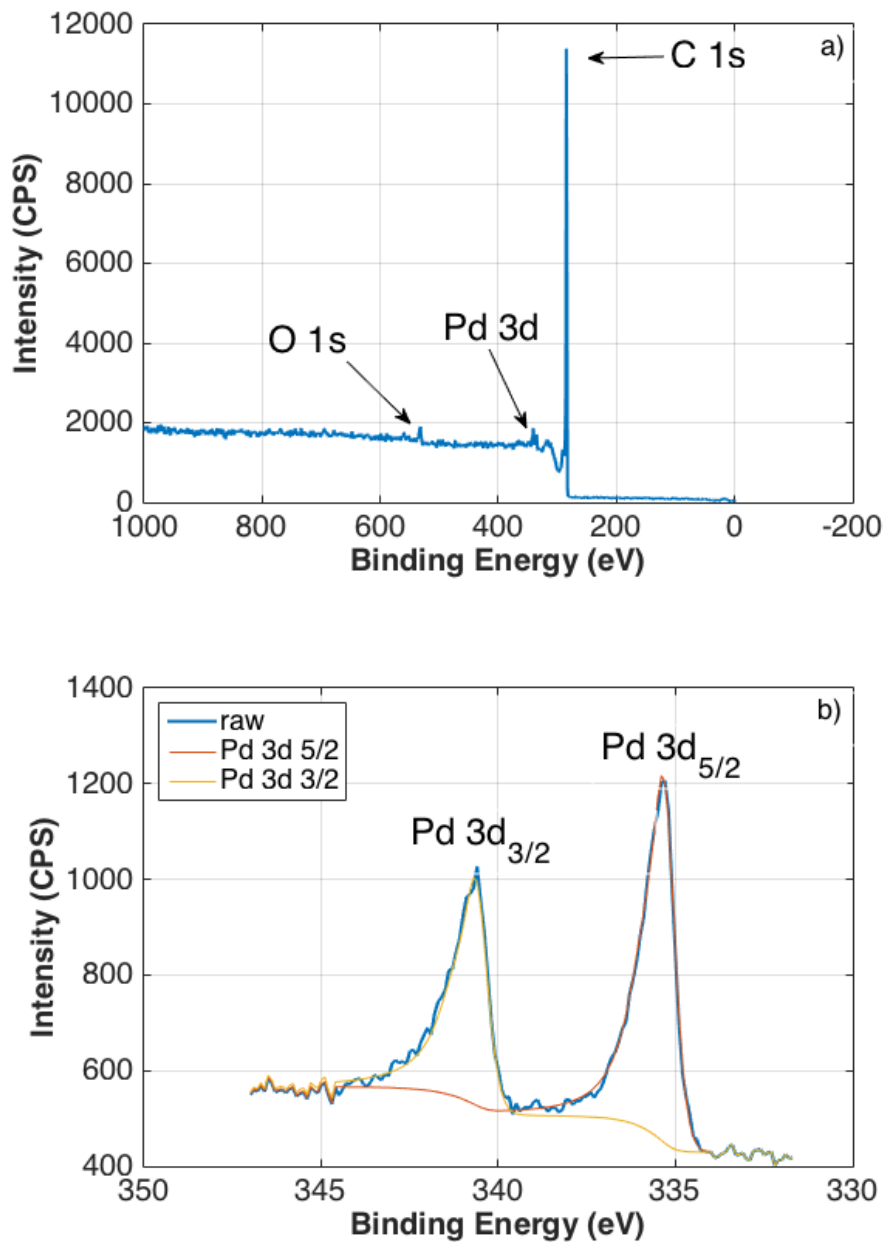


**Figure 4. 7 XPS spectra of a) survey scan of Pd attached CNTCFC hybrid b) high-resolution Pd 3d core level.**

#### 4.4 Conclusion

In this chapter, Pd-NPs were attached to porous carbon structures. Three types of substrates were compared: bare carbon fiber cloth (CFC), CNT grafted fabric (CNTCFC) and palladium nanoparticle attached CNTCFC hybrid material (Pd-CNTCFC). It is expected that high concentration of catalyst nanoparticles can be attached on hierarchical structures to provide very high surface activity for smaller and lighter components. Sets of identical experiments were conducted to compare the distribution of PdNP on differently modified substrates. Surface wettability tuning was applied to those substrate, showing that hydrophilic surface will have the highest Pd loading, acceptable Pd loading on untreated CNT covered CFC, and no PdNPs onto the bare fiber cloth. However, due to the agglomeration of over-sized particles on the SOL-GEL silica modified (hydrophilic) fiber cloth surface, it was determined that untreated CNT grafted support (CNTCFC) would be more suitable for future applications. These materials have better nanoparticle size distribution, and no agglomeration was observed. Therefore, CNTCFC was utilized as the optimized support for the Pd nanoparticle attachment. On the basis of XRD, XPS analysis, as well as the SEM and HRTEM results, the deposited Pd on the surface is as individual metallic nanoparticles.

As discussed in the next chapter, those nano-catalysts can be used easily for contaminated water treatment, as they are adhered to larger supports. This makes them reusable and eco-friendly as the NPs and the CNT are immobilized on larger porous supports.

## **Chapter 5 Reusable Flexible Hierarchical Hybrid Nanocatalysts for Degradation of Triclosan in water**

### **5.1 Introduction**

Chlorine and Chlorinated Hydrocarbon (CCH) is a major category of environmental contaminants that comes from a wide variety of industries, pharmaceutical, personal care products [180-183]. According to recent U.S EPA reports, more than 100 different CCHs have been found to date, which are contaminating the soil, groundwater, and air in large quantities [184].

Recent studies have been focused on CCHs removal from water. Since most CCHs are non-biodegradable, common methods of removing them involve mitigation through adsorption, combustion, and sedimentation, etc. Those techniques may have efficiency issue or difficult to reach complete removal. For example, using commercial granular activated carbon(GAC) to adsorb CCHs may take several days for treatment, still achieving only partial removal [185,186]. Moreover, these techniques may require follow-up steps to treat the resulting by-product. Additionally, while dealing with the halogenated compound, removing the halogen groups, especially chlorinated or fluorinated compounds, as in this case, oxidation becomes difficult. Usually, substantial energy-consuming

techniques such as UV radiation or dielectric barrier discharge(DBD) plasma [187,188] are required.

A novel approach is to target the toxic group of the compound and use an eco-friendlier way to degrade the CCH into some non-toxic or easier to treat intermediate (daughter) products. Reductive dechlorination reactions under STP can be utilized, where a hydrogen source, with the help of a catalyst, can break down the carbon-halogen bond (carbon-chlorine bond in this case). The molecular hydrogen will initially associate with the metal catalyst, forming a metal hydride, following the introduction of CCH, hydrogen will dissociate from the catalyst surface, subsequently, replaces the chlorine in the compound that produces a reduced chlorinated compound. Among all catalysts, palladium based catalysts have been proven as a good candidate via coupling reaction and therefore a promising method of water treatment [222]. Pt or Rh based catalysts also show potential in dehalogenation, however, their catalytic activity for dehalogenation is lower than Pd-based catalysts. While Ni-based catalysts are showing stronger activity than Pd in certain contaminants, especially nitrogen-based pollutants, however, leaching is a massive issue for Ni-based catalysts [189,190,191].

Previously, work has been done to use a Pd-based catalyst to target aromatic CCHs, rate constant varies from 0.1-100 mmol/min/g<sub>catalyst</sub>, according to the

model compound and form of the catalyst [191-195]. Comparing with conventional catalysts, nanocatalyst is showing better catalytic activity and selectivity, it stands out due to its high SSAs, since most functional materials are heavily surface dependent. Moreover, nano catalyst has better dispersion in solvent which would help mixing with the reactants for catalytic activity enhancement.

Even though nanomaterials have significant advantages, they on the other hand pose environmental risks since they can be released into the surroundings, and recovery of nano dimensional materials is costly and challenging. Meanwhile, environmental risk remains undiscussed. In this team, we have investigated how to address this issue by attaching nanocatalysts onto a robust, flexible, inert, and multiscale hierarchical carbon structure by attaching Pd nanoparticles (PdNP) onto a CNT grafted carbon fiber cloth(CNTCFC) hybrid material. Just like dew on the spider web, CNTs can play very well support for the Pd-nanoparticles, with an enhanced surface area, attached nanoparticles become more effective, furthermore, the stable physical and chemical property of CNT, chemical inertness and resistance to acidic or basic environment, as well make itself a suitable support. Last but not least, the actual amount of catalyst used is reduced whiling used in nanoscale, makes it economically affordable.

Carbon nanotubes (CNTs) consist of one or more graphene sheets rolled into a cylindrical tube with a nanoscale outer diameter [7, 13], commercially available CNTs have potential in environmental applications due to their enhanced specific surface area(SSA) as sorbents, which can facilitate the removal of contaminants [8,196,197]. Because of their outstanding physical and chemical properties, both SWCNTs and MWCNTs are being produced in large quantities to achieve desired functionalities, and they are among the most commonly used engineered nanomaterials [14, 22].

In this study, we were using the add-on effect of CNT and Pd based catalysts. Firstly, CNT's large surface area will be providing a good amount of adsorption sites for the contaminant. If the Pd-based catalysis targets all adsorbed contaminants, efficiency will increase and after treatment will not be needed. Previous chapters we have discussed and optimized hybrid material for of Pd nanoparticle(PdNP) deposited CNTCFC hybrid material. The CNTCFC hybrid material provides not only a large SSA, but also its flexibility opens the door for utilization of these materials in a different environment.

Furthermore, palladium is anchored onto this hierarchical substrate in nanoscale, forming palladium nanoparticles (PdNPs), the PdNPs are strongly attached to the supports, preventing the nano-catalyst posing hazardous effect to the outside

environment. The objective of this work is to first investigate the morphology of PdNPs decorated material study the surface chemistry of this hybrid catalyst (discussed in the chapter 4),). Secondly, demonstrate the use of a hierarchical substrate as effective catalyst support for water treatment applications and also to evaluate the reactivity, capability, and durability of this novel catalyst.

In this study, we have chosen triclosan(TCS) as our model compound, a widely used disinfecting agent, and a potential endocrine disruptor [198]. TCS is highly hydrophobic, so it's likely to stay in human fatty acid or other animals' bodies [199]. Recent work using nanocatalyst targeting triclosan showing a rate constant of 0.03 – 0.1 mmol/min/g<sub>catalyst</sub>. TCS degradation was performed, tests using high-performance liquid chromatography and (HPLC) and Gas chromatography-mass spectrometry (GC-MS) for the kinetic and dechlorination pathway studies, respectively. The concentration of TCS in the liquid was monitored. Removal results were compared with other forms of catalysts or other techniques. Catalysts were also tested repeated for durability and anti-poisoning ability.

## 5.2. Experimental

### 5.2.1 Materials

The chemical reagents used in this study were of analytical grade and consumed without further purification. These include Triclosan (TCS,  $C_{12}H_7Cl_3O_2$ , HPLC, Sigma Aldrichds), the water used in this study was MiliQ DI water that has a resistivity of 18 Megaohm-cm ( $M\Omega$ -cm). Other materials are laboratory grade high purity gases that include 5% $H_2$  balanced  $N_2$ . Gas-tight syringes (Hamilton, Inc.) and end-to-end rotators at 60 rpm (Glas-Col®) were used. The pH of the buffer solution was monitored using a pH meter. Teflon-lined butyl rubber stopper (PTFE-lined) of size 20mm and aluminum crimp were purchased from Wheaton Inc.

### 5.2.2 Palladium nanoparticle (PdNP) deposition

As mentioned in the previous chapter, palladium nanoparticles (PdNPs) were synthesized via a two-step method, step one Tetraamine palladium (II) nitrate (TAPN) of known concentration (62.5 mM TAPN) is used as the metal precursor solution, the wetted carbon fiber cloths are immersed in a diluted solution of TAPN for a certain time. The carbon supports are recovered from the solution, and the excess non-interacting solution on the sample is washed-off by briefly dipping the support in methanol, shown in Fig 4.1. The following thermal reduction step is

performed in a quartz furnace. As discussed in chapter 4, CNTCFC was chosen as the appropriate support for the PdNP deposition, the prepared Pd-CNTCFC hybrid material is further analyzed in this chapter for the degradation purpose. 5.2.3

#### Dechlorination batch test

The stock solution of triclosan(TCS) was separately prepared as 50 g/L (0.173M) in methanol, and 10 mg/L (0.035 mM) in water, the stock solution was kept in shaker prior to use for 48 hours for complete mixing. Investigation of TCS degradation is carried out in a batch reactor, shown in Fig 5.1. Carbon supports (with and without catalyst) were rinsed prior putting inside the reactor; hydrogen gas was introduced and the reactor pressured was kept at 1 atm throughout the reaction. During the process, since reaction was studied in both water and methanol environment, there will be evaporation mass loss due to the high volatile property of methanol solvent, methanol was supplied constantly and the reactor mass was kept constant throughout the whole degradation process. 2 ml Samples collected from the reactor via the syringe at the different reacting time, then filtered and kept for further high-performance liquid chromatography (HPLC) analysis.

#### 5.2.4 Morphology and Chemistry analysis

SEM analysis is performed using the JOEL-7401 system; XPS analysis is carried out using a Kratos Ultra system mentioned in previous chapters. An HPLC system (Waters Micromass Quattro Micro) equipped with a Waters Xselect CSH C18 (3.5  $\mu\text{m}$ , 4.6x50 mm) column and a UV-vis detector was used to measure the triclosan concentrations at a detection wavelength of 235 nm. The mobile phase used for elution was deionized water (polar component) and acetonitrile (non-polar component) using reverse phase HPLC. Liquid mixture was delivered at  $1\text{ml}\cdot\text{min}^{-1}$  through the column. Samples are stationed at an auto sampler tray and each time 50  $\mu\text{l}$  of sample was taken for test. Column temperature was maintained at room temperature. For kinetic study, a calibration curve was performed in the range of experimental concentrations, details of the HPLC method is in appendix A.

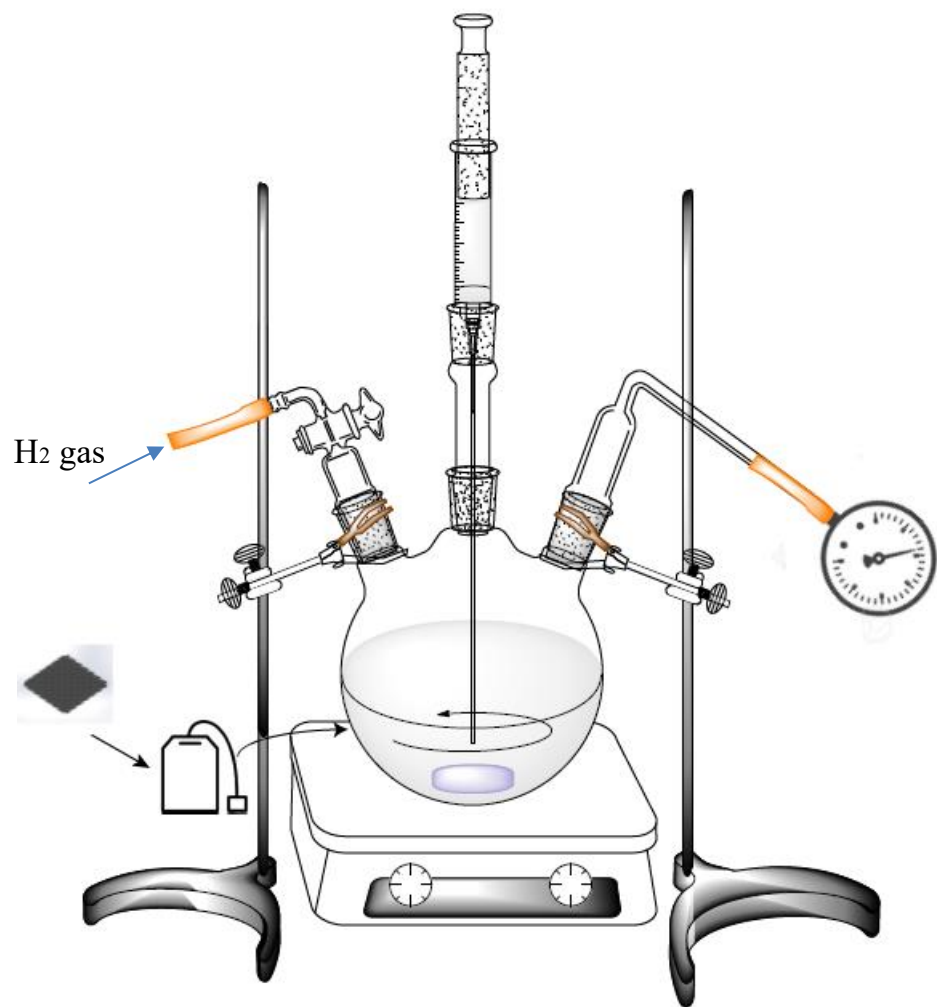


**Figure 5. 1 The reactor of triclosan catalytic degradation**

## 5.3. Results and Discussion

### 5.3.1 Attachment of nano catalytic particle: Palladium

Previous chapter we have discussed the Pd deposition on CNTCFC hybrid material, Figure 5.2 shows the SEM/TEM images of Palladium nanoparticles(Pd-NPs) deposition on CNTCFC. From image 5.2b and 5.2c, the attachment of Pd is desired, and the high surface area carbon nanotubes have provided an excellent support for anchoring the PdNPs. It can be observed, first of all, the overall coverage of CNT onto the CFC support is complete, 5.2a showing the all surface of CFC is covered by CNT forest. 5.2b and 5.2c showed an even distribution of palladium nanoparticles on the support, the size of the palladium particles is measured based on the TEM images, moreover, from the TEM image, it can be seen that PdNPs are well attached to the CNT surface. 5.2c showed a detailed uniform distribution of the PdNPs on the hierarchical substrate. The diameter of the PdNPs was measured subsequently based on multiple groups of samples; diameter distribution was shown in Figure 5.3, the result shows an average diameter of PdNPs is 10.9 nm ( $\pm 0.97$  nm). The composition of the material obtained using EDS was shown the table 5.1 below. In comparison with the deposition on the bare fiber cloth, we can see for the bare fiber cloth; it's very difficult for the NPs to be deposited on, hardly NPs were observed from the SEM

or detected by EDS. This can be the reason for the surface sizing of CFC, the treated inert surface is almost unwettable, which may lead to the failure of step one of Pd deposition. While the CNT-CFC sample, the weight percent of the Pd on the sample is around 11 wt %, we can hence conclude the PdNPs can only be deposited onto the sample with grafted CNTs, and the Pd will stay only on the CNT surface, which agrees with the SEM observation. Hence, since the CNT on the sample is about 11%, and the Pd also holds an 11% weight percentage, resulting in a 1.3% of the overall material weight is composed of PdNPs. XPS analysis was also conducted, will be discussed in the later part of the chapter in order to compare the material chemical state before and after degradation test.

Furthermore, investigation of the PdNPs mass and surface area are calculated based on the observed palladium particle diameter; all palladium particle is assumed to be spherical.

$$\# \text{ of PdNP per unit mass material} = m_{Pd}/M_{Pd} * N_{avogadro} = 7.35 * 10^{19} / g$$

$$SSA \text{ of Pd per unit mass material} = 4\pi r^2 * \# = 1.1 * 10^5 \text{ m}^2/g$$

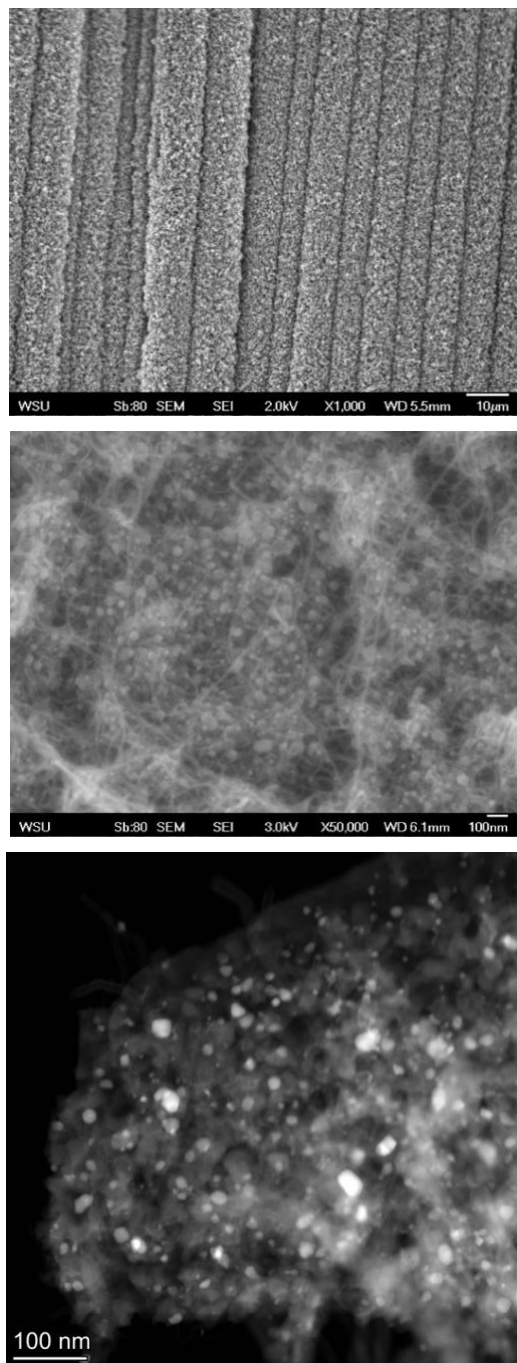


**Figure 5. 2 SEM/TEM Micrographs of PdNPs synthesized on CNT-CFC hierarchical substrate**

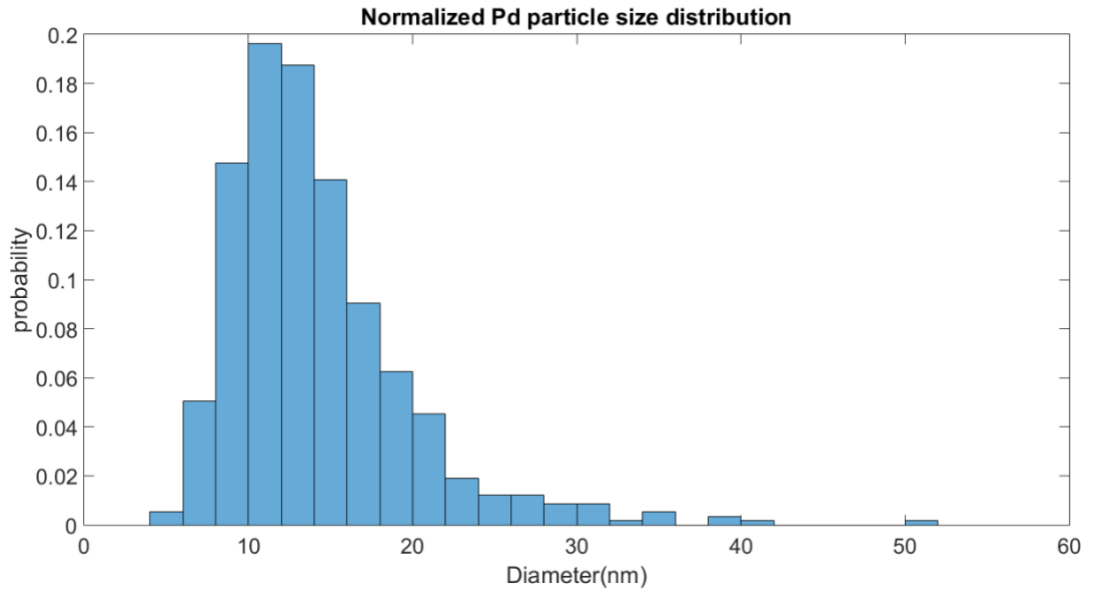


**Figure 5. 3 Normalized PdNP diameter distribution histogram**

**Table 5.1 The elemental composition obtained from EDS analysis of Pd-NPs fabricated on fiber cloth material**

Element	weight percentage (wt%)	
	CFC	CNT-CFC
C K	97.72	77.38
O K	00.76	07.49
Si K	00.14	03.76
Pd L	01.38	11.37

### 5.3.2 Catalytic reduction of triclosan via hierarchical hybrid material

Firstly, we compared the adsorption capability of different material for the model compound TCS, test was carried out in aqueous environment first, result is shown in Fig 5.4. Both carbon fiber cloth and CNT decorated CFC are not shown promising results, for the CFC, TCS was barely adsorbed onto the surface of CFC, a total of 1.5 ppm of TCS removal was observed (15% removal); meanwhile, as the CNTs are attached to the CFC, CNTCFC hybrid material showed an improved adsorption percentage, however, the overall adsorption percentage stays around 30% after the adsorption stabilizes in 2 hours, which is not desired. Additionally, since the concentration of triclosan is low in aqueous solution (solubility 10 ppm), the same adsorption test was performed in methanol, while the concentration of triclosan is increased up to 50ppm, shown in Fig 5.5, it was observed the similar amount TCS was removed by adsorption, for the CFC sample group, a total around 2 ppm (4%) removal was observed, and the CNTCFC counterpart shows a 4 ppm (8%) removal. It can be seen that in organic solvent, TCS is easier to be adsorbed onto the adsorbate surface, however, in both cases, TCS removal is limited, an alternative approach for TCS removal is needed.

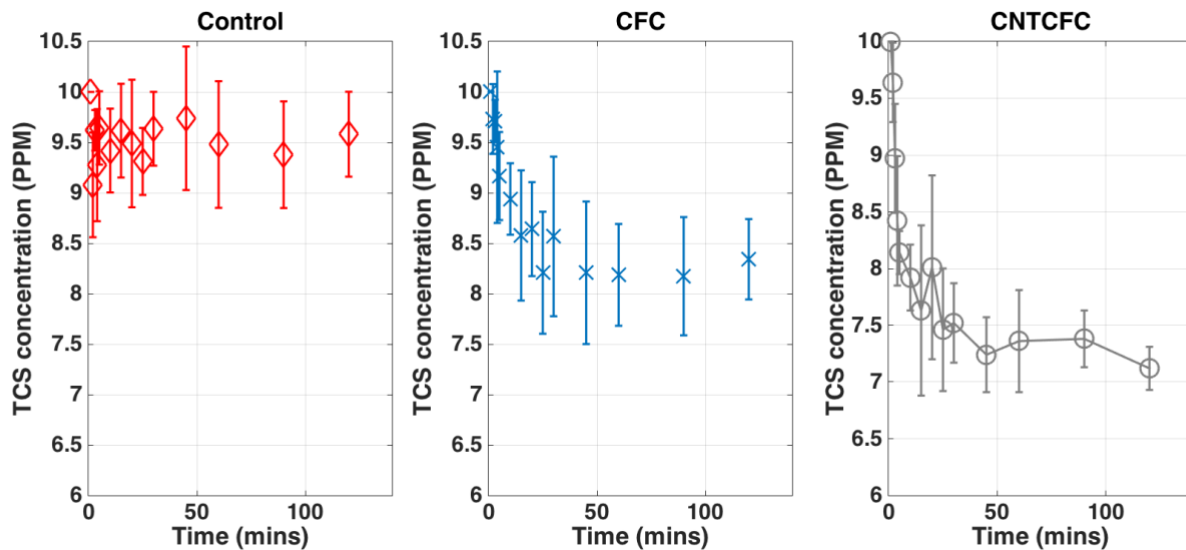
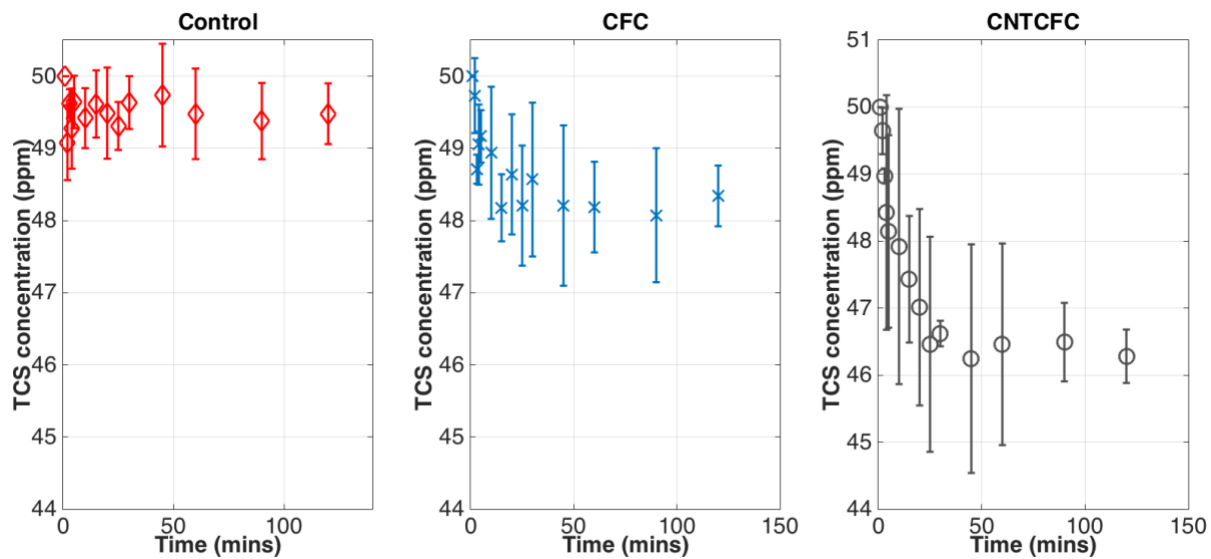


Figure 5. 4 Adsorption comparisons of TCS from different materials in water.



**Figure 5. 5 Adsorption comparisons of TCS from different materials in methanol.**

Degradation test results were given in Fig.5.6 below. From Fig 5.6a, dehalogenation was carried out in aqueous solution, it can be seen that the TCS will be completely removed within 10 mins, showing the hybrid material holds a very high efficiency of removing the contaminant. Also, it indicates that the degradation reaction of TCS using PdNP catalyst is carried with the aid of H<sub>2</sub>. A study by Nadagouda et. al. For degradation of TCS using Pd catalyst in ambient air conditions shows no significant removal of TCS using only a palladium catalyst [191]. Therefore, without the presence of both Pd and hydrogen gas, only the adsorption process happened. Unfortunately, this rapid removal won't be able to provide too much information regarding the kinetics and degradation pathway, the calculated pseudo-first order rate constant shows a rate constant for TCS degradation in water is 0.9338 min<sup>-1</sup>, which is very high and might not be accurate. As a result, TCS in methanol with higher concentration was studied.

Fig 5.6b shows the result of TCS degradation in methanol environment, a detailed kinetic study was followed. From 5.6b, it can be obviously observed that the degradation process was finished throughout the two hours period, an over 97% removal was achieved. Same as the degradation in water, the degradation process

requires the presence of both PdNPs and hydrogen, otherwise the catalytic reduction reaction won't happen. In comparison with the adsorption process, degradation is much quicker, more complete and efficient, even with TCS concentration increased up to 50 ppm, TCS can be removed completely in two hours. Pseudo-first-order rate constant was extrapolated from the catalytic reaction as shown before:

*Pseudo - first order rate equation*

$$\ln N_t = \ln N_0 - kt$$

*where  $N_0$  and  $N_t$  is the mole amount of TCS at time 0 and time  $t$   
 $k$  is the rate constant,  $t$  is the time*

From the equation above, we can obtain a rate constant of 0.041 min<sup>-1</sup>. In comparison with the previous study, the table 5.2 below shows the result. If the rate constant is normalized by the amount of TCS and catalyst loading, we can see the rate constant will pass 100 mmol/min/g<sub>catalyst</sub>, which is two to three orders of magnitude higher than reported in the reference. From this comparison, it can be seen when catalysts are distributed on to the hierarchical support at nanoscale, the required mass of catalyst is reduced, but the capability and efficiency of TCS removal is increased enormously.



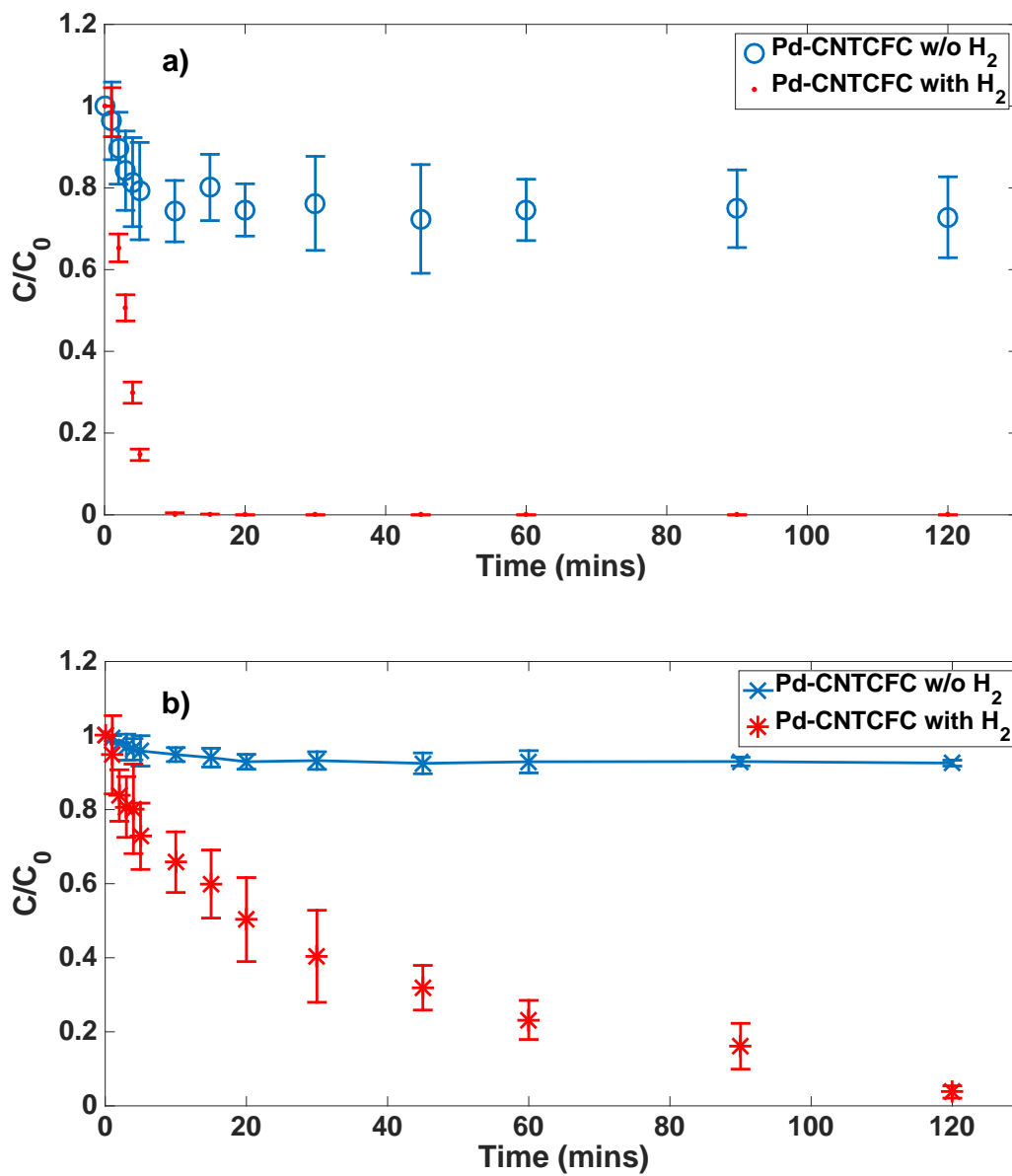


**Figure 5. 6 TCS catalytic degradation in a) aqueous environment, b) methanol environment**

**Table 5. 2 Catalytic rate constant comparisons**

<b>Rate constant (min<sup>-1</sup>)</b>	<b>Pd mass (mg)</b>	<b>TCS amount (mmol)</b>	<b>Adjusted rate constant (mmol/min/g catalyst)</b>	<b>Source</b>
0.041	2.6	6.372	100.48	this work
0.043	60	0.5	0.36	[223]
0.0183	100	0.02	0.003	[191]

The durability test is followed up to check the catalyst activity and poisoning for long term, result is shown in Fig 5.7. Catalyst activated carbon fiber cloth was kept inside the reactor for the whole time in solution, durability tests were carried out in both aqueous condition and methanol condition too, each cycle was taking two hours, which is the TCS complete removal time in methanol. Fig 5.7a shows the catalyst activity in aqueous environment, due to the high efficiency and low solubility of TCS in water, all 4 repeats Pd-CNTCFC hybrid material is able to remove the TCS completely. Fig 5.7b shows the catalyst hybrid behavior in methanol, high concentration of TCS is desired to explore the limit of the catalyst. It can be seen that the removal drops from 97% to 85% after the 4<sup>th</sup> run, which shows the catalytic activity of the hybrid material is falling, however, this durability test shows the catalyst even after multiple runs of degradation, it still maintains a high percentage of TCS removal. This efficiency drop may cause the catalyst a longer time to fully remove the TCS after couple of runs, with enough time, Pd based catalyst matrix might still able to fully dechlorinate TCS.

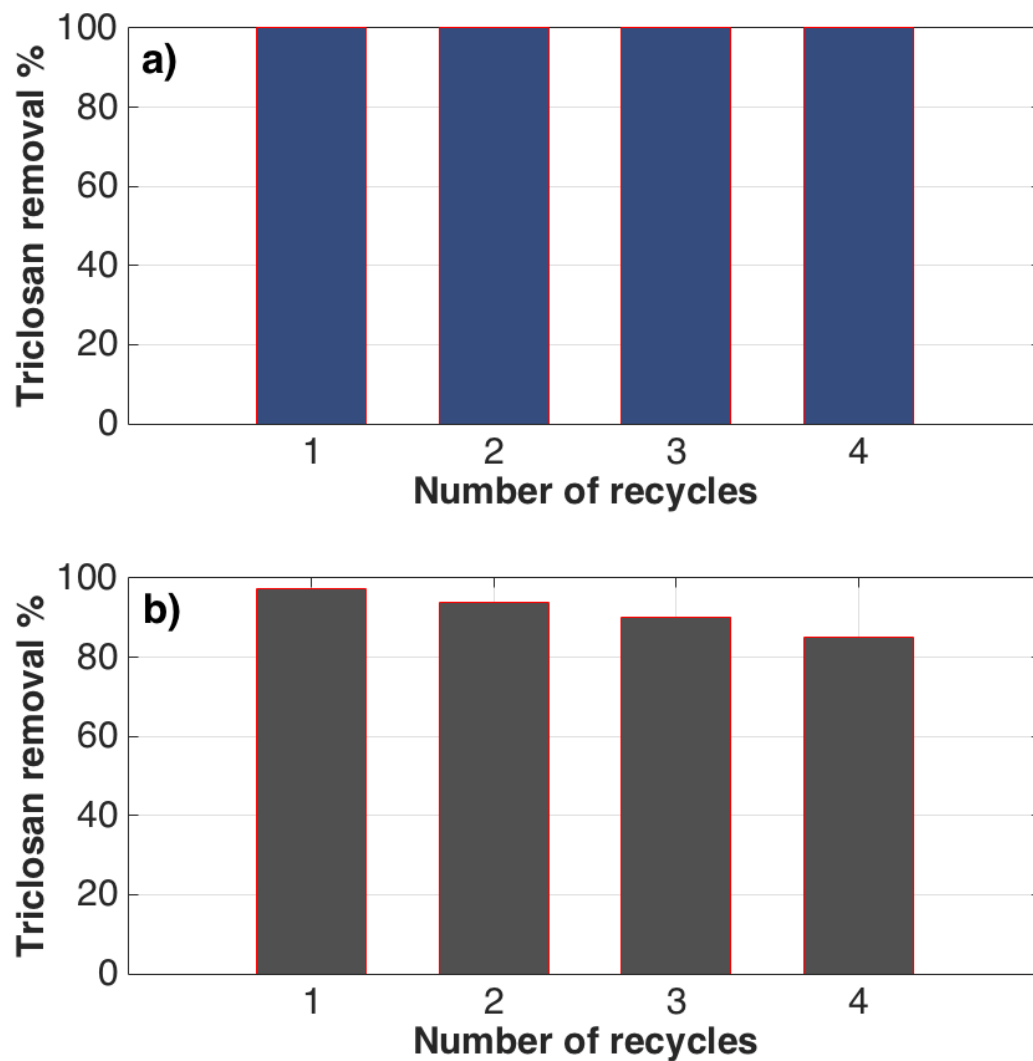


**Figure 5. 7 Stability and durability test of PdNP loaded CNTCFC hybrid material in a) aqueous environment, b) MeOH environment**

### 5.3.3 Palladium catalyst chemistry analysis

XPS surface analysis was conducted to investigate the chemical state of the Pd-CNTCFC hybrid material before and after the degradation, shown in Fig 5.8 and Fig 5.9. From Fig 5.8, survey scan and high resolved Pd  $3d$  peak scan was performed. Survey scan shows the existence of carbon, oxygen and palladium, detailed high resolution scan of Pd observed the Pd  $3d$  peak at 335.3 eV for Pd  $3d_{5/2}$  and 340.6 eV for Pd  $3d_{3/2}$ , which are peaks for metallic palladium nanoparticles. After the degradation, Pd-CNTCFC sample is retrieved from the solution, rinsed with DI water and air dried before XPS analysis. Fig 5.9 shows the survey scan and high resolution Pd scan shows similar result as Fig 5.8, Pd fine scan peaks shows the Pd  $3d_{5/2}$  and Pd  $3d_{3/2}$  are at 335.4 eV and 340.6 eV, no significant difference was found of the palladium before or after catalytic degradation, it remains at metallic state.

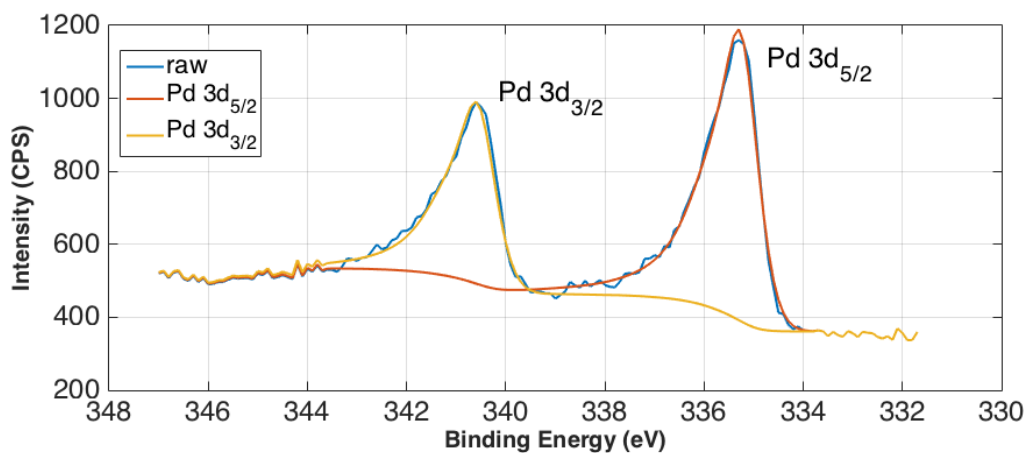
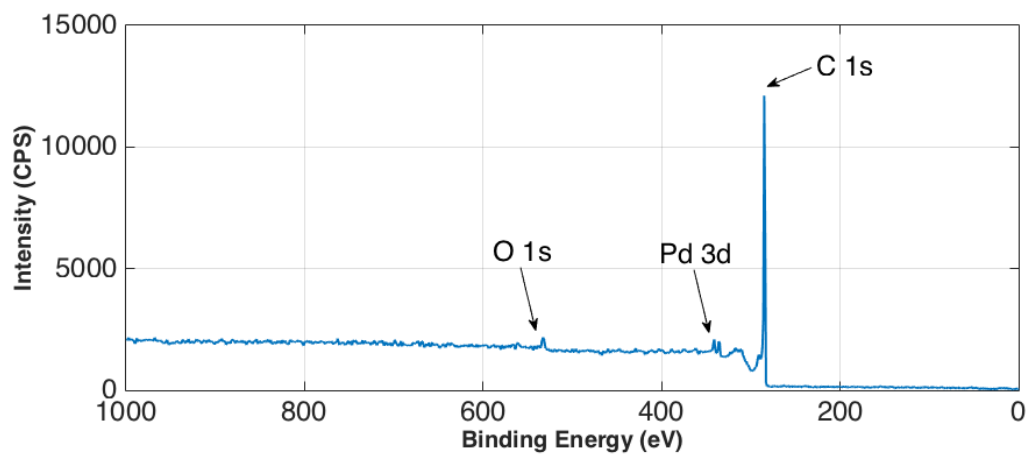


**Figure 5. 8 XPS surface analysis of Pd attached CNTCFC hybrid material before dechlorination**

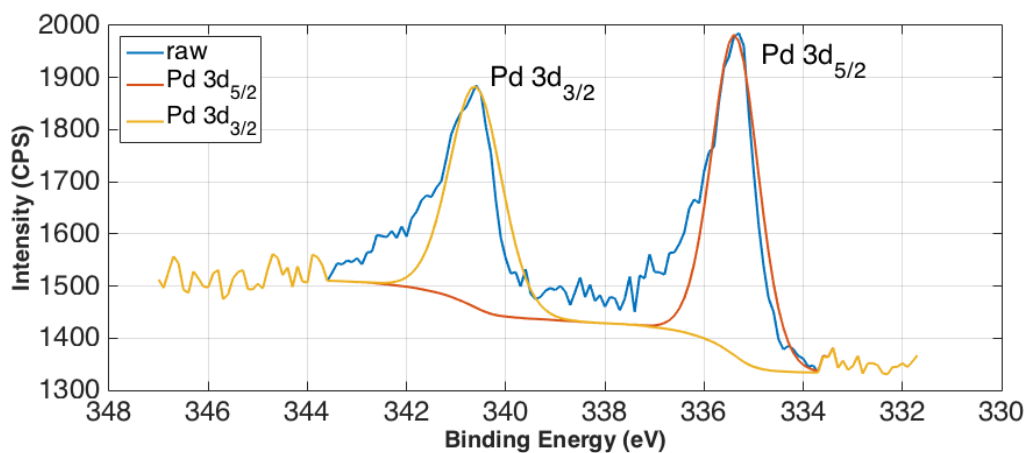
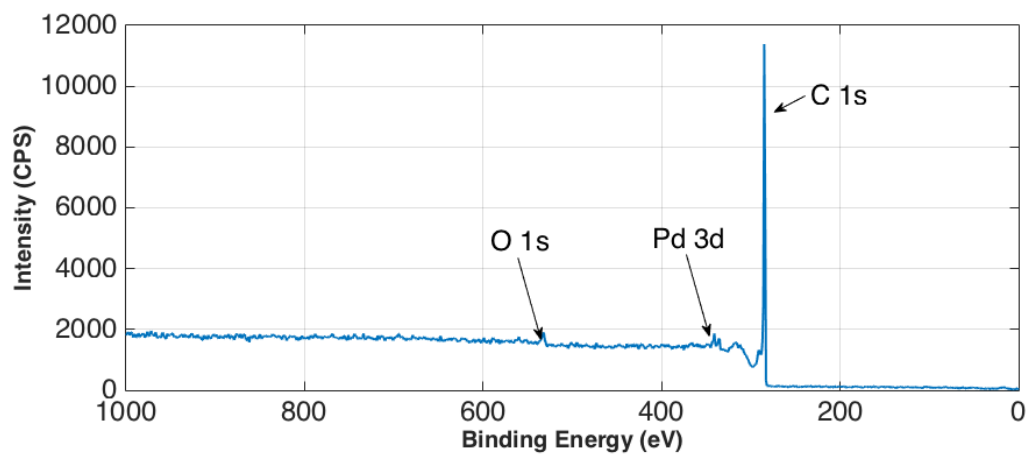


**Figure 5. 9 XPS surface analysis of Pd attached CNTCFC hybrid material post dechlorination**

#### 5.3.4 Degradation pathway study

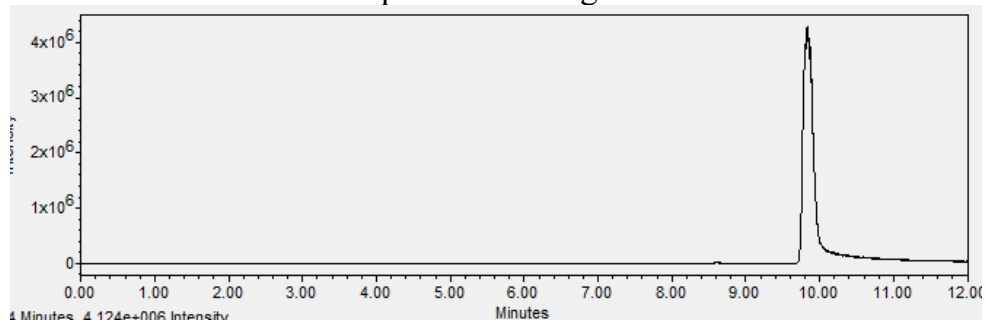
Degradation of triclosan forms various daughter compounds. Liquid chromatography-mass spectrum(LC-MS) was employed to analyze the daughter compound from the reduction reaction. The daughter compounds include significant amounts of dechlorinated TCS. As the reaction proceeds, more daughter products were observed, the formation of trace amounts of other daughter products indicate further degradation of TCS.

In this study, heterogeneous liquid-phase degradation of TCS at ambient temperatures was accomplished. As mentioned earlier in context, only with the presence of PdNPs and hydrogen source, reduction reaction will happen. A timestamp tracing of daughter product was done to estimate the reduction path. As shown in Fig 5.10. From time 0, where the sample is as prepared TCS solution, shows a single peak at retention time of 10 mins, when sample was taken after 1 hour reaction, multiple peaks were observed. Since the coupling reaction is replacing the chlorine with hydrogen, three chlorines are on the molecular, from the multiple peaks of the chromatogram, we assume the chlorine atoms get removed one after another, not all together, therefore there is intermediate compound existing during the process. From the qualitative LC, attempts were made to detect daughter product using LC-MS analysis. Table 5.3 shows the

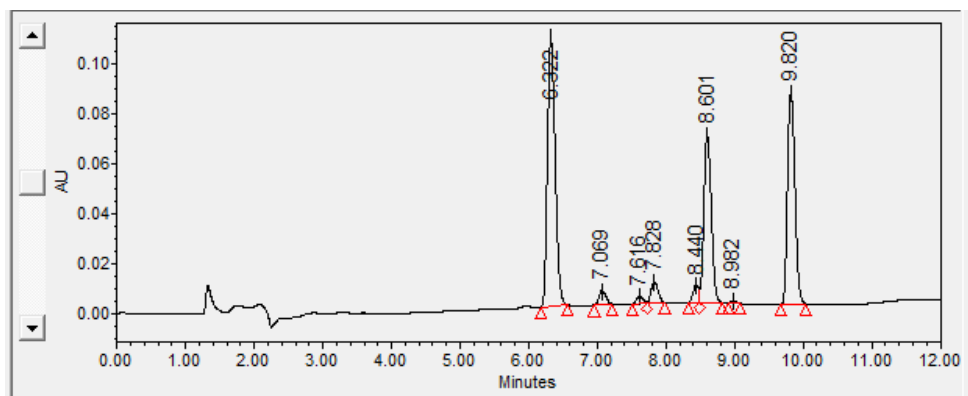
possible daughter product from dehalogenation. From Fig 5.10. we can see there are three neighboring peaks around 8.6 mins and 7.6 mins, there can be assigned to the diclosan and monoclosan due to both chemicals have three isomers, thus lead to three peaks in chromatogram. A typical MS chromatogram is shown in Fig 5.11, it can be seen from the LC-MS that throughout the whole degradation, all di-chloro and mono-chloro intermediates are detected. Also, the LC-MS matched well with the HPLC chromatogram, for example, 5.11a shows a LC-MS extracted from time 9.81 mins retention time, which corresponds to the HPLC peak in Fig 5.10, showing a molecular weight of 299.9 g/mol, similarly, 5.11b shows a extraction time at 8.6 mins, which corresponds to the three peaks in HPLC, which could be the isomers of diclosan. In this study, the LC-MS wasn't able to successfully detect the final product 2-phenoxyphenol, therefore analysis technique was switched to GC-MS and successfully detected the final product 3-phenoxyphenol, shown in Fig 5.10c. From the three HPLC peaks, there is significant evidence showing one isomer is the main intermediate, however, in this study, we are focusing on the hybrid catalyst capabilities of breaking down the triclosan compound, detailed structure study of intermediate isomers were not performed, which may require detailed NMR analysis.

Sample  
Time 0

### Liquid Chromatogram

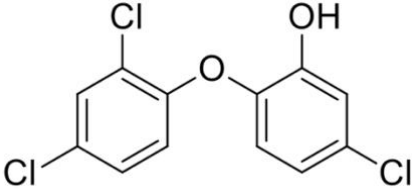
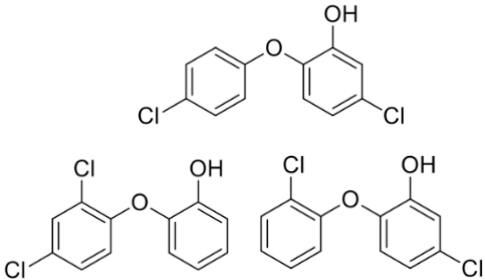
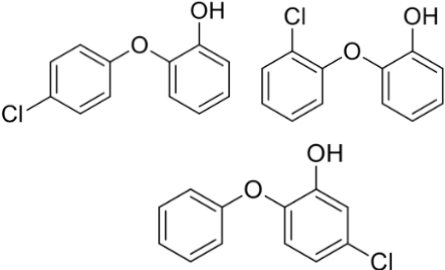
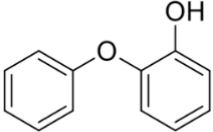
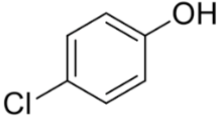


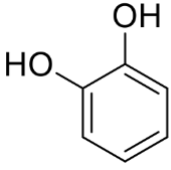
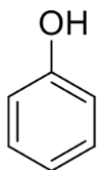
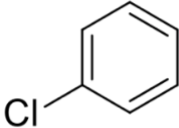
Time  
60mins



**Figure 5. 10 sample liquid chromatogram of TCS at different reaction time**

**Table 5. 3 Chemical information of Triclosan and Triclosan related daughter product**

Chemical information	Chemical structure
<p>Triclosan (Irgasan)            Formula: C<sub>12</sub>H<sub>7</sub>Cl<sub>3</sub>O<sub>2</sub>            IUPAC ID: 5-chloro-2-(2,4-dichlorophenoxy)phenol            Molecular Weight: 289.54</p>	
<p>Diclosan (Soneclosan)            Formula: C<sub>12</sub>H<sub>8</sub>Cl<sub>2</sub>O<sub>2</sub>            IUPAC ID: 5-chloro-2-(4-chlorophenoxy)phenol            Molecular Weight: 255.10</p>	
<p>Monoclosan            Formula: C<sub>12</sub>H<sub>9</sub>ClO<sub>2</sub>            IUPAC ID: 3-chlorobiphenyl-2,2'-diol            Molecular Weight: 220.65</p>	
<p><b>2-Phenoxyphenol</b>            Formula: C<sub>12</sub>H<sub>10</sub>O<sub>2</sub>            IUPAC ID: <b>2-Phenoxyphenol</b>            Molecular Weight: 186.21</p>	
<p>p-Chlorophenol  <b>Formula:</b> C<sub>6</sub>H<sub>4</sub>ClOH  <b>IUPAC ID:</b> 4-CHLOROPHENOL  <b>Molecular Weight:</b> 128.56</p>	

<p>Pyrocatechol  Formula: C<sub>6</sub>H<sub>6</sub>O<sub>2</sub>  IUPAC ID: 1,2-benzenediol  Molecular Weight: 110.11</p>	
<p>Phenol  Formula: C<sub>6</sub>H<sub>5</sub>OH  IUPAC ID: Hydroxybenzene  Molecular Weight: 94.11</p>	
<p>Chlorobenzene  Formula: C<sub>6</sub>H<sub>5</sub>Cl  IUPAC ID: Chlorobenzene  Molecular Weight: 112.55</p>	

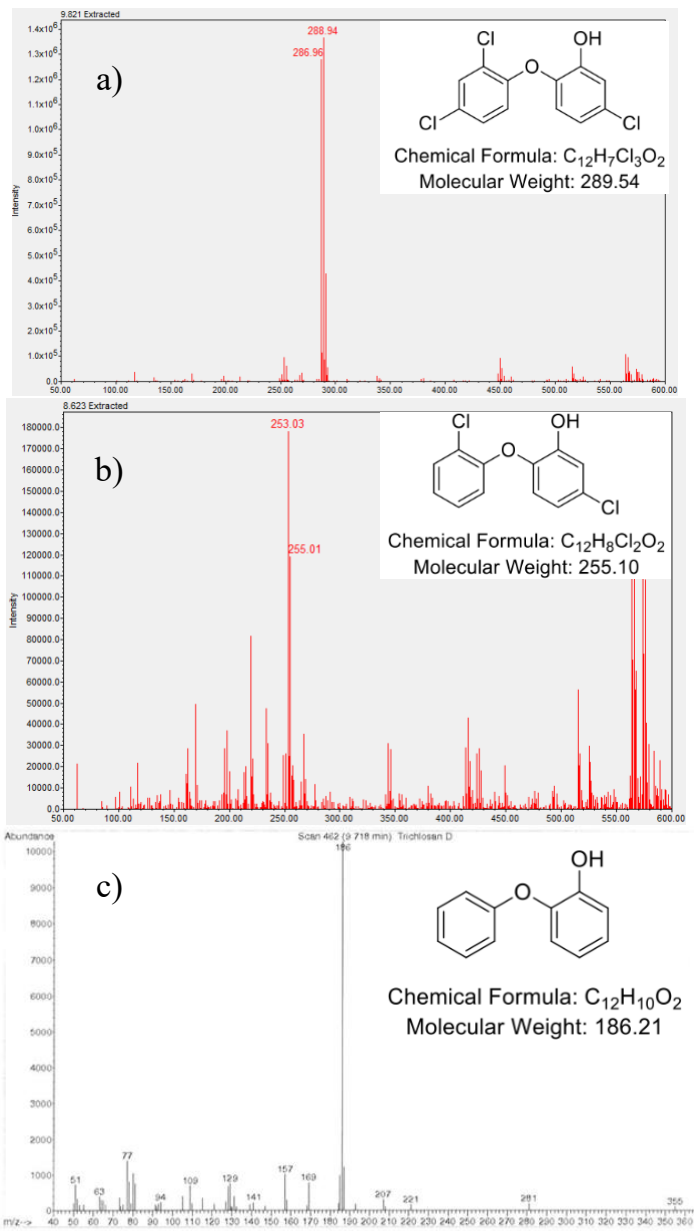


Figure 5. 11 Typical a,b) LC mass spectrum c) GC-MS acquired

Fig 5.12 shows a timestamp of the TCS degradation and intermediate/daughter product formation. From the timestamp curve (Fig 5.12) together with HPLC chromatogram (Fig 5.10), it can be seen that, before the reaction starts, the only compound detected is the triclosan itself, as the reaction starts, daughter product starts to form, chromatogram starts to change. As time passes, TCS goes through a gradual loss of chlorine one at a time, forming diclosan and monoclosan. Fig 5.12, the diclosan and monoclosan shows themselves peak at different reaction time, this can be explained as since the chlorine gets knocked out one at a time, diclosan was formed first and therefore peaked first. Soon, monoclosan becomes the major intermediate and peaks. At last, the sole peak in Fig 5.10 corresponds to the final product 2-Phenoxyphenol (purple line) in Fig 5.12, and all three chlorines were removed, it can be seen that from the beginning of the reaction and till the end, the amount of final product keeps increasing, and becomes the only remained compound after the degradation is accomplished, all reactant and intermediate were removed. A proposed pathway for the degradation of TCS is shown in Fig 5.11. As mentioned earlier, this pathway is limited since the focus of this study is on the material side but not on the chemistry side, detailed isomer ratio identification is required in order to establish a complete mechanism.

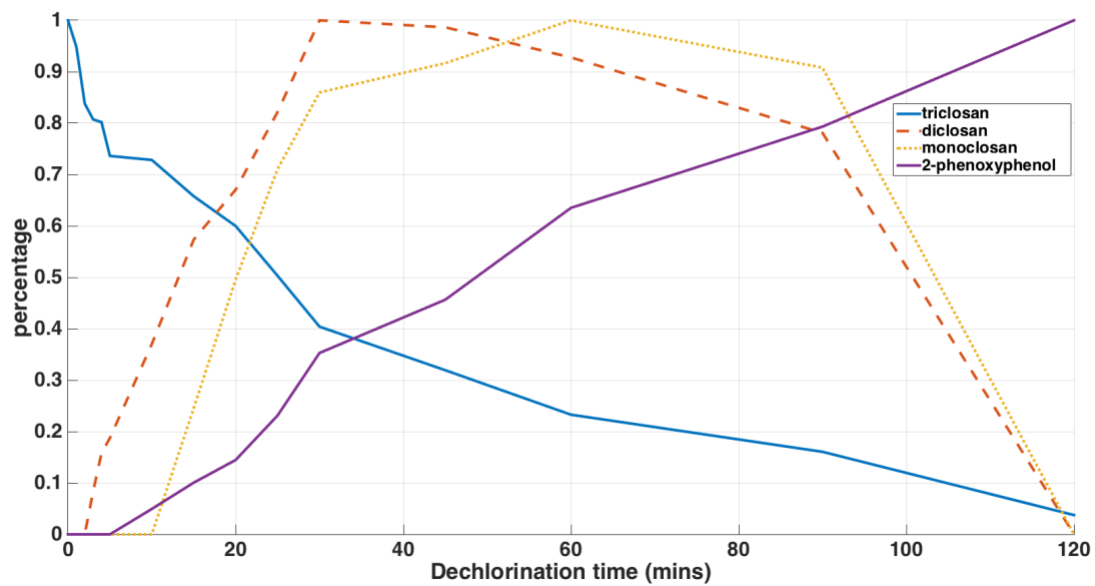


Figure 5.12 Triclosan dechlorination and daughter products formation curve

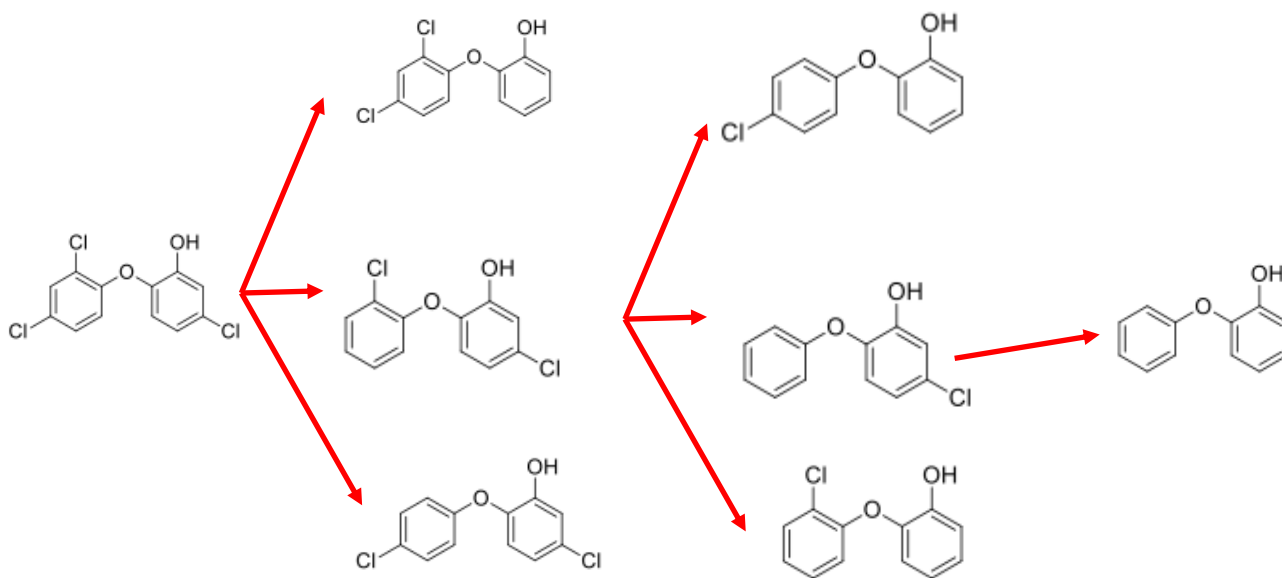


Figure 5.13 Proposed pathway of degradation

## 5.4. Conclusion

In this study, Pd-NPs were synthesized on vertically aligned carbon nanotubes attached to flexible carbon fiber cloth, forming a hierarchical architecture. Thermal oxidation of Pd-NPs in air forms oxidized palladium nanoparticles. XPS analysis shows that Pd-NPs were in metallic form, SEM shows an even distributed PdNPs attached to the CNTs. The palladium-based hierarchical structures were employed in water purification for removal of emerging contaminants, and triclosan was used as the model compound. The catalytic activity of this hybrid material was investigated, the result showing complete dechlorination of TCS. Compared with former studies, this new catalyst on hierarchical structures provides enhanced surface area and high efficiency. Therefore, this method provides a promising approach of creating robust material with the fully utilized surface and keeping the catalyst nanoparticles anchored onto the substrate from leaching into the environment. Moreover, this novel material shows higher efficiency and capabilities of contaminant removal. With its efficient, durable, environmental-friendly properties, it can be a future capable candidate for more hazardous contaminant and harsh environment.

## Chapter 6: Use porous carbon support for stimuli responsive composite

### 6.1 Introduction

Previous chapters, properties of CNTCFC hybrid material and the PdNP enhanced catalytic application were discussed. In reality, there are not only static water purification devices, but also dynamic scenario. In this case, fluid dynamics through the porous materials will be substantial [200]. Understanding of fluid flow in a confined area will therefore open the door to many real-world engineering and biological applications, such as petroleum engineering [201], catalyst carrier [202], ion transfer through ion channels [203,204], lubrication [205] etc. Fluid flow in confined area is determined by the pressure drop over a distance in the absence of gravity [206]. Darcy, H. (1856) was the first person described the fluid flow through porous structure [207]. He and Karumuri et al in this group connected the fluid flow behavior with CNT grafted RVC foam and CFC [208, 209]. It has been discovered the CNT grafted samples will be able to increase permeability of fluid (water in this case) flow by controlling the drag effect.

Smart polymers or stimuli-responsive polymers are macromolecules that can receive stimulus signals from environment, by making changes to their own molecular structure accordingly, and adjust into the environment [210, 211]. Such materials can be sensitive to different factors from environment, such as pH value,

temperature, humidity, light, gas or an electrical or magnetic field etc. Poly(N-isopropylacrylamide (PNIPAM) is one such smart polymer which responds to temperature by changing its size and volume [212, 213]. When heated in water above 32 °C, which is its reversible lower critical solution temperature (LCST), it goes through a phase transition from a swollen hydrated state to a shrunken dehydrated state. This occurs because of a coil-to-globule transition. At room temperature (or below LCST), fluid flow through PNIPAM will be hindered or even blocked since PNIPAM will stay at swollen phase, however, at elevated temperature (or above LCST), PNIPAM will shrink and therefore impose minimum impact on the liquid flow, since the reinforcement material is high porous (CFC or RVC), fluid will be free to pass.

PNIPAM polymer gels can be synthesized using the monomer, a cross –linking agent, an initiator, and a solvent through free radical crosslinking polymerization [214]. This gel, when infiltrated into the porous carbon substrates, composite is prepared. These composites will have different porosities above and below the Lower Critical Solution Temperature (LCST) and hence can act as “Smart Valves” only allowing water above the LCST to flow through. With the help of CNTs, the composite is supposed to possess superior qualities like higher strength, faster responsiveness etc. To understand the flow mechanism, a steady- state flow

experiment was conducted to demonstrate the relationship between pressure drop (resistance of the water flow from composite) to flow velocity, in order to understand how material influences the flow passing through it while surface modification was applied.

In this work, the goal is to incorporate stimuli responsive polymers, as matrix, into the porous 3D carbon structures to form a robust and highly temperature sensitive composite. We are also trying to investigate how CNT attached carbon substrate will influence the behavior of this composite.

## 6.2 Experimental

### 6.2.1 PNIPAM synthesis

The method used to prepare the PNIPAM gel is free radical crosslinking polymerization. One pot reaction is used. In this study, we are using PNIPAM as matrix to form composite. Two different porous carbon materials were chosen for composite: RVC foam and CFC, unfortunately, CFC material is not a good candidate for this “smart valve” system, since the PNIPAM wasn’t able to infiltrate only into the whole material but also stay on the surface, in another word, wrapping the material. Therefore, further experiment (flow test) was only carried out on the highly porous RVC counterpart (97% porosity).

There were certain differences in our method as compared to the method in reference [214]. They are as follows:

- Inert Gas used : Argon instead of Nitrogen (lab grade, 99.99% purity)
- Solvent Used : Ethyl Alcohol instead of 1,4- dioxane
- Duration of Polymerization : 4 hours instead of 2 hours

N-isopropylacrylamide is from , *N*-Isopropylacrylamide ( $\geq 99\%$ ) from Sigma-Aldrich. Ethyl alcohol used is lab grade, 200 proof, Fisher Scientific. 2,2’-

Azobis(2-methylpropionitrile), 98% from Sigma-Aldrich. N,N'-methylenebisacrylamide, 99% from Sigma Aldrich. Table 6.1 shows the chemicals used and their functions has been shown below:

**Table 6. 1 Parameters of polymerization**

<b>Chemical short name</b>	<b>Chemical full name</b>	<b>Function</b>
NIPAM	N-isopropylacrylamide	Monomer
MBAm	N,N'-methylenebisacrylamide	Cross-linking agent
AIBN	Azobisisobutyronitrile	Initiator of the free radical polymerization
Ethyl Alcohol	Ethyl Alcohol	Solvent

### 6.2.2 Background mathematical model and water filtration test

Darcy's law, as refined by Morris Muskat, of fluid permeability is given in equation 6.1 form based on the experimental observations [215,216].

$$Q = -\frac{kA}{\mu L} \Delta P \quad \dots \dots (6.1)$$

where Q is the volumetric flow rate in ml/min; k is the permeability in m<sup>2</sup>; A is the cross-section area of porous medium in m<sup>2</sup>; ΔP is the total pressure drop in Pa; L is the length of the sample in m, μ is the dynamic viscosity in Pa·s.

Proposed by Basak [217], there is flow regimes in porous media, moves from pre-laminar, laminar to turbulent as Reynolds number increases. Darcy's law is restricted to laminar flow, or viscous flow with low Reynolds number. A Forchheimer term (inertial term) was added to the Darcy's equation [218]. Therefore eqn 6.1 turns into eqn 6.2 as below:

$$\frac{\Delta P}{L} = -\frac{\mu}{k} q - \frac{\rho}{k'} q^2 \quad \dots \dots (6.2)$$

where k' is known as inertial permeability in m<sup>-1</sup>, q is the fluid velocity defined as the ratio of Q/A. ρ is the liquid density in kg/m<sup>3</sup>, all other parameters remain the same. The focus of this work is on the material property influence on the flow,

therefore, flow is experimentally fixed at the laminar zone (Darcy zone). Equation 6.3 below shows the Reynolds number in a pipe

$$Re = \frac{QD}{\mu A} \quad \dots \dots (6.3)$$

Where D is the diameter of the pipe in m, all other parameters remain the same. laminar flow occurs when  $Re < 2300$  and turbulent flow occurs when  $Re > 2900$  [219], since the sample in this experiment is using RVC foam with 11.5 mm in diameter. Therefore, the flow rate is controlled at  $Q < 11.43 \text{ m}^3/\text{s}$  ( $6.8 \cdot 10^8 \text{ ml/min}$ ), which in our experiment, the machine is not able to pass this flow rate, as a matter of fact all flows are treated as laminar flow.

The water filtration test is to measure the thermal responsiveness of polymer during water going through the carbon foam (RVC foam). Pressure difference is measured in order to monitor the process. The polymer is grafted on the porous carbon structure with or without CNT, the results are compared.

The water filtration test is to measure the thermal responsiveness of polymer during water going through the porous carbon material. Pressure difference is measured in order to monitor the process. The polymer is grafted on the RVC foam with or without CNT, the results are compared. Schematic illustration of the

in-house built pressure drop test setup is shown in Fig. 6.1. In this experiment, water volumetric flow rate ( $Q$ , ml/min) was controlled by master flex L/S (master flex 7518-10)] controller. A U-manometer was connected to the fluid with a T-connected on the plastic tube. Pressure drop was measured by the manometer at different flow rate. Pressure drop is tested in mm H<sub>2</sub>O (1 mm H<sub>2</sub>O = 9.8 Pa)

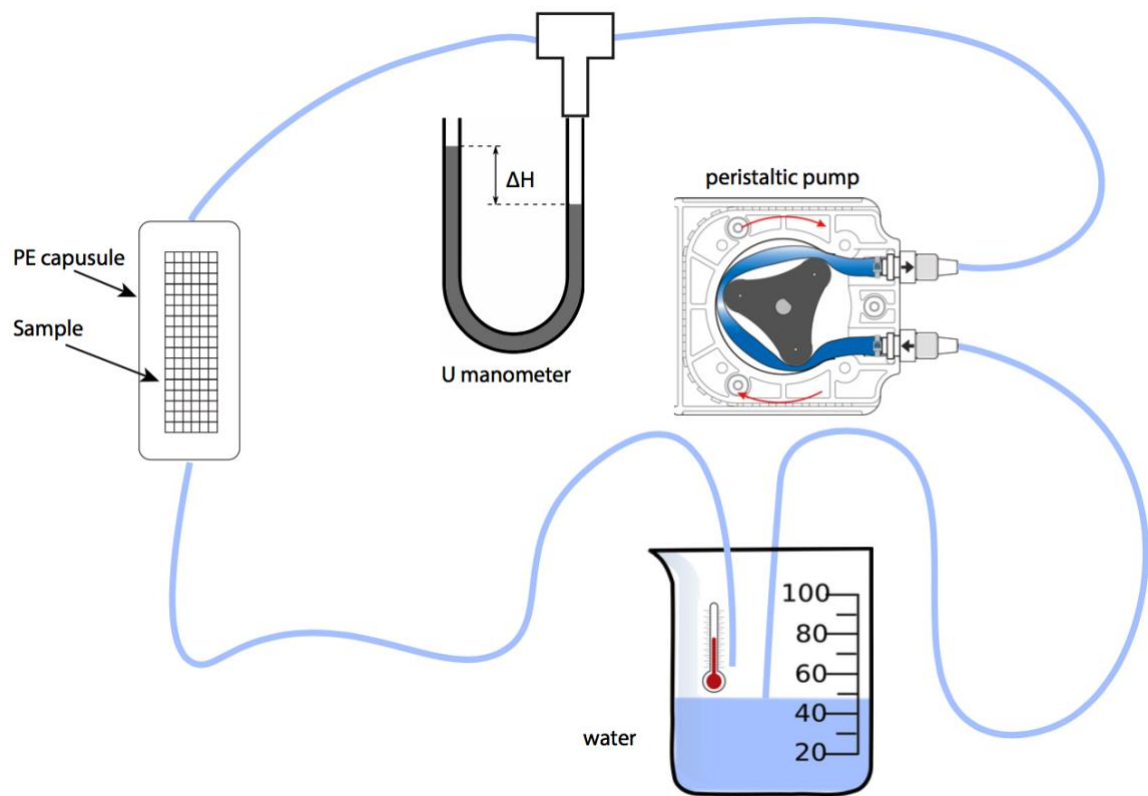


**Figure 6. 1 Schematic water flow set**

### 6.2.3 Mechanical strength measurement

Standard ASTM compression [220] test was performed on three samples; an as received RVC foam, a PNIPAM composite with CNT and a PNIPAM composite without CNT. The setup of the compression test has been shown in Fig 6.2. The setup applied a compressive force on the composite and measured the value of compressive stress as well as compressive strain. The setup had a load cell which reported the force and the distance moved by the load cell was used to compute the compressive strain.

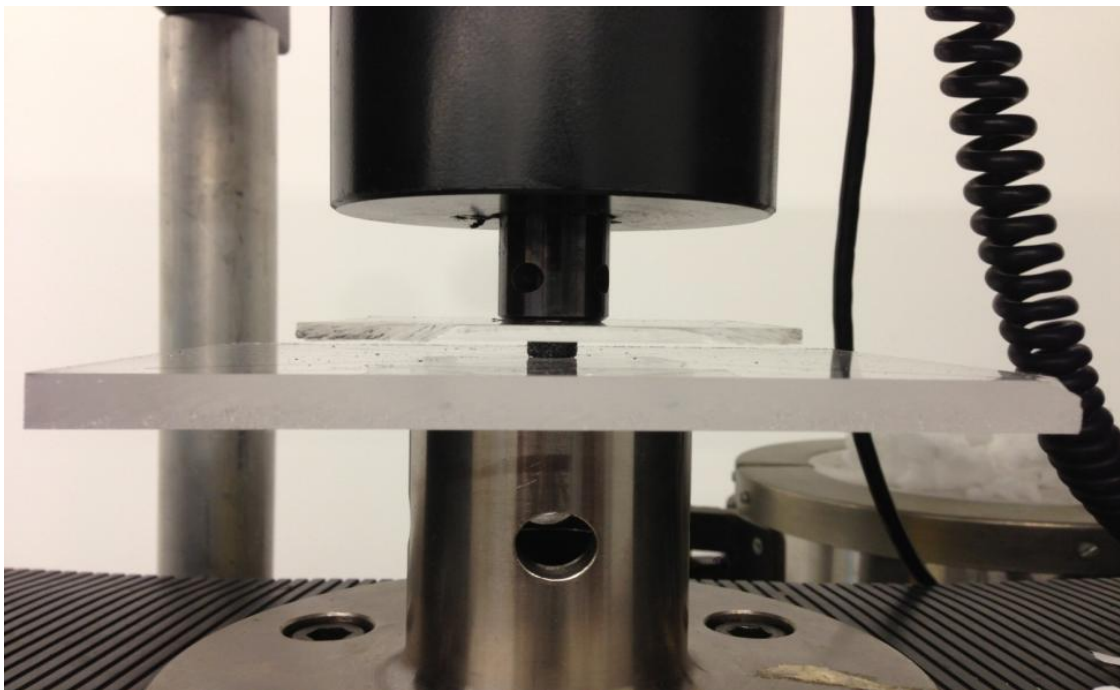
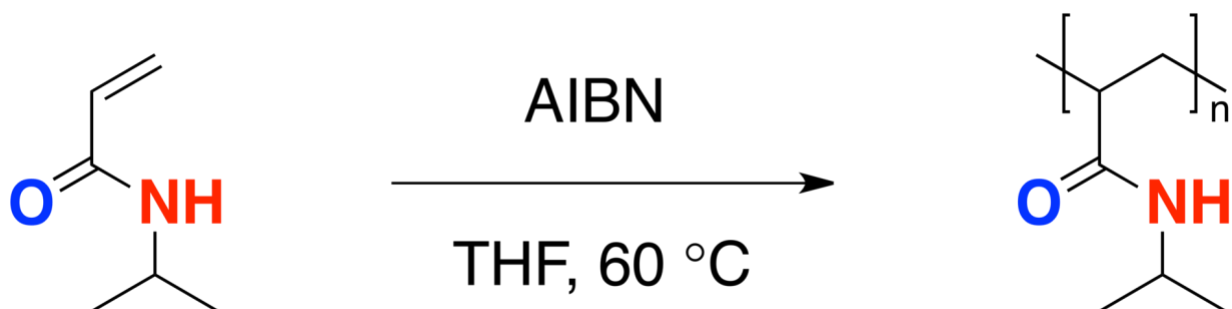


**Figure 6. 2 Setup for the compression test**

## 6.3 Results and discussion

### 6.3.1 Polymerization



PNIPAM carbon composite was successfully synthesized through a one-pot free radical reaction as mentioned earlier. After the polymer is synthesized, an optical microscope is used to check if the polymer has fully penetrated through the substrate and covers all empty pores of the RVC foam. As shown in Fig 6.3, the polymer has penetrated into the porous RVC foam completely, even sample was mechanically crushed, it still can be seen the polymer matrix is holding the foam strut.

Same polymerization synthesis on carbon fabric structure, unfortunately, the composite created was not be able to function as a thermal responsive valve but a structural composite. Therefore, further detailed tests were focused on the RVC foam structure only. In order to further understand the synthesis process, mass measurement was compared, result is shown in table 6.1. There is significant

evidence that with the growth of CNT on the RVC foam, the amount (mass) of PNIPAM hydrogel is increased, which means better polymer permeation inside the support, which will consequently affect the thermal responsiveness of the composite itself, as well as the mechanical property of the composite. Since the composite was used in water flow test next, wet weight was measured.

A simple temperature responsiveness test is done in order to check the PNIPAM behavior. Shown in Fig 6.4. Apparently, PNIPAM crosslinks when temperature reaches 39 degrees C, which is its lower critical solution temperature (LCST). Polymer under LCST is behaving a transparent hydrogel form, which means the majority of the polymer is at amorphous state, as soon as the temperature passes PNIPAM's LCST, the polymer is not providing transparency property, which attributed to the increasing crystallinity of the polymer.

**Table 6. 2 Mass measurement comparisons of composite of different support**

	Pristine RVC foam	CNT grafted RVC foam
Mass before polymerization (g)	0.0234	0.0263
Mass after polymerization and hydrated (g)	0.5264	0.6347
Weight change (%)	2149.6%	2313.3%

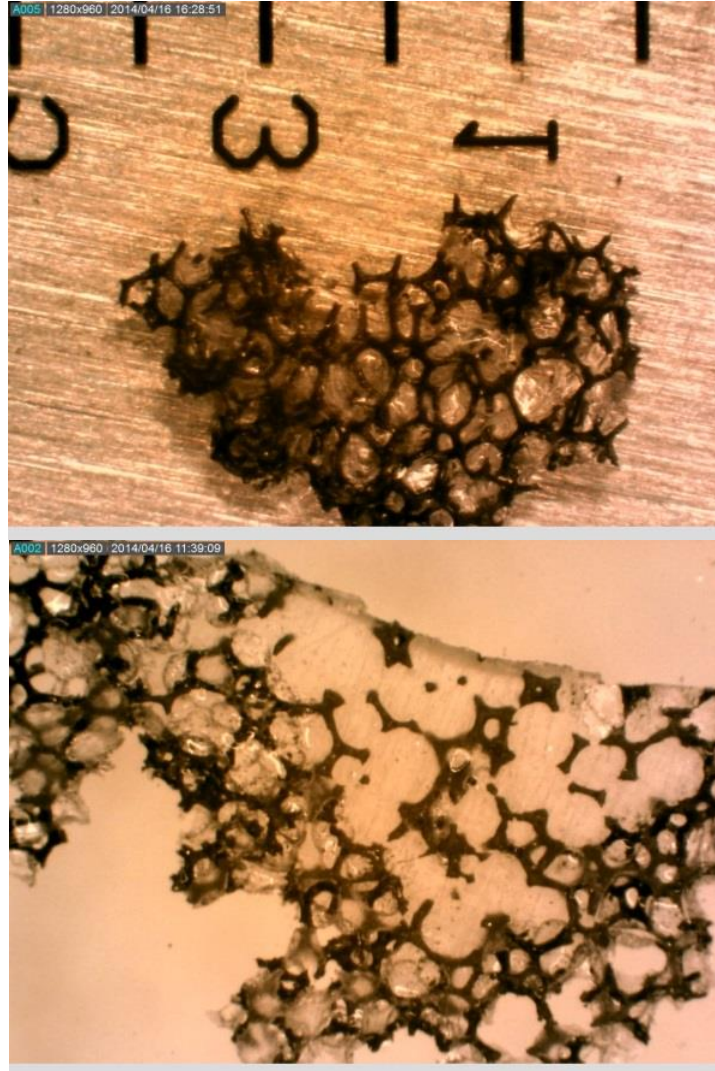


**Figure 6. 3 Optical microscopy image of RVC foam with polymer infiltrated**



**Figure 6. 4 Composite response to temperature a)below LCST b) above LCST**

### 6.3.2 Fluid flow test

Firstly, a constant flow rate ( $Q = 100 \text{ ml/min}$ ) is applied to the flow set. In this case, PNIPAM-RVC sample was used for the thermal response of the composite. The pressure change in manometer was plotted against temperature, shown in Fig 6.5. It is clear that the PNIPAM-RVC sample was behaving drastically different as the temperature was cooled down by adding tap water into the water reservoir. As the temperature drops, the coil-globule transition starts to happen, and the crosslinked PNIPAM gradually swells into the hydrogel form, which is proven by the increasing pressure change in the tube. The larger pressure change means the gradual “close down” of the pores on the RVC foam and vice versa.

In order to see the detailed behavior of the composite with different composition at different flow rate, two sets of tests were conducted. At room temperature ( $20 \text{ }^{\circ}\text{C}$ ), the behavior of different samples at different flow rate is shown in Fig 6.6. It can be easily noticed as the flow rate increases, polymer samples have a drastic pressure build-up, beyond  $50 \text{ H}_2\text{O}$ , the detection limit of manometer is reached, therefore no more data points could be collected. This is because at room temperature, PNIPAM stayed at expanded coil state, all pores on RVC and CNTRVC samples are closed. No water could be able to pass through the valve. The orange dashed line and green dotted are representing the CNTRVC and

pristine RVC samples, respectively. It can be also observed the both samples are showing a linear pattern of the pressure drop as a function of time, which has good agreement with Darcy's law at laminar flow region. One thing needed to be point out is the CNTRVC sample has a higher pressure drop than its counterpart (pristine RVC), this is the due to the porosity reduction by CNT attachment.

On the other hand, at elevated temperature (50 °C), 4 samples: RVC, CNT-RVC, PNIPAM-RVC, PNIPAM-CNT-RVC were studied and result is plotted in Fig 6.7. It can be seen all 4 samples are having a similar linear pattern as the flow rate increases, because PNIPAM is above its LCST, the whole structure is no longer at expanded coil state but at contracted globule state. According to Darcy's law, permeability's reciprocal is a linear to the pressure drop. Linear fitting is applied to all sets of data. Corresponding permeability is calculated based on equation 6.1, results are shown in Table 6.3 below. Obviously, the RVC media has the best permeability due to its large porosity, and PNIPAM-CNT-RVC sample has the lowest permeability due to the crosslinked polymer is attached to the CNTs throughout the whole material. CNT-RVC and PNIPAM-RVC samples have similar permeability, but still the polymer sample is providing slightly higher number, this can be from either experiment error or, the crosslinked polymer gel is

soft comparing with the rigid CNTs which could providing larger fluid channels for the water, an analogue to the half-closed door.

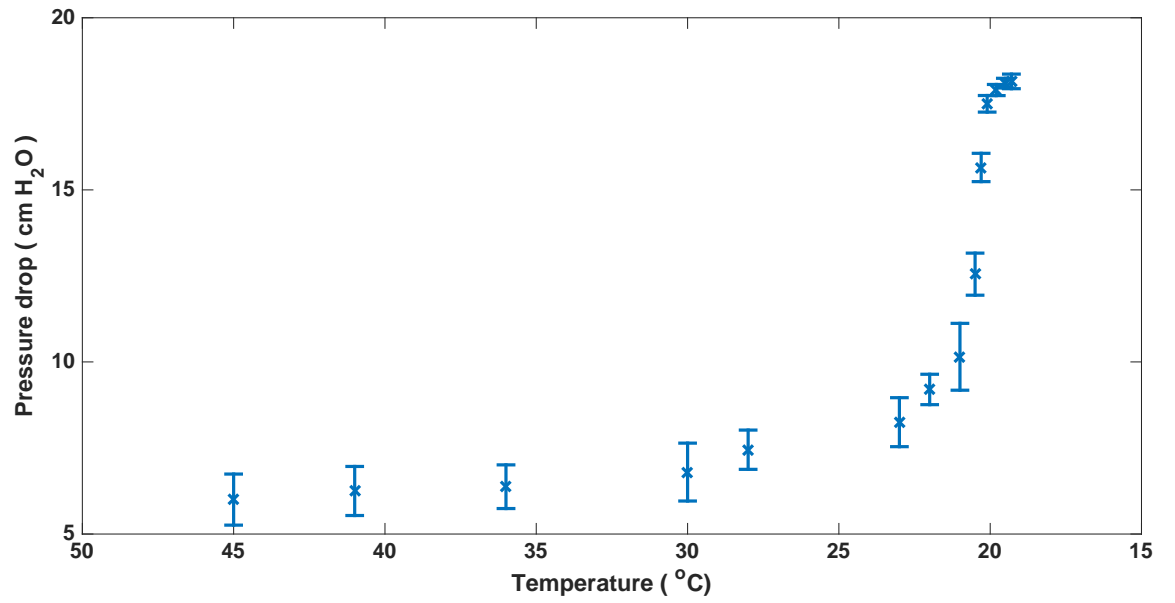


**Figure 6. 5 Thermosensitive valve response on the temperature of constant rate water flow**

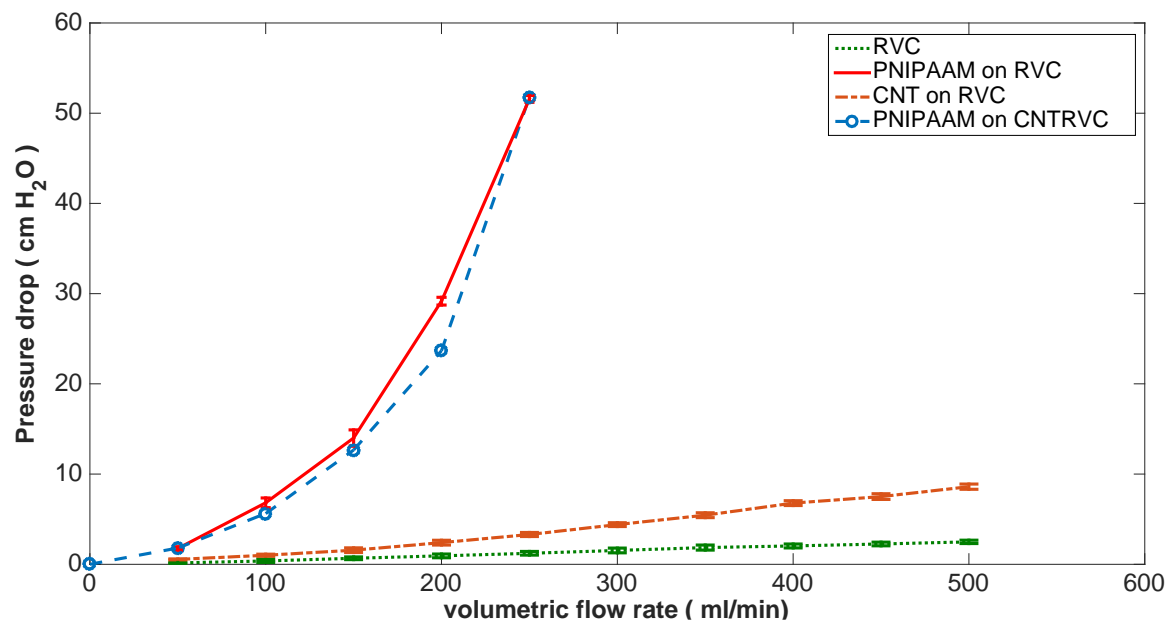


**Figure 6. 6 Pressure drop as a function of volumetric flow rate at room temperature**

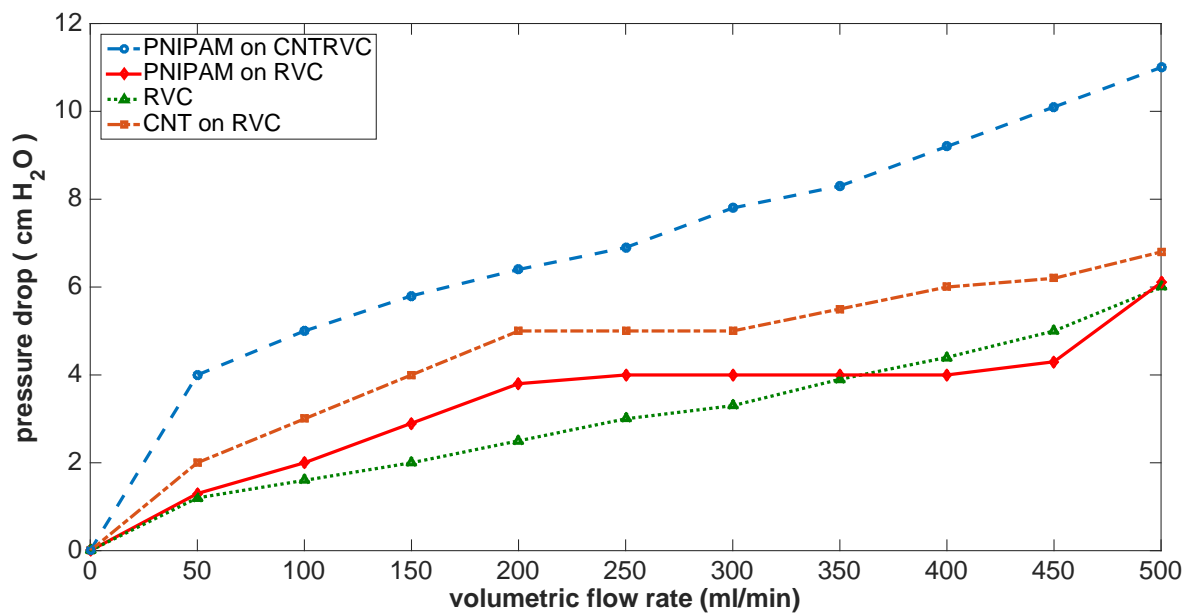


**Figure 6. 7 Pressure drop as a function of volumetric flow rate at elevated temperature (50 °C)**

**Table 6. 3 Permeability of different materials**

Sample	Fitted linear coefficient	Calculated permeability (m <sub>2</sub> )
RVC	0.0093	107.53
CNT-RVC	0.0114	87.72
PNIPAM-RVC	0.0106	94.34
PNIPAM-CNT-RVC	0.0179	52.63

#### 6.3.4 Mechanical testing

From the compression test, stress vs strain curve was plotted from three different samples: pristine RVC, PNIPAM-RVC composite and PNIPAM-CNTRVC composite, shown in Fig 6.8. This curve clearly shows that the mechanical strength of the composite with CNT is greater than the composite without CNT, which in turn both composites exhibit much greater compressive strength than the that of as received RVC foam. RVC foam shows an ultimate compressive strength around 160 kPa and fractured, with 5% deformation. Meanwhile, the both composites didn't fracture up to 30% strains. It can be seen than the CNT attached composite has a very high modulus from the elastic zoom, for 10% deformation, CNT attached composite requires a stress around 250 kpa while the RVC only composite only takes 150 kPa, this is significant evidence that the integrity of the composite will hold better if CNT was introduced to the system, which can be explained as via the introduction of CNT, the interfacial strength and toughness at the phase boundaries between the matrix and reinforcement material is improved, this agrees with previous work from Karumuri *et al* [221].

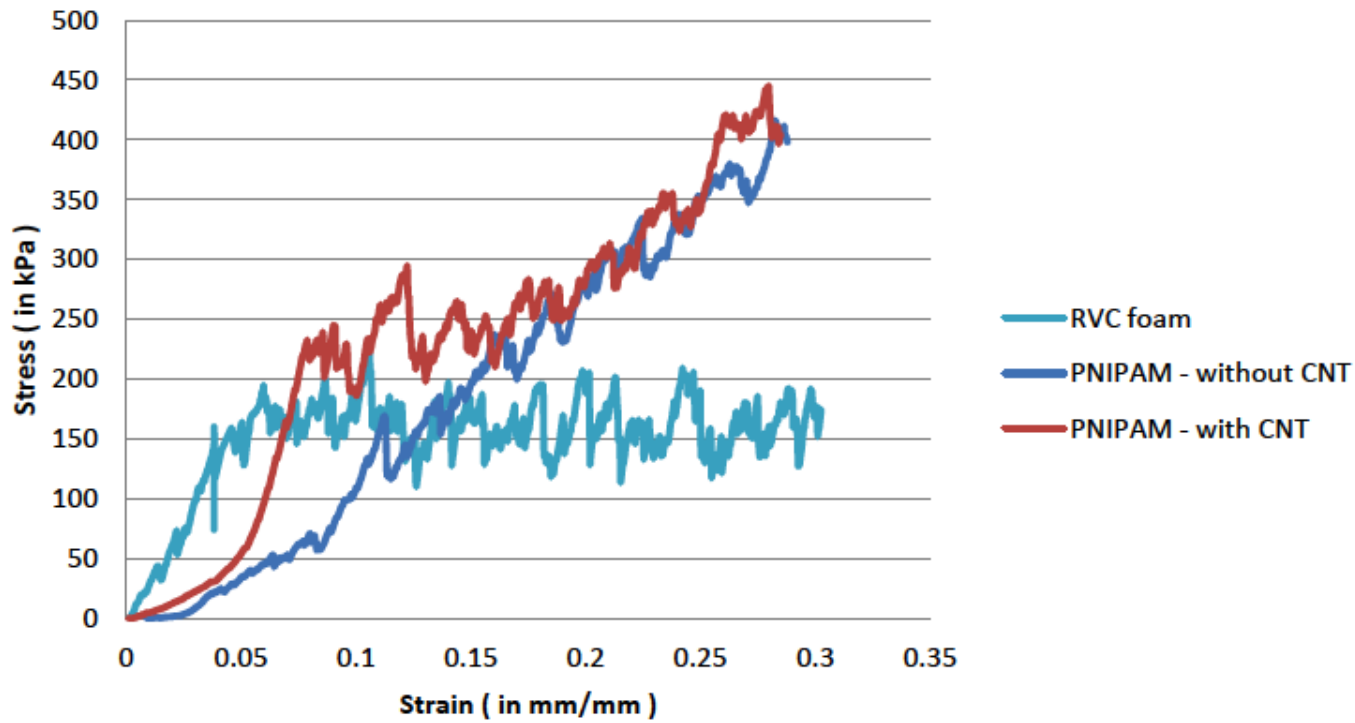


**Figure 6. 8 Stress-strain curve from a uniaxial compression test on foam samples.**

## 6.4 Conclusion

Temperature responsive polymer, PNIPAM (Poly(N-isopropylacrylamide)) was prepared on carbon substrates to form composites. The carbon substrates used were either as received RVC (Reticulated Vitreous Carbon ) foam or CNT(carbon nanotubes ) grafted RVC foam. Preliminary tests were conducted to measure the strength, thermal responsiveness and polymer retention of the two composites and the results showed that the CNT grafted RVC foam had superior strength, faster thermal response and greater polymer retention (further tests are required to confirm these facts). These composites were tested for their application as “Smart Valves” which allow water only above a particular temperature to pass through them. Additional tests are needed for the detailed mechanism.

## Summary

In this dissertation, the research interest lies on the investigation of a novel functional hierarchical material for next generation fluid purification devices. Flexible and porous woven carbon fiber cloth was used to fabricate hierarchical structure by grafting carbon nanotubes (CNTs) via a two-step chemical vapor deposition technique. Nanotubes were successfully grown on to the 2D networking woven fiber cloth, using optimized CNT growth parameters from previous studies. In depth investigation of surface properties of these types of hierarchical materials were performed. Longer CVD runtime will linearly increase the CNT carpet length. This type of hierarchical morphology provides the capability of increasing surface area by several orders of magnitude, as well as tuning the morphology for targeted applications by varying the growth time of the CNT array. Analytical model using surface morphologies to estimate the specific surface area (SSA) of CNT arrays on porous structures were developed using input from two experimental methods: microstructural analysis and weight gain method. It was seen that SSA can indeed be tuned by this process, and several orders of magnitude increase is possible. The SSA increase matches well with BET measurements and reported surface adsorption data, indicating that the surface functionality of individual nanotubes are retained in this multiscale architecture.

Moreover, the good agreement of those two methods can bring confident estimation of the future properties of the material.

The surfaces were modified with silicon oxide coatings via sol gel method using a silica precursor solvent. Secondary, microstructural analysis, and spectroscopic studies showed that the individual CNT were indeed coated with amorphous silica. The layers are not very uniform, however, and there is scope for future improvement to control coating uniformity. Water contact angle measurements were made to understand the wettability and water permeation behavior of these surface modified materials. It was seen that those surface modification techniques can tune the material from hydrophobic to hydrophilic back and forth.

An engineering property that will depend on surface-liquid interaction is water flow. A stimuli-responsive polymer PolyN-isopropylacrylamide (PNIPAm) was prepared via polymerization on the CNT grafted RVC foam. Preliminary tests were conducted to measure the strength, thermal responsiveness and polymer retention of the two composites and the results showed that the CNT grafted RVC foam had superior strength, faster thermal response and greater polymer retention (further tests are required to establish these facts). These composites were tested for their application as “Smart Valves” which allow water only above a particular temperature to pass through them.

CNT grafted carbon fiber cloth was further functionalized with palladium nanoparticles(Pd-NPs) capable of organic pollutant removal and water purification. SEM, XPS, EDS analysis were applied indicating the Pd-NPs were evenly deposited with complete coverage. This palladium modified hierarchical structures were further employed in removal of model organic contaminant triclosan. With the presence of hydrogen source, the reduction Dechlorination reacts rapidly. Kinetic studies and daughter product identification was done showing dechlorination was complete.

The catalyst particles on the hierarchical structures can provide very high surface activity from a compact material. This study therefore shows that anchoring carbon nanotube carpets on woven fiber cloth substrates may be a very promising approach to create flexible solid devices that fully utilize the surface area benefits of carbon nanotubes without dispersing loose nanomaterials into the environment. This flexible architecture proves to be effective for water purification, which makes it reusable and eco-friendly as the nanoscale particles and CNT are immobilized on larger porous supports.

## Future work

During the research investigation, issues had been discovered in some areas.

There are portions of study can follow up this investigation are mentioned below:

- Stimuli-responsive polymer and carbon materials incorporation, in this study only preliminary studies have been accomplished showing the possibilities of “smart composite”. Due to the advantageous properties such as lightweight but high strength of CNTCFC hybrid material, if the infiltration and dispersion issues are solved, a flexible stimuli responsive composite is possible.
- Palladium hydrogen absorbing and storage abilities can be explored further. This work has shown the excellent capabilities of Pd catalytic activity for chlorinated emerging contaminants, tougher compounds such as fluorinated chemical (Perfluorooctanoic acid, PFOA) could be considered.
- CNT has shown itself a good candidate for nanoparticle supports, different nanoparticles could be synthesized and assembled onto this robust hybrid material for specific application, especially a surface sensitive application is desired. This CNTCFC hybrid material could be a solid support for chemical sensors and biosensors.

## Reference

- [1] Li, H., Eddaoudi, M., O'Keeffe, M. & Yaghi, O. M. Design and synthesis of an exceptionally stable and highly porous metal-organic framework. *Nature* **402**, 276–279 (1999)
- [2] Davis, M. “Ordered porous materials for emerging applications.” *Nature* **417**, 813–821 (2002)
- [3] Peter Fratzl., Richard Weinkamer. “Nature’s hierarchical materials, Progress in Materials Science”, Volume 52, Issue 8, November 2007, Pages 1263-1334
- [4] L.J. Gibson, M.F. Ashby. Cellular solids, structure and properties (2nd ed.), Cambridge University Press, Cambridge (1999), p. 510
- [5] D.A. Tirrell. Hierarchical structures in biology as a guide for new materials technology, National Academy Press, Washington (1994), p. 130
- [6] Christopher M. A. Parlett, Karen Wilson and Adam F. Lee, “Hierarchical porous materials: catalytic applications” ,*Chem. Soc. Rev.*, 2013,42, 3876-3893
- [7] Tang, Z. K. et al. Superconductivity in 4 Å single-walled carbon nanotubes. *Science* **292**, 2462–2465 (2001)

- [8] Joo, S. H. et al. Ordered nanoporous arrays of carbon supporting high dispersions of platinum nanoparticles. *Nature* **412**, 169–172 (2001)
- [9] Pop M, Kosack DS, Salzberg SL., “Hierarchical scaffolding with Bambus”, *Genome Res.* 2004 Jan;14(1):149-59.
- [10] Oxana V. Kharissova, Boris I. Kharisov, “Variations of interlayer spacing in carbon nanotubes”, *RSC Adv.*, 2014,**4**, 30807-30815
- [11] Yahachi Saito, Tadanobu Yoshikawa, Shunji Bandow, Masato Tomita, and Takayoshi Hayashi, “Interlayer spacings in carbon nanotubes”, *Phys. Rev. B* 48, 1907, Jul 1993
- [12] Iijima, S. “Helical microtubules of graphitic carbon.” *Nature* **354**, 56–58 (1991).
- [13] M. Endo, S. Iijima, and M. S. Dresselhaus, *Carbon Nanotubes*, 1st ed. Pergamon, 1996.
- [14] Yao, M.; Liu, B.; Zou, Y.; Wang, L.; Li, D.; Cui, T.; Zou, G.; Sundqvist, B. Synthesis of singlewall carbon nanotubes and long nanotube ribbons with Ho/Ni as catalyst by arc discharge. *Carbon* 2005, 43, 2894–2901.

- [15] Yang, L.C.; Shi, Y.; Gao, Q.S.; Wang, B.; Wu, Y.P.; Tang, Y. The production of carbon nanospheres by the pyrolysis of polyacrylonitrile. *Carbon* 2008, 46, 1816–1818.
- [16] Azami, T.; Kasuya, D.; Yoshitake, T.; Kubo, Y.; Yudasaka, M.; Ichihashi, T.; Iijima, S. Production of small single-wall carbon nanohorns by CO<sub>2</sub> laser ablation of graphite in Ne-gas atmosphere. *Carbon* 2007, 45, 1364–1369.
- [17] Hsu, W.K.; Hare, J.P.; Terrones, M.; Kroto, H.W.; Walton, D.R.M.; Harris, P.J.H. Condensed-phase nanotubes. *Nature* 1995, 377, 687.
- [18] Matveev, A.T.; Golberg, D.; Novikov, V.P.; Klimkovich, L.L.; Bando, Y. Synthesis of carbon nanotubes below room temperature. *Carbon* 2001, 39, 155–15.
- [19] Qian, H.; Han, F.; Zhang, B.; Guo, Y.; Yue, J.; Peng, B. Non-catalytic CVD preparation of carbon spheres with a specific size. *Carbon* 2004, 42, 761–766
- [20] Mori, S.; Suzuki, M. Catalyst-free low-temperature growth of carbon nanofibers by microwave plasma-enhanced CVD. *Thin Solid Films* 2009, 517, 4264–4267.

- [21] A. Yokoyama, M. Yoshida, A. Ishii, Y. K. Kato, “Giant circular dichroism in individual carbon nanotubes induced by extrinsic chirality”, *Phys. Rev. X* 4, 011005 (2014).
- [22] L. Yuan et al., “Ethylene flame synthesis of well-aligned multi-walled carbon nanotubes”, *Chemical Physics Letters*, Volume 346, Issues 1–2, 28 September 2001, Pages 23-28
- [23] Liming Yuan, Tianxiang Li, Kozo Saito. “Synthesis of multiwalled carbon nanotubes using methane/air diffusion flames”, *Proceedings of the Combustion Institute*, Volume 29, Issue 1, 2002, Pages 1087-1092
- [24] Mei Zhang, Jian Li, “Carbon nanotube in different shapes”, *Materials Today*, Volume 12, Issue 6, June 2009, Pages 12-18
- [25] Sigeo Ihara, Satoshi Itoh, and Jun-ichi Kitakami, “Helically coiled cage forms of graphitic carbon”, *Phys. Rev. B*, vol 48, pp. 5643, August 1993
- [26] C. Dekker, “Carbon Nanotubes As Molecular Quantum Wires,” *Phys. Today*, vol. 52, no. 5, p. 22, 1999

[27] Min Ouyang, Jin-Lin Huang, Charles M. Lieber, “Fundamental Electronic Properties and Applications of Single-Walled Carbon Nanotubes”, *Acc. Chem. Res.* 2002, 35, 12, 1018-1025

[28] Wenzhong Tang, Michael H Santare, Suresh G Advani. “Melt processing and mechanical property characterization of multi-walled carbon nanotube/high density polyethylene (MWNT/HDPE) composite films”, *Carbon*, Volume 41, Issue 14, 2003, Pages 2779-2785

[29] Wei Zhang, Zhiyuan Zhu, Feng Wang, Tingtai Wang, Litao Sun and Zhenxia Wang, “Chirality dependence of the thermal conductivity of carbon nanotubes”, *Nanotechnology* 15 (2004) 936–939

[30] George E. Froudakis, “Hydrogen storage in nanotubes & nanostructures”, *Materials Today*, Volume 14, Issues 7–8, July–August 2011, Pages 324-328

[31] Hirohiko Murakami, Masaaki Hirakawa, Chiaki Tanaka, and Hiroyuki Yamakawa, “Field emission from well-aligned, patterned, carbon nanotube emitters”, *Appl. Phys. Lett.* 76, 1776 (2000)

[32] Shenghong Yao, Jinkai Yuan, Hasanal Mehedi, Etienne Gheeraert, Alain Sylvestre, “Carbon nanotube forest based electrostatic capacitor with excellent dielectric performances”, *Carbon*, Volume 116, May 2017, Pages 648-654

- [33] Y.M.Wong, W.P.Kang, J.L.Davidson, A.Wisitsora-at, K.L.Soh, “A novel microelectronic gas sensor utilizing carbon nanotubes for hydrogen gas detection”, *Sensors and Actuators B: Chemical*, Volume 93, Issues 1–3, 1 August 2003, Pages 327-332
- [34] Zhu Z, “An Overview of Carbon Nanotubes and Graphene for Biosensing Applications”, *Nanomicro Lett.* 2017;9(3):25
- [35] Liubing Dong, Feng Hou, Yang Li, Lei Wang, Hongxu Gao, Yanlong Tang, “Preparation of continuous carbon nanotube networks in carbon fiber/epoxy composite”, *Composites: Part A* 56 (2014) 248–255
- [36] T.W.Ebbesen, H.Hiura, J.Fujita, Y.Ochiai, S.Matsui, K.Tanigaki, “Patterns in the bulk growth of carbon nanotubes”, *Chemical Physics Letters*, Volume 209, Issues 1–2, 25 June 1993, Pages 83-90
- [37] J.-P. Salvetat, G. A. D. Briggs et al, “Elastic and Shear Moduli of Single-Walled Carbon Nanotube Ropes”, *Phys. Rev. Lett.* 82, 944-947, 1999
- [38] M Terrones, “Science and Technology of the Twenty-First Century: Synthesis, Properties, and Applications of Carbon Nanotubes”, *Annu. Rev. Mater. Res.* 2003. 33:419–501

- [39] Treacy, M., Ebbesen, T. & Gibson, J. “Exceptionally high Young's modulus observed for individual carbon nanotubes.” *Nature* 381, 678–680 (1996).
- [40] Eric W. Wong, et al, “Nanobeam Mechanics: Elasticity, Strength, and Toughness of Nanorods and Nanotubes”, *Science* 277, 1971 (1997);
- [41] J. P. Lu, “Elastic Properties of Carbon Nanotubes and Nanoropes”, *Phys. Rev. Lett.* 79(7), 1297-1300 (1997)
- [42] Zhou Xin, Zhou Jianjun, and Ou-Yang Zhong-can, “Strain energy and Young’s modulus of single-wall carbon nanotubes calculated from electronic energy-band theory”, *Phys. Rev. B* 62, 13692 –, 2000
- [43] Hu, J., Ouyang, M., Yang, P. et al. “Controlled growth and electrical properties of heterojunctions of carbon nanotubes and silicon nanowires”, *Nature* **399**, 48–51 (1999).
- [44] Dai, H., Wong, E. W. & Lieber, C. M. “Probing electrical transport in nanomaterials: conductivity of individual carbon nanotubes”, *Science* **272**, 523–526 (1996).
- [45] Hong, S., Myung, S. “A flexible approach to mobility”. *Nature Nanotech* 2, 207–208 (2007)

[46] Ernesto Joselevich and Charles M. Lieber, “Vectorial Growth of Metallic and Semiconducting Single-Wall Carbon Nanotubes”, *Nano Letters* 2002 2 (10), 1137-1141

[47] M. S. Saito, R., Fujita, M., Dresselhaus, G., Dresselhaus, “Electronic structure of chiral graphene tubules,” *Appl. Phys. Lett.*, vol. 60, no. 18, pp. 2204–2206, 1992.

[48] Qingfeng Liu, Wencai Ren, Zhi-Gang Chen, Lichang Yin, Feng Li, Hongtao Cong, Hui-Ming Cheng. “Semiconducting properties of cup-stacked carbon nanotubes”, *CARBON* 47 (2009) 731 – 736

[49] Debjit Chattopadhyay, Izabela Galeska and Fotios Papadimitrakopoulos, “A Route for Bulk Separation of Semiconducting from Metallic Single-Wall Carbon Nanotubes”, *J. Am. Chem. Soc.* 2003, 125, 11, 3370-3375

[50] Zhihong Chen, Xu Du, Mao-Hua Du, C. Daniel Rancken, Hai-Ping Cheng, and Andrew G. Rinzler, “Bulk Separative Enrichment in Metallic or Semiconducting Single-Walled Carbon Nanotubes”, *Nano Lett.*, Vol. 3, No. 9, 2003, 1245-1249

[51] Hiroshi Ajiki, Tsuneya Ando, “Energy Bands of Carbon Nanotubes in Magnetic Fields”, *J. Phys. Soc. Jpn.* 65, pp. 505-514 (1996)

[52] Uhland Weissker, Silke Hampel, Albrecht Leonhardt and Bernd Buchner, “Carbon Nanotubes Filled with Ferromagnetic Materials”, *Materials* 2010, 3, 4387-4427;

[53] Andrea Masotti<sup>1</sup>, Andrea Caporali, “Preparation of Magnetic Carbon Nanotubes (Mag-CNTs) for Biomedical and Biotechnological Applications”, *Int J Mol Sci.* 2013 Dec; 14(12): 24619–24642.

[54] Atsushi Nagata, Hideki Sato, Yusuke Matsui, Tetsuya Kaneko, Yuji Fujiwara, “Magnetic properties of carbon nanotubes filled with ferromagnetic metals”, *Vacuum*, Volume 87, January 2013, Pages 182-186

[55] Jie Li, Changlun Chen, Shouwei Zhanga and Xiangke Wang, “Surface functional groups and defects on carbon nanotubes affect adsorption–desorption hysteresis of metal cations and oxoanions in water”, *Environ. Sci.: Nano*, 2014,1, 488-495

[56] Y H Li et al, “Carbon nanotubes - the promising adsorbent in wastewater treatment”, 2007 *J. Phys.: Conf. Ser.* 61 140

[57] Liheng Xu, Jinye Li, and Ming Zhang, “Adsorption Characteristics of a Novel Carbon-Nanotube-Based Composite Adsorbent toward Organic Pollutants”, *Ind. Eng. Chem. Res.* 2015, 54, 8, 2379-2384

- [58] Bo Pan and Baoshan Xing, “Adsorption Mechanisms of Organic Chemicals on Carbon Nanotubes”, *Environ. Sci. Technol.* 2008, 42, 24, 9005-9013
- [59] Daohui Lin and Baoshan Xing, “Adsorption of Phenolic Compounds by Carbon Nanotubes: Role of Aromaticity and Substitution of Hydroxyl Groups”, *Environ. Sci. Technol.* 2008, 42, 19, 7254-7259
- [60] Yanqing Wang, Can Pan, Wei Chu, Adavan Kiliyankil Vipin, and Ling Sun, “Environmental Remediation Applications of Carbon Nanotubes and Graphene Oxide: Adsorption and Catalysis”, *Nanomaterials* 2019, 9(3), 439
- [61] Chungsyng Lu, Fengsheng Su, “Adsorption of natural organic matter by carbon nanotubes”, *Separation and Purification Technology*, Volume 58, Issue 1, 1 December 2007, Pages 113-121
- [62] Yan-Hui Li, Shuguang Wang, Zhaokun Luan, Jun Ding, Cailu Xu, Dehai Wu, “Adsorption of cadmium(II) from aqueous solution by surface oxidized carbon nanotubes”, *Carbon* Volume 41, Issue 5, 2003, Pages 1057-1062
- [63] Balandin, A. “Thermal Properties of graphene and nanostructured carbon material.” *Nat. Mater.* 2011, 10, 569–581.

[64] Eric Pop, David Mann, Qian Wang, Kenneth Goodson, and Hongjie Dai, “Thermal Conductance of an Individual Single-Wall Carbon Nanotube above Room Temperature”, *Nano Lett.* 2006, 6, 1, 96-100

[65] John A. Thomas, Ryan M. Iutzi, and Alan J. H. McGaughey, “Thermal conductivity and phonon transport in empty and water-filled carbon nanotubes.”, *Phys. Rev. B* 81, 045413

[66] Takahiro Yamamoto and Kazuyuki Watanabe, “Nonequilibrium Green’s Function Approach to Phonon Transport in Defective Carbon Nanotubes”, *Phys. Rev. Lett.* 96, 255503 –

[67] Quinton, B.T.; Elston, L.; Scofield, J.D.; Mukhopadhyay, S.M. “Aligned Carbon Nanotube Arrays Bonded to Solid Graphite Substrates: Thermal Analysis for Future Device Cooling Applications.” *Carbon* 2018, 4, 28.

[68] Ebbesen, T., Ajayan, P. Large-scale synthesis of carbon nanotubes. *Nature* 358, 220–222 (1992)

[69] Guo, Ting; Nikolaev, P; Thess, A; Colbert, D; Smalley, R (1995). "Catalytic growth of single-walled nanotubes by laser vaporization". *Chem. Phys. Lett.* 243 (1–2): 49–54.

- [70] Thess, A, Lee, R, & Nikolaev, P. “Crystalline ropes of metallic carbon nanotubes”, *Science*, Vol. 273, Issue 5274, pp. 483-487
- [71] H. W. Zhu, C. L. Xu, D. H. Wu, B. Q. Wei, R. Vajtai, and P. M. Ajayan, “Direct synthesis of long single-walled carbon nanotube strands.”, *Science*, vol. 296, no. 5569, pp. 884–6, May 2002.
- [72] H.M.Cheng, F.Li, X.Sun, S.D.M.Brown, M.A.Piment, A.Marucci, G.Dresselhaus, M.S.Dresselhaus, “Bulk morphology and diameter distribution of single-walled carbon nanotubes synthesized by catalytic decomposition of hydrocarbons”, *Chemical Physics Letters* Volume 289, Issues 5–6, 19 June 1998, Pages 602-610
- [73] M. Yudasaka, R. Yamada, N. Sensui, T. Wilkins, T. Ichihashi, S. Iijima, “Mechanism of the Effect of NiCo, Ni and Co Catalysts on the Yield of Single-Wall Carbon Nanotubes Formed by Pulsed Nd:YAG Laser Ablation”, *J. Phys. Chem. B* 1999, 103, 30, 6224-6229
- [74] Weizhong Qian, Tang Liu, Fei Wei, Zhanwen Wang, Guohua Luo, Hao Yu, Zhifei Li, “The evaluation of the gross defects of carbon nanotubes in a continuous CVD process”, *Carbon* Volume 41, Issue 13, 2003, Pages 2613-2617

- [75] Firoozeh Danafar, A. Fakhru'l-Razi, Mohd Amran Mohd Salleh, Dayang Radiah Awang Biak, "Fluidized bed catalytic chemical vapor deposition synthesis of carbon nanotubes—A review", *Chemical Engineering Journal* 155 (2009) 37–48
- [76] Lucie Jodin, Anne-Claire Dupuis, Emmanuelle Rouvière, and Peter Reiss, "Influence of the Catalyst Type on the Growth of Carbon Nanotubes via Methane Chemical Vapor Deposition", *J. Phys. Chem. B* 2006, 110, 14, 7328-7333
- [77] J Prasek et al, "Methods for carbon nanotubes synthesis—review", *J. Mater. Chem.*, 2011,21, 15872-15884
- [78] Ali Eatemadi et al, "Carbon nanotubes: properties, synthesis, purification, and medical applications", *Nanoscale Res Lett.* 2014; 9(1): 393.
- [79] I. T. Barney, "Fabrication and Testing of Hierarchical Carbon Nanostructures for Multifunctional Applications," Wright State University, 2012.
- [80] A. K. Karumuri, "Hierarchical Porous Structures Functionalized with Silver Nanoparticles : adaptation for antibacterial applications," Wright State University, 2014.

- [81] R. V. and S. M. Mukhopadhyay, “Nanoscale coatings for control of interfacial bonds and nanotube growth,” *Appl. Surf. Sci.*, vol. 253, no. 17, pp. 7342–7352, Jun. 2007.
- [82] Wilder, J., Venema, L., Rinzler, A. et al. “Electronic structure of atomically resolved carbon nanotubes.” *Nature* 391, 59–62 (1998).
- [83] Wang, N., Tang, Z. K., Li, G. D. & Chen, J. S. “Single-walled 4 Å carbon nanotube arrays”. *Nature* **408**, 50–51 (2000)
- [84] Walt A. de Heer, A. Châtelain, D. Ugarte , “A Carbon Nanotube Field-Emission Electron Source”, *Science* 17 Nov 1995: Vol. 270, Issue 5239, pp. 1179-1180
- [85] Tans, S., Devoret, M., Dai, H. et al. “Individual single-wall carbon nanotubes as quantum wires.” *Nature* 386, 474–477 (1997).
- [86] Zhou L, Sun Y, Yang Z, Zhou Y. “Hydrogen and methane sorption in dry and water loaded multiwall carbon nanotubes.”, *J Colloid Interface Sci.* 2005 Sep 15;289(2):347-51.
- [87] Hui-Ming Cheng, Quan-Hong Yang, Chang Liu,, “Hydrogen storage in carbon nanotubes.”, *Carbon* Volume 39, Issue 10, August 2001, Pages 1447-1454

- [88] Chong Luo, Hui Xie, Qin Wang, Geng Luo, and Chao Liu, “A Review of the Application and Performance of Carbon Nanotubes in Fuel Cells.”, *Journal of Nanomaterials* Volume 2015, Article ID 560392
- [89] Kong J, Franklin NR, Zhou C, Chapline MG, Peng S, Cho K, Dai H., “Nanotube Molecular Wires as Chemical Sensors”, *Science*. 2000 Jan 28;287(5453):622-5.
- [90] Seongjeen Kim, “CNT Sensors for Detecting Gases with Low Adsorption Energy by Ionization”, *Sensors* 2006, 6(5), 503-513
- [91] Philip G. Collins, Keith Bradley, Masa Ishigami, A. Zettl, “Extreme Oxygen Sensitivity of Electronic Properties of Carbon Nanotubes”, *Science* 10 Mar 2000: Vol. 287, Issue 5459, pp. 1801-1804
- [92] Vera Schroeder, Suchol Savagatrup, Maggie He, Sibol Lin, and Timothy M. Swager, “Carbon Nanotube Chemical Sensors”, *Chem. Rev.* 2019, 119, 1, 599-663
- [93] Kannan Balasubramanian. Marko Burghard, “Biosensors based on carbon nanotubes”, *Anal Bioanal Chem* (2006) 385: 452–468

- [94] Qing Liu, Xianbo Lu, Jun Li, Xin Yao, Jinghong Li, “Direct electrochemistry of glucose oxidase and electrochemical biosensing of glucose on quantum dots/carbon nanotubes electrodes”, *Biosensors and Bioelectronics* Volume 22, Issue 12, 15 June 2007, Pages 3203-3209
- [95] Jun Wang and Yuehe Lin, “Functionalized carbon nanotubes and nanofibers for biosensing applications”, *Trends Analyt Chem.* 2008; 27(7): 619–626.
- [96] Amal Rabti, Nouredine Raouafi, Arben Merkoçi, “Bio(Sensing) devices based on ferrocene–functionalized graphene and carbon nanotubes”, *Carbon* Volume 108, November 2016, Pages 481-514
- [97] Yossi Weizmann, David M. Chenoweth, and Timothy M. Swager, “DNA–CNT Nanowire Networks for DNA Detection”, *J. Am. Chem. Soc.* 2011, 133, 10, 3238-3241
- [98] Lee, J., Lee, D., Jung, Y. et al. “Direct spinning and densification method for high-performance carbon nanotube fibers.”, *Nat Commun* 10, 2962 (2019).
- [99] Johann Cho, Aldo R. Boccaccini, Milo S. P. Shaffer, “Ceramic matrix composites containing carbon nanotubes”, *J Mater Sci* (2009) 44:1934–1951

- [100] Arash, B., Wang, Q. & Varadan, V. “Mechanical properties of carbon nanotube/polymer composites.”, *Sci Rep* 4, 6479 (2015).
- [101] SR Bakshi, D Lahiri, A Agarwal, “Carbon nanotube reinforced metal matrix composites-a review.”, *International materials reviews*, Volume 55, 2010 - Issue 1, Pages 41-64
- [102] Philippe Serp, Massimiliano Corrias, Philippe Kalck, “Carbon nanotubes and nanofibers in catalysis.”, *Applied Catalysis A: General*. Volume 253, Issue 2, 28 October 2003, Pages 337-358
- [103] Anya Kuznetsova, Irene Popova, John T. Yates, Jr., Michael J. Bronikowski, Chad B. Huffman, Jie Liu, Richard E. Smalley, Henry H. Hwu, and Jingguang G. Chen, “Oxygen-Containing Functional Groups on Single-Wall Carbon Nanotubes: NEXAFS and Vibrational Spectroscopic Studies”, *J. Am. Chem. Soc.* 2001, 123, 43, 10699-10704
- [104] Juliette Simon, Emmanuel Flahaut, and Muriel Golzio, “Overview of Carbon Nanotubes for Biomedical Applications.”, *Materials* 2019, 12(4), 624
- [105] Hua He, Lien Ai Pham-Huy, Pierre Dramou,<sup>1</sup> Deli Xiao, Pengli Zuo, and Chuong Pham-Huy, “Carbon Nanotubes: Applications in Pharmacy and

Medicine.”, *BioMed Research International*. Volume 2013, Article ID 578290, 12 pages

[106] Eatemadi, A., Daraee, H., Karimkhanloo, H. et al. Carbon nanotubes: properties, synthesis, purification, and medical applications. *Nanoscale Res Lett* 9, 393 (2014).

[107] Liu, Z., Tabakman, S., Chen, Z. et al. “Preparation of carbon nanotube bioconjugates for biomedical applications.”, *Nat Protoc* 4, 1372–1381 (2009).

[108] Stanislaus S. Wong, James D. Harper, Peter T. Lansbury, Jr., and, and Charles M. Lieber, “Carbon Nanotube Tips: High-Resolution Probes for Imaging Biological Systems.”, *J. Am. Chem. Soc.* 1998, 120, 3, 603-604

[109] Bianco A1, Kostarelos K, Prato M., “Applications of carbon nanotubes in drug delivery.”, *Curr Opin Chem Biol.* 2005 Dec;9(6):674-9.

[110] S.K.Smart, A.I.Cassady, G.Q.Lu, D.J.Martin, “The biocompatibility of carbon nanotubes.”, *Carbon*. Volume 44, Issue 6, May 2006, Pages 1034-1047

[111] Constantine P.Firme III, Prabhakar R.Bandaru, “Toxicity issues in the application of carbon nanotubes to biological systems”, *Nanomedicine*:

Nanotechnology, Biology and Medicine. Volume 6, Issue 2, April 2010, Pages 245-256

[112] He, B., Shi, Y., Liang, Y. et al. "Single-walled carbon-nanohorns improve biocompatibility over nanotubes by triggering less protein-initiated pyroptosis and apoptosis in macrophages.", *Nat Commun* 9, 2393 (2018).

[113] Mattson, M.P., Haddon, R.C. & Rao, A.M. Molecular functionalization of carbon nanotubes and use as substrates for neuronal growth. *J Mol Neurosci* 14, 175–182 (2000).

[114] Zanello LP, Zhao B, Hu H, Haddon RC., "Bone cell proliferation on carbon nanotubes.", *Nano Lett.* 2006 Mar;6(3):562-7.

[115] Anderson T, Hu R, Yang C, Yoon H-S, Yong K-T. "Pancreatic cancer gene therapy using an siRNA-functionalized single walled carbon nanotubes nanoplex.", *Biomater. Sci.*, 2014,2, 1244-1253

[116] Newbury DE, Ritchie NW., "Is scanning electron microscopy/energy dispersive X-ray spectrometry (SEM/EDS) quantitative?", *Scanning.* 2013 May-Jun;35(3):141-68

- [117] Stephen Brunauer, P. H. Emmett, and Edward Teller, “Adsorption of Gases in Multimolecular Layers”, *J. Am. Chem. Soc.* 1938, 60, 2, 309-319
- [118] Borm PJ, Robbins D, Haubold S, et al. The potential risks of nanomaterials: a review carried out for ECETOC. *Part Fibre Toxicol.* 2006;3:11. Published 2006 Aug 14. doi:10.1186/1743-8977-3-11
- [119] Z.-Y. Yuan, B.-L. Su, Insights into hierarchically meso–macroporous structured materials, *J. Mater. Chem.* 16 (2006) 663–677. doi:10.1039/b512304f
- [120] Rushikesh S. Ambekar and Balasubramanian Kandasubramanian, “Progress in the Advancement of Porous Biopolymer Scaffold: Tissue Engineering Application”, *Industrial & Engineering Chemistry Research* 2019 58 (16), 6163-6194 DOI: 10.1021/acs.iecr.8b05334
- [121] Patricia M. Taylor, Anthony E.G. Cass, Magdi H. Yacoub, Extracellular matrix scaffolds for tissue engineering heart valves, *Progress in Pediatric Cardiology*, Volume 21, Issue 2, 2006, Pages 219-225,
- [122] C. Lai, Q. Guo, X. Wu, D.H. Reneker, H. Hou, Growth of carbon nanostructures on carbonized electrospun nanofibers with palladium nanoparticles, *Nanotechnology.* 19 (2008) 195303. doi:10.1088/0957-4484/19/19/195303

[123] G.G. Wildgoose, C.E. Banks, R.G. Compton, Metal nanoparticles and related materials supported on carbon nanotubes: methods and applications., *Small*. 2 (2006) 182–93. doi:10.1002/sml.200500324.

[124] A. Stein, Z. Wang, M. a. Fierke, Functionalization of Porous Carbon Materials with Designed Pore Architecture, *Adv. Mater.* 21 (2009) 265–293. doi:10.1002/adma.200801492.

[125] Dong, L., Li, Y., Wang, L., Xu, S. & Hou, F. Effect of frozen conditions on dispersion morphologies of carbon nanotubes and electrical conductivity of carbon fiber/epoxy composites. *Mater. Lett.* 130, 180–183 (2014).

[126] Perera, S. D. et al. Vanadium oxide nanotube spherical clusters prepared on carbon fabrics for energy storage applications. *ACS Appl. Mater. Interfaces* 3, 4512–4517 (2011).

[127] Di, J. et al. Carbon-Nanotube Fibers for Wearable Devices and Smart Textiles. *Adv. Mater.* 10529–10538 (2016).

[128] T. Tong, Y. Zhao, L. Delzeit, A. Kashani, M. Meyyappan, and A. Majumdar, “Dense Vertically Aligned Multiwalled Carbon Nanotube Arrays as Thermal Interface Materials,” *IEEE Trans. Components Packag. Technol.*, vol. 30, no. 1, pp. 92–100, 2007.

- [129] P. B. Amama, C. L. Pint, S. M. Kim, L. McJilton, K. G. Eyink, E. a Stach, R. H. Hauge, and B. Maruyama, "Influence of alumina type on the evolution and activity of alumina-supported Fe catalysts in single-walled carbon nanotube carpet growth.," *ACS Nano*, vol. 4, no. 2, pp. 895–904, Feb. 2010.
- [130] H. Wang, Q. Cai, C.-L. Chen, D. Wang, and Z. Ren, "Growth of aligned carbon nanotubes on ALD-Al<sub>2</sub>O<sub>3</sub> coated silicon and quartz substrates," *J. Exp. Nanosci.*, vol. 6, no. 5, pp. 464–472, Oct. 2011.
- [131] Sugime, H. et al. Growth kinetics and growth mechanism of ultrahigh mass density carbon nanotube forests on conductive Ti/Cu supports. *ACS Appl. Mater. Interfaces* 6, 15440–15447 (2014).
- [132] S. M. Mukhopadhyay, R. V. Pulikollu, E. Ripberger, and A. K. Roy, "Surface modification of graphitic foam," *J. Appl. Phys.*, vol. 93, no. 2, pp. 878–882, 2003.
- [133] P.W.A.M. Wenmakers, J. van der Schaaf, B.F.M. Kuster, J.C. Schouten, "Hairy Foam": carbon nanofibers grown on solid carbon foam. A fully accessible, high surface area, graphitic catalyst support, *J. Mater. Chem.* 18 (2008) 2426–2436. doi:10.1039/b718673h.

[134] S.M. Mukhopadhyay, A. Karumuri, I.T. Barney, Hierarchical nanostructures by nanotube grafting on porous cellular surfaces, *J. Phys. D. Appl. Phys.* 42 (2009) 195503. doi:10.1088/0022-3727/42/19/195503.

[135] B.Q. Wei, R. Vajtai, Y. Jung, J. Ward, R. Zhang, G. Ramanath, et al., Assembly of Highly Organized Carbon Nanotube Architectures by Chemical Vapor Deposition, *Chem. Mater.* 15 (2003) 1598–1606.

[136] A.K. Karumuri, A.A. Maleszewski, D.P. Oswal, H. a. Hostetler, S.M. Mukhopadhyay, Fabrication and characterization of antibacterial nanoparticles supported on hierarchical hybrid substrates, *J. Nanoparticle Res.* 16 (2014) 2346. doi:10.1007/s11051-014-2346-x.

[137] B.T. Quinton, K.D. Leedy, J.W. Lawson, B. Tsao, J.D. Scofield, J.N. Merrett, et al., Influence of oxide buffer layers on the growth of carbon nanotube arrays on carbon substrates, *Carbon N. Y.* 87 (2015) 175–185. doi:10.1016/j.carbon.2015.02.015.

[138] S.M. Mukhopadhyay, A. Karumuri, I.T. Barney, Hierarchical nanostructures by nanotube grafting on porous cellular surfaces, *J. Phys. D. Appl. Phys.* 42 (2009) 195503. doi:10.1088/0022-3727/42/19/195503.

- [139] R. V. Pulikollu, S.M. Mukhopadhyay, Nanoscale coatings for control of interfacial bonds and nanotube growth, *Appl. Surf. Sci.* 253 (2007) 7342–7352. doi:10.1016/j.apsusc.2007.03.026.
- [140] Guadagno, L. et al. RSC Advances carbon fiber reinforced composites. 6033–6042 (2015).
- [141] Compston P, Jar PYB, Davies P. Matrix effect on the static and dynamic interlaminar fracture toughness of glass–fibre marine composites. *Compos Part B Eng* 1998;29(4):505–16.
- [142] H. Vijwani, M.N. Nadagouda, V. Namboodiri, S.M. Mukhopadhyay, Hierarchical hybrid carbon nano-structures as robust and reusable adsorbents: Kinetic studies with model dye compound, *Chem. Eng. J.* 268 (2015) 197–207. doi:10.1016/j.cej.2015.01.027.
- [143] T Martin Pumera, The Electrochemistry of Carbon Nanotubes: Fundamentals and Applications, *Chemistry a European journal*, Volume15, Issue20, May 11, 2009, Pages 4970-4978
- [144] Fernando T. Andón et al, Biodegradation of Single-Walled Carbon Nanotubes by Eosinophil Peroxidase, *Small*, Volume9, Issue16, August 26, 2013, Pages 2721-2729

- [145] Akhil Patel et al, Carbon-based hierarchical scaffolds for myoblast differentiation: Synergy between nano-functionalization and alignment, *Acta Biomaterialia* Volume 32, 1 March 2016, Pages 77-88
- [146] JunWang, YueheLin ,Functionalized carbon nanotubes and nanofibers for biosensing applications, *TrAC Trends in Analytical Chemistry* Volume 27, Issue 7, July–August 2008, Pages 619-626
- [147] Laurent, C., Flahaut, E. & Peigney, A. The weight and density of carbon nanotubes versus the number of walls and diameter. *Carbon* N. Y. 48, 2994–2996 (2010).
- [148] C. Gommès, S. Blacher, C. Bossuot, P. Marchot, J.B. Nagy, J.-P. Pirard, Influence of the operating conditions on the production rate of multi-walled carbon nanotubes in a CVD reactor, *Carbon* N. Y. 42 (2004) 1473–1482.  
doi:10.1016/j.carbon.2004.01.063
- [149] 2016, Aligned Carbon Nanotube Carpets on Carbon Substrates for High Power Electronic Applications, Betty Tun-Huan Quinton, Wright State University
- [150] SPECIFICATION FOR THE SIZE OF ABRASIVE GRAIN - GRINDING WHEELS, POLISHING AND GENERAL INDUSTRIAL USES. ANSI B74.12 2018 Edition, 2018

[151] 2015, Hierarchical Porous Structures with Aligned Carbon Nanotubes as Efficient Adsorbents and Metal-Catalyst Supports, Hema Vijwani, Wright State University

[152] Evans J.W., De Jonghe L.C. (2016) “Advanced Materials and Processes. In: The Production and Processing of Inorganic Materials.”, Springer, Cham

[153] Peigney, Alain and Laurent, Christophe and Flahaut, Emmanuel and Bacsa, Revathi and Rousset, Abel, “Specific surface area of carbon nanotubes and bundles of carbon nanotubes.”, (2001) Carbon, vol. 39 (n° 4). pp. 507-514.

[154] Yibo Yan, Xinli Jia, Yan huiYang, “Palladium nanoparticles supported on CNT functionalized by rare-earth oxides for solvent-free aerobic oxidation of benzyl alcohol.”, Catalysis Today Volume 259, Part 2, 1 January 2016, Pages 292-302

[155] V.Selvaraj, M.Alagar, K. Sathish Kumar, “Synthesis and characterization of metal nanoparticles-decorated PPY–CNT composite and their electrocatalytic oxidation of formic acid and formaldehyde for fuel cell applications.”, Applied Catalysis B: Environmental Volume 75, Issues 1–2, 29 August 2007, Pages 129-138

- [156] F. Avilés, J.V. Cauich-Rodríguez, L. Moo-Tah, A. May-Pat, R. Vargas-Coronado, "Evaluation of mild acid oxidation treatments for MWCNT functionalization.", *Carbon* Volume 47, Issue 13, November 2009, Pages 2970-2975
- [157] Min Zhang, Tao Zhang, and Tianhong Cui, "Wettability Conversion from Superoleophobic to Superhydrophilic on Titania/Single-Walled Carbon Nanotube Composite Coatings", *Langmuir* 2011 27 (15), 9295-9301
- [158] J. Yang, Z. Zhang, X. Men, X. Xu, and X. Zhu, "Reversible superhydrophobicity to superhydrophilicity switching of a carbon nanotube film via alternation of UV irradiation and dark storage.," *Langmuir*, vol. 26, no. 12, pp. 10198–202, Jun. 2010.
- [159] Young, T. (1805). "An Essay on the Cohesion of Fluids". *Philosophical Transactions of the Royal Society of London*. 95: 65–87.
- [160] Guillaume Lamour, Ahmed Hamraoui, Andrii Buvailo, Yangjun Xing, Sean Keuleyan, Vivek Prakash, Ali Eftekhari-Bafrooei, and Eric Borguet, "Contact Angle Measurements Using a Simplified Experimental Setup.," *J. Chem. Educ.* 2010, 87, 12, 1403-1407

[161] SPECIFICATION FOR THE SIZE OF ABRASIVE GRAIN - GRINDING WHEELS, POLISHING AND GENERAL INDUSTRIAL USES. ANSI B74.12 2018 Edition, 2018

[162] ASTM E407 - 07(2015)e1. Standard Practice for Microetching Metals and Alloys

[163] Diana Vilela, María Cristina González, Alberto Escarpa, “Sensing colorimetric approaches based on gold and silver nanoparticles aggregation: Chemical creativity behind the assay. A review”, *Analytica Chimica Acta* Volume 751, 2 November 2012, Pages 24-43

[164] Peter Majewski & Benjamin Thierry, “Functionalized Magnetite Nanoparticles—Synthesis, Properties, and Bio-Applications.”, *Critical Reviews in Solid State and Materials Sciences* Volume 32, 2007 - Issue 3-4, Pages 203-215

[165] Richard D. Glover, John M. Miller, and James E. Hutchison, “Generation of Metal Nanoparticles from Silver and Copper Objects: Nanoparticle Dynamics on Surfaces and Potential Sources of Nanoparticles in the Environment.”, *ACS Nano* 2011 5 (11), 8950-8957

- [166] Lichen Liu and Avelino Corma, “Metal Catalysts for Heterogeneous Catalysis: From Single Atoms to Nanoclusters and Nanoparticles.”, *Chem. Rev.* 2018, 118, 10, 4981-5079
- [167] Yan Qiao, Chang Ming Li, “Nanostructured catalysts in fuel cells.”, *J. Mater. Chem.*, 2011,21, 4027-4036
- [168] Yang, X., Li, H., Ahuja, R. et al. “Formation and electronic properties of palladium hydrides and palladium-rhodium dihydride alloys under pressure.”, *Sci Rep* 7, 3520 (2017).
- [169] Paresh Chandra Ray, Hongtao Yu, and Peter P. Fu, “Toxicity and Environmental Risks of Nanomaterials: Challenges and Future Needs.”, *J Environ Sci Health C Environ Carcinog Ecotoxicol Rev.* 2009 Jan; 27(1): 1–35
- [170] Heming Wang, Zhiyong Jason Ren, “Bioelectrochemical metal recovery from wastewater: A review”, *Water Research* Volume 66, 1 December 2014, Pages 219-232
- [171] Creamer, N.J., Baxter-Plant, V.S., Henderson, J. et al. Palladium and gold removal and recovery from precious metal solutions and electronic scrap leachates by *Desulfovibrio desulfuricans* . *Biotechnol Lett* 28, 1475–1484 (2006).

[172] Schreiber, R., Do, J., Roller, E. et al. “Hierarchical assembly of metal nanoparticles, quantum dots and organic dyes using DNA origami scaffolds.”, *Nature Nanotech* 9, 74–78 (2014).

[173] R. M. Rioux, H. Song, J. D. Hoefelmeyer, P. Yang, and G. A. Somorjai, “High-Surface-Area Catalyst Design: Synthesis, Characterization, and Reaction Studies of Platinum Nanoparticles in Mesoporous SBA-15 Silica.”, *J. Phys. Chem. B* 2005, 109, 2192-2202

[174] Suresh Babu Kalidindi, Udishnu Sanyal, and Balaji R. Jagirdar, “Metal Nanoparticles via the Atom-Economy Green Approach.”, *Inorganic Chemistry* 2010 49 (9), 3965-3967

[175] Takashi Onoe, Shinji Iwamoto, Masashi Inoue, “Synthesis and activity of the Pt catalyst supported on CNT”, *Catalysis Communications*, Volume 8, Issue 4, April 2007, Pages 701-706

[176] H. Vijwani and S. M. Mukhopadhyay, “Palladium nanoparticles on hierarchical carbon surfaces : A new architecture for robust nano-catalysts,” *Appl. Surf. Sci.*, vol. 263, pp. 712–721, 2012.

- [177] T. Teranishi and M. Miyake, "Size Control of Palladium Nanoparticles and Their Crystal Structures," *Chem. Mater.*, vol. 4756, no. 23, pp. 594–600, 1998.
- [178] Xu L, Wu XC, Zhu JJ., "Green preparation and catalytic application of Pd nanoparticles.", *Nanotechnology*. 2008 Jul 30;19(30):305603.
- [179] R. Wojcieszak, M. J. Genet, P. Eloy, P. Ruiz, and E. M. Gaigneaux, "Determination of the Size of Supported Pd Nanoparticles by X-ray Photoelectron Spectroscopy. Comparison with X-ray Diffraction, Transmission Electron Microscopy, and H<sub>2</sub> Chemisorption Methods.", *J. Phys. Chem. C* 2010, 114, 39, 16677-16684
- [180] Prof. Dr. Dietrich Henschler, "Toxicity of Chlorinated Organic Compounds: Effects of the Introduction of Chlorine in Organic Molecules", *Angew. Chem. Int. Ed. Engl.* Volume 33, Issue 19, Pages: 1897-1994, October 17, 1994
- [181] Godwin O. Olutona, Stephen O. Olatunji, and Joshua F. Obisanya, "Downstream assessment of chlorinated organic compounds in the bed-sediment of Aiba Stream, Iwo, South-Western, Nigeria", *Springerplus*. 2016; 5: 67.
- [182] EPA/635/R-00/007, TOXICOLOGICAL REVIEW OF CHLORINE DIOXIDE AND CHLORITE (CAS Nos. 10049-04-4 and 7758-19-2), 2000

- [183] Walter RK, Lin PH, Edwards M, Richardson RE., “Investigation of factors affecting the accumulation of vinyl chloride in polyvinyl chloride piping used in drinking water distribution systems.”, *Water Res.* 2011 Apr;45(8):2607-15.
- [184] U.S. Environmental Protection Agency. Integrated Risk Information System (IRIS) on Chlorine. National, Center for Environmental Assessment, Office of Research and Development, Washington, DC. 1999.
- [185] Beijer K, Björlenius B, Shaik S, Lindberg RH, Brunström B, Brandt I, “Removal of pharmaceuticals and unspecified contaminants in sewage treatment effluents by activated carbon filtration and ozonation: Evaluation using biomarker responses and chemical analysis.”, *Chemosphere.* 2017 Jun;176:342-351.
- [186] Katsigiannis, A., Noutsopoulos, C., Mantziaras, J., Gioldasi, M., “Removal of emerging pollutants through Granular Activated Carbon”, *Chemical Engineering Journal* 280 (2015) 49–57
- [187] Lu Xina, Yabing Sun, Jingwei Feng, Jian Wang, Dong He, “Degradation of triclosan in aqueous solution by dielectric barrier discharge plasma combined with activated carbon fiber.”, *Chemosphere* 144 (2016) 855–863 Contents
- [188] S. Murgolo, F. Petronella, R. Ciannarella, R. Comparelli, A. Agostiano,

M.L. Curri, G. Mascolo, “UV and solar-based photocatalytic degradation of organic pollutants by nano-sized TiO<sub>2</sub> grown on carbon nanotubes.”, *Catalysis Today* 240 (2015) 114–124

[189] Brian P. Chaplin, Martin Reinhard, William F. Schneider, Christoph Schüth, John R. Shapley, Timothy J. Strathmann, and Charles J. Werth, “Critical Review of Pd-Based Catalytic Treatment of Priority Contaminants in Water” , *Environ. Sci. Technol.* 2012, 46, 7, 3655-3670

[190] Charlie Corredor, Mark D. Borysiak, Jay Wolfer, Paul Westerhoff, and Jonathan D. Posner, “Colorimetric Detection of Catalytic Reactivity of Nanoparticles in Complex Matrices.”, *Environ. Sci. Technol.* 2015, 49, 6, 3611-3618

[191] Mallikarjuna N. Nadagouda, Ishan Desai, Carlo Cruz and Duck J. Yang, “Novel Pd based catalyst for the removal of organic and emerging contaminants”, *RSC Adv.*, 2012, 2, 7540-7548

[192] Varima Bokare, Kumarasamy Murugesan, Young-Mo Kim, Jong-Rok Jeon, Eun-Ju Kim, Yoon Seok Chang, “Degradation of triclosan by an integrated nano-bio redox process”, *Bioresource Technology*, Volume 101, Issue 16, August 2010, Pages 6354-6360

- [193] Kumarasamy Murugesan, Varima Bokare, Jong-Rok Jeon, Eun-Ju Kim, Jae-Hwan Kim, Yoon-Seok Chang, “Effect of Fe-Pd bimetallic nanoparticles on *Sphingomonas* sp. PH-07 and a nano-bio hybrid process for triclosan degradation, *Bioresource Technology*”, Volume 102, Issue 10, May 2011, Pages 6019-6025
- [194] Man Zhang, Deborah B. Bacik, Christopher B. Roberts, Dongye Zhao, “Catalytic hydrodechlorination of trichloroethylene in water with supported CMC-stabilized palladium nanoparticles.”, *Water Research*, Volume 47, Issue 11, 1 July 2013, Pages 3706-3715
- [195] Cedric Fischmeister and Henri Doucet, “Greener solvents for ruthenium and palladium-catalysed aromatic C–H bond functionalization”, *Green Chem.*, 2011, 13, 741-753
- [196] Hyun-Hee Cho, Haiou Huang, and Kellogg Schwab, “Effects of solution chemistry on the adsorption of ibuprofen and triclosan onto carbon nanotubes”, *Langmuir* 2011, 27, 21, 12960-12967
- [197] Zhou, S, Shao, Y, Gao, N, Deng, J, Tan, C, “Equilibrium, Kinetic, and Thermodynamic Studies on the Adsorption of Triclosan onto Multi-Walled Carbon Nanotubes”, *Clean – Soil, Air, Water* 2013, 41 (6), 539–547

- [198] Mei-Fei Yueh and Robert H. Tukey, “Triclosan: A Widespread Environmental Toxicant with Many Biological Effects”, *Annu Rev Pharmacol Toxicol.* 2016 Jan 6; 56: 251–272.
- [199] Lisa M. Weatherly and Julie A. Gosse, “Triclosan Exposure, Transformation, and Human Health Effects”, *J Toxicol Environ Health B Crit Rev.* 2017; 20(8): 447–469.
- [200] Štěpánek F., Šoóš M. and P. Rajniak, “Characterization of porous media by the virtual capillary condensation method”, *Colloids and Surfaces A.* (2007), 300, 11-20
- [201] B. Henrich, C. Cupelli, M. Santer, and M. Moseler, “Continuum concepts in nanoscale capillary impregnation”, *New J. Phys.* 10, 113022 (2008).
- [202] Hettel M., Wörner M., Deutschmann O. (2018) Computational Fluid Dynamics of Catalytic Reactors. In: Andreoni W., Yip S. (eds) *Handbook of Materials Modeling.* Springer, Cham
- [203] W. A. Catterall, “Structure and function of voltage-sensitive ion channels”, *Science* 242, 50 (1988).

[204] van der Straaten, T., Kathawala, G. & Ravaioli, U. “BioMOCA: A Transport Monte Carlo Model for Ion Channels.”, *Journal of Computational Electronics* 2, 231–237 (2003).

[205] Bernard J. Hamrock, Steven R. Schmid, Bo O. Jacobson, *Fundamentals of Fluid Film Lubrication*, 2nd Edition

[206] M.J.Buntain, S.Bickerton, “Compression flow permeability measurement: a continuous technique”, *Composites Part A: Applied Science and Manufacturing* , Volume 34, Issue 5, May 2003, Pages 445-457,

[207] Whitaker, S. “Flow in porous media I: A theoretical derivation of Darcy's law.”, *Transp Porous Med* 1, 3–25 (1986).

[208] 2015, *Surface Treatments to Tailor the Wettability of Carbon Nanotube Arrays*, He, Lvmeng, Wright State University

[209] 2014, *Hierarchical Porous Structures Functionalized with Silver Nanoparticles: Adaptation for Antibacterial Applications*, Karumuri, Anil Kumar, Wright State University

[210] Menglian Wei, Yongfeng Gao, Xue Li and Michael J. Serpe, “Stimuli-responsive polymers and their applications.”, *Polym. Chem.*, 2017, 8, 127-143

[211]. Cabane, E., Zhang, X., Langowska, K. *et al.* Stimuli-Responsive Polymers and Their Applications in Nanomedicine. *Biointerphases* 7, 9 (2012).

[212] Muhammad Abdul Haq, Yunlan Su, Dujin Wang, “Mechanical properties of PNIPAM based hydrogels: A review”, *Materials Science and Engineering: C* , Volume 70, Part 1, 1 January 2017, Pages 842-855

[213] Prof. Avraham Halperin, Prof. Martin Kröger, Prof. Françoise M. Winnik, “Poly(*N*-isopropylacrylamide) Phase Diagrams: Fifty Years of Research”, *Angewandte Chemie International Edition*, Volume 54, Issue 51 December 14, 2015, Pages 15342-15367

[214] Qun Feng Liu et al, “A Simple Method to Synthesize PNIPAM Hydrogel with Improved Response Rate by Conventional Radical Crosslinking Polymerization ”, 2011, *Advanced Materials Research*, 236-238, 1483,

[215]. D. R. Simpson, “Biofilm processes in biologically active carbon water purification,” *Water Res.*, vol. 42, no. 12, pp. 2839–2848, 2008.

[216]. G. O. Brown, “Henry Darcy and the making of a law,” *Water Resour. Res.*, vol. 38, no. 7, pp. 1–12, 2002.

[217]. Basak, P. 1977. *Non-Darcy Flow and Its Implications to Seepage Problems*, *Journal of the Irrigation and Drainage Division, American Society of Civil Engineers*, 103, 459.

[218] M. Peszyńska, A. Trykozko, and W. Sobieski, “Forchheimer law in computational and experimental studies of flow through porous media at porescale and mesoscale,” *Math. Sci. Appl.*, vol. 32, pp. 463–482, 2010.

[219] *Heat transfer* / Jack P. Holman.—10th ed. 2010.

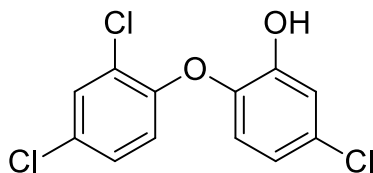
[220] ASTM D695–15 *Standard Test Method for Compressive Properties of Rigid Plastics*

[221] Sharmila M Mukhopadhyay and Anil K Karumuri, “Nanotube attachment for prevention of interfacial delamination”, *J. Phys. D: Appl. Phys.* 43 (2010) 365301 (7pp)

[222] Jerzy. Dec and Jean Marc. Bollag, “Dehalogenation of Chlorinated Phenols during Oxidative Coupling.”, *Environ. Sci. Technol.* 1994, 28, 3, 484-490

[223] Ryu Nakao, Hakjune Rhee and, and Yasuhiro Uozumi, "Hydrogenation and Dehalogenation under Aqueous Conditions with an Amphiphilic-Polymer-Supported Nanopalladium Catalyst", *Org. Lett.* 2005, 7, 1, 163-165

## Appendix A: HPLC analysis of Triclosan (Irgasan)



Chemical Formula:  $C_{12}H_7Cl_3O_2$

Molecular Weight: 289.54

### Beer–Lambert law

$$A = -\log T = \log \frac{I_0}{I} = \varepsilon \cdot c \cdot d$$

A Absorption

T Transmission,  $T = I/I_0$

$I_0$  Intensity of the light going to the flow cell

I Intensity of the light that has passed the flow cell

$\varepsilon$  extinction coefficient: how strong does a specific substance absorb light

c concentration of the substance

d length of the beam path through the cell, cell length

Stock solution: 1 mg/ml(1000 ppm).

- Weigh 53.2 mg of the standard (97%), dissolve in MeOH, adjust the volume to 25 ml, giving the final concentration at 2.07 mg/ml.
- Dilute the solution by 100 fold (100 ul to 10.0 ml, MeOH) to give 20.7 ug/ml solution

Solution	Stock	MeOH	Concentration (ppm)	235 nm Area (mAu*sec)	202 nm Area (mAu*sec)
1	1	0	20.7	595.4	2183.3
2	0.7	0.3	14.49	418.1	1481.7
3	0.4	0.6	8.28	233.5	822.3
4	0.2	0.8	4.14	129.9	431.0
5	0.1	0.9	2.07	76.3	233.6
6	0.05	0.95	1.035	46.7	131.4

### HPLC Method

Column: waters Xselect CSH C18 3.5 um, 4.6x50 mm, part #: 186005267

Solvent: **A** 1% MeCN/0.2%H<sub>3</sub>PO<sub>4</sub>/Water; **B** Acetonitrile

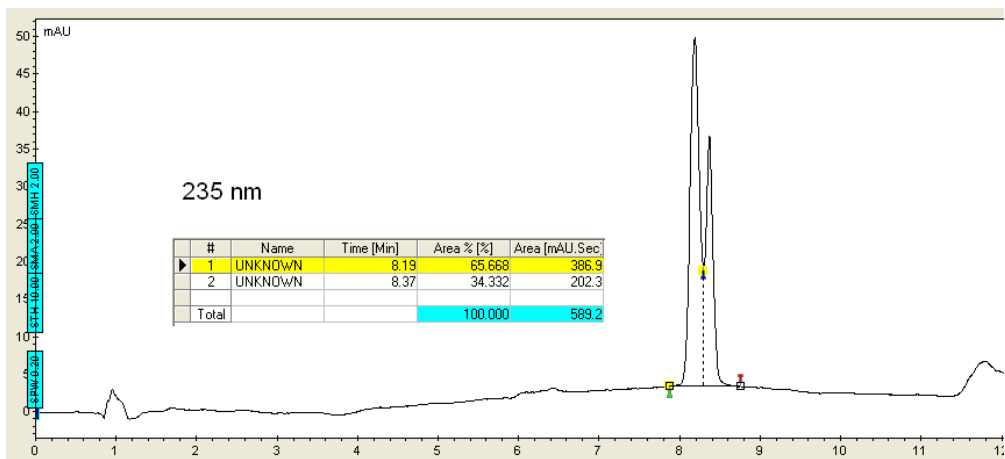
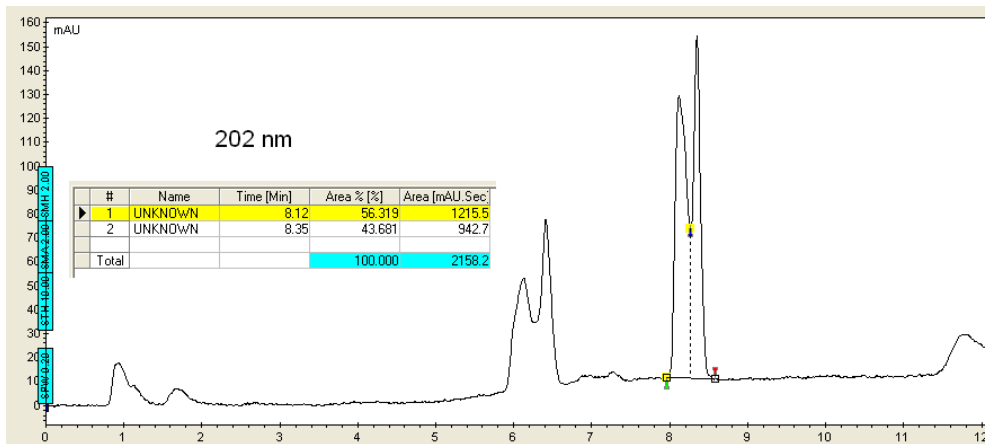
Flow:

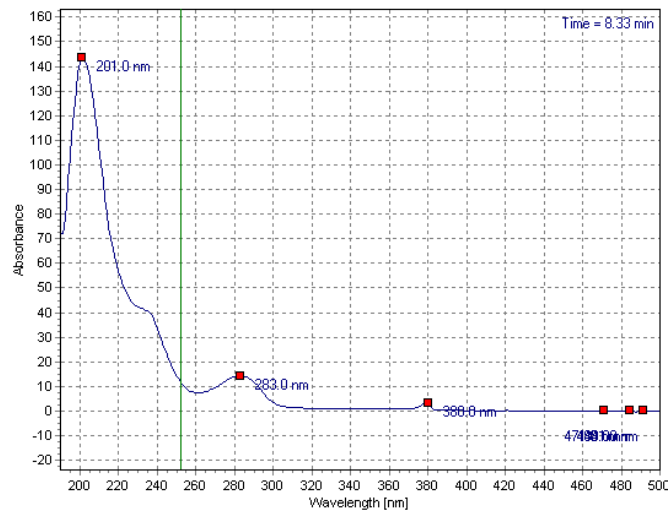
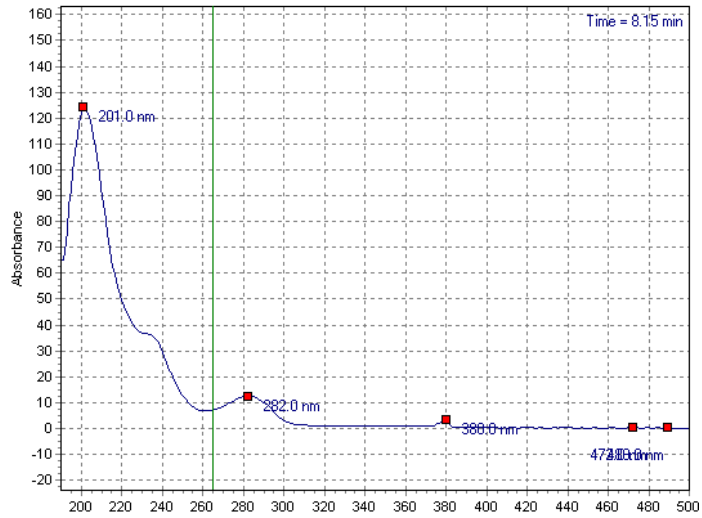
Time (min)	Flow (ml/min)	A (%)	B (%)
0	1	70	30
2	1	70	30
8	1	10	90
10	1	10	90
11	1	70	30

## Detection

UV at 235 nm or 202nm

Retention time, spectra





## Standard curve calibration

